AD-A015 723

EVALUATION OF LEAD FINISHES FOR MICROCIRCUIT PACKAGES

G. Schaefer, et al

General Electric Company

Prepared for:

Rome Air Development Center

July 1975

294097

RADC-TR-75-171
Final Technical Report
July 1975

EVALUATION OF LEAD FINISHES FOR MICROCIRCUIT PACKAGES

General Electric Company

Rome Air Development Center
Air Force Systems Command
Griffiss Air Force Base, New York 13441

This report has been reviewed by the RADC Information Office (OI) and is releasable to the National Technical Information Service (NTIS). At NTIS it will be releasable to the general public, including foreign nations.

This technical report has been reviewed and approved for publication.

APPROVED: John E. McCormick

JOHN E. McCORMICK
Project Engineer

APPROVED: Joseph J. Naresky

JOSEPH J. NARESKY
Chief, Reliability & Compatibility Division

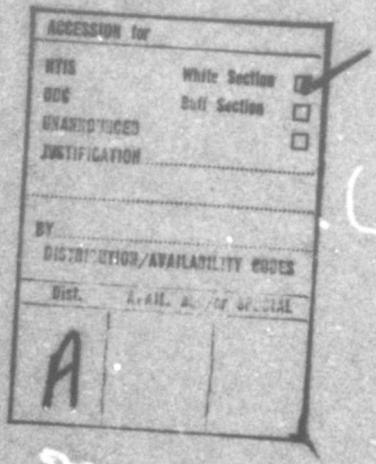

FOR THE COMMANDER: John P. Huss

JOHN P. HUSS
Acting Chief, Plans Office

Do not return this copy. Retain or destroy.

UNCLASSIFIED

SECURITY CLASSIFICATION OF THIS PAGE (When Data Entered)

REPORT DOCUMENTATION PAGE	READ INSTRUCTIONS BEFORE COMPLETING FORM
1. REPORT NUMBER: RADC-TR-75-171	2. GOVT ACCESSION NO. / 3. RECIPIENT'S CATALOG NUMBER
4. TITLE (and Subtitle): EVALUATION OF LEAD FINISHES FOR MICROCIRCUIT PACKAGES	5. TYPE OF REPORT & PERIOD COVERED: Final Technical Report 23 Jan 74 - 23 Apr 75
	6. PERFORMING ORG. REPORT NUMBER: N/A
7. AUTHOR(s): G. Schaefer, R. Ward, L. Zakraysek	8. CONTRACT OR GRANT NUMBER(s): F30602-74-C-0118
9. PERFORMING ORGANIZATION NAME AND ADDRESS: General Electric Company, Aerospace Electronic Systems Department, Utica NY 13503	10. PROGRAM ELEMENT, PROJECT, TASK AREA & WORK UNIT NUMBERS: 62702F, 55190438
11. CONTROLLING OFFICE NAME AND ADDRESS: Rome Air Development Center (RBRM), Griffiss AFB NY 13441	12. REPORT DATE: July 1975
	13. NUMBER OF PAGES: 140
14. MONITORING AGENCY NAME & ADDRESS (if different from Controlling Office): Same	15. SECURITY CLASS. (of this report): UNCLASSIFIED
	15a. DECLASSIFICATION/DOWNGRADING SCHEDULE: N/A

16. DISTRIBUTION STATEMENT (of this Report)

Approved for public release; distribution unlimited.

17. DISTRIBUTION STATEMENT (of the abstract entered in Block 20, if different from Report)

Same

18. SUPPLEMENTARY NOTES

RADC Project Engineer
John E. McCormick (RBRM)

19. KEY WORDS (Continue on reverse side if necessary and identify by block number)

Microcircuit Package Lead Finishes
Glass Sealing Alloys
Oxidation of Fe-Ni-Co
Solderability of Fe-Ni-Co

20. ABSTRACT (Continue on reverse side if necessary and identify by block number)

Oxidation studies made on several vendor Fe-Ni-Co (ASTM-F15) glass sealing alloys show these alloys to differ in both rate of oxidation and adherence of the oxide to the metal. Differences in surface preparation, surface roughness, and atmosphere control on rate and adherence were shown to affect both rate of oxidation and adherence. Using the curves established in these rate studies, samples were oxidized to predetermined thickness. Those selectively oxidized samples were "sealed" with commercial glasses. Adherence of the glass to

DD FORM 1 JAN 73 1473 EDITION OF 1 NOV 65 IS OBSOLETE

UNCLASSIFIED

SECURITY CLASSIFICATION OF THIS PAGE (When Data Entered)

metal is shown to be related to oxide thickness and the energy input used in sealing.

Samples, both in the cleaned as-received and cleaned-after oxidation conditions, were plated with bright acid tin (BAT), bright acid solder (BAS), high purity gold (99.9%), lesser purity gold (99.7%), with some gold plated samples receiving under plates of sulfamate nickel (NiS). Duplex coatings of gold also were made. Studies of corrosion, salt fog, bend tests, solderability, and flying lead bondability investigations of these plated samples show: (1) BAT and BAS protect the base lead material by sacrificial corrosion and are excellent in solderability, (2) high purity gold plates to be superior to gold plates of lesser purity in bend, corrosion, solderability and bondability. Ultrasonic soldering was found beneficial in restoring solderability to samples showing dewet areas where the dewetting was produced intentionally by several different techniques.

EVALUATION

This effort supports RADC TPO-13, Reliability. The purpose of this study was to determine the compatibility and effectiveness of surface finishes and undercoats being used on microelectronic package leads. The study covered the actions and interactions resulting from the various process steps the lead materials undergo, from initial rolled sheet condition through the final process of plating to preserve solderability. Results of the experimental work have indicated two areas, beyond the scope of this program, which require further study.

A serious need exists for documentation controlling the processing and production of integrated circuit lead frame materials. Presently, only the chemical makeup of the alloys are partially controlled. No documentation exists for the control of heat treat operations and associated metallurgical processes that directly affect the glass sealing properties and solderability of this lead frame material.

The second problem area is concerned with solderability testing. A need exists for a program updating Test Method 2003, Solderability, of MIL-STD-883, Test Methods and Procedures for Microelectronics. This program should also include an investigation of the applicability and repeatability of alternate solderability test methods for inclusion in Method 2003.

John E McCormick

JOHN E. McCORMICK
Solid State Applications Section
Reliability Branch

TABLE OF CONTENTS

TABLE OF CONTENTS (Continued)

TABLE OF CONTENTS (Continued)

LIST OF ILLUSTRATIONS

LIST OF ILLUSTRATIONS (Continued)

LIST OF ILLUSTRATIONS (Continued)

LIST OF ILLUSTRATIONS (Continued)

LIST OF TABLES

SECTION 1

INTRODUCTION

OBJECTIVES

The purpose of this study was to determine the compatibility and effectiveness of surface finishes and undercoats being used on microelectronic package leads. The study was to determine optimum combination of materials and processes, including those in use and those proposed for use, for various lead frame sealing glass combinations. The study covered the actions and interactions resulting from the various process steps the lead materials undergo, from initial rolled sheet condition through the final process of plating to preserve solderability.

BACKGROUND

Microcircuit packages, which have been in use for a considerable period of time, employ surface preservation and glass sealing techniques developed in the vacuum tube and electrical feedthrough industries. In addition, the surface preservation techniques used in these packages have been those which "worked best", as adapted from the jewelry industry. These combinations of sealing and surface preservation techniques have had both advantages and disadvantages for producers as well as users of the packages.

Because of hermeticity requirements, microelectronic package lead frame material must be compatible dimensionally with the sealing glasses used in the packages. Therefore, lead materials have been limited to those whose thermal characteristics would match those of the glasses. Because both compression and oxide type glass sealing techniques are used, lead materials compatible with both techniques have been developed. In addition, variations in types of glass and adjustment of the properties of the various types have led to similar variations in lead material processing. These variations have occurred in production of microcircuit packages, but even more so in their application. This is because a typical producer usually specializes in certain package types, while a user may require as many as

50 different types in just one application. Even this number could double with dual source of supply. Each of these types could use different glass or base lead material processing.

Two particular conditions highlighted the need for this study contract. These become evident because users of microelectronic circuit packages, in particular manufacturers of military electronic systems for all branches of the armed services, were experiencing increased costs and schedule delays due to the need for corrective action on soldered leads. The first condition was actual solderability problems encountered with parts. The second involved failure of solder joints to meet inspection criteria. The latter condition became apparent as the surface mounting of microelectronic circuit techniques became more prevalent due to the need to increase the density of electronic functions. Surface mounting exposed greater portions of solder joints and made more critical inspection possible. In addition, solder joints had traditionally not been designed for mechanical support. In any case, the solder joints were failing inspection criteria of "95% wetted" or "5% pin holes/voids".

Another condition leading to the study was the failure of microcircuits due to corrosion or stress corrosion during salt fog testing. Such failures are generally at the external lead-to-glass interface.

STUDY PLAN

The study described in this report was accomplished in several stages, as follows:

- Vendor visits and acquisition of samples of lead materials and glass
- Oxide experiments
- Sealing experiments
- Plating and solderability experiments
- Ultrasonic tinning study
- Gold and aluminum bondability study

The study involved actually setting up oxidation and glass sealing equipment and establishing cleaning and plating procedures. Statistical analyses were also performed for all separate tests conducted. Each of the separate tasks is described in the following sections.

SECTION 2

VENDOR SURVEY

As an initial step in the study, a survey of several flat pack/ microcircuit package vendors was made. Three vendors were actually visited. They were:

- A large supplier of flat pack packages in addition to a wide variety of other hermetically sealed glass insulated parts
- A new supplier of microcircuit packages
- A large volume supplier of a wide variety of microcircuit packages (visited by a representative of the GE Technical Services Laboratory)

In addition, other vendors were contacted although not actually visited.

Results of this survey may be summarized as follows:

1. Lead frame suppliers generally order sheet material from single sources to ASTM-F15 or to their own internal requirements with slight variations to ASTM-F15.
2. Lead frame producers perform controlling receiving inspection for items found critical for their processing -- generally dimensions plus other items.
3. Most frame producers perform the decarburizing step. Etching or stamping of sheet material into the lead frame configuration may be performed by an outside vendor, depending on the size of the producer.
4. Frames are oxidized and glass sealing is generally accomplished using procedures and equipment developed in-house. Fixturing is developed to produce the configurations catalogued.

5. De-oxidation and surface preservation are performed in-house by large volume producers, but are frequently subcontracted by smaller volume producers. Final inspection and packaging are performed by the frame producers.

6. Producers have adequate hermeticity testing equipment and are generally able to insure that specified frame package requirements are being met. Some producers do not have the ability or procedures to perform complete in-depth failure analysis, or may not be aware of material variations which are causing part failures or borderline quality from a stable in-house process.

ASTM-F15 materials were acquired from each of the vendors visited. Samples were obtained of the materials at the various stages of their production sequence. However, these samples were found to be inadequate for the study. Samples used were acquired from General Electric stock (identified) and from other sources where identification was known.

No identification of material vendors is given in this report as the study is not considered to be exhaustive and represents only those characteristics observed in those lots sampled. Vendors are referred to simply as Vendors A, B, C, etc.

Subsequent sections of this report detail the steps taken to study materials and process variations.

SECTION 3

EXPERIMENTAL WORK

INTRODUCTION

TEST PROGRAM OVERVIEW

In the electronic industry, high reliability in the operation of sensitive components is often achieved by packaging these components in hermetically sealed containers. A common alloy used for the electrical feedthrough leads and for the container is an iron-nickel-cobalt alloy of the ASTM-F15 type which is oxidized prior to sealing. Sealing is obtained by fusing a glass of a properly matched thermal coefficient to the oxidized surface of the alloy. The degree of hermeticity and the strength of the joint depend upon the chemical and physical properties of the metal/metal oxide/glass interfaces.

The objectives of the experimental portion of this study were to define the materials and the conditions for processing those materials that can cause failures either in the glass-to-metal seals through loss of hermeticity or by breakage of leads, as well as those factors that can cause variations of solderability of lead surfaces. Lead materials for microcircuit packages not only must have the mechanical and physical properties required for electrical leads to make them easy to fabricate and use, but also must have the proper coefficient of expansion and must form desireable oxides that adhere to the metal and combine with the glass to form a seal. These oxides must also be readily removable to present a clean surface for protective plating and an active surface for soldering. The alloys must have predictable performance; i.e., they must behave in a predictable reproducible manner when they are exposed to the temperatures, atmospheres and other environmental conditions during fabrication. Thus, these materials must have not only the correct combination of properties, but also consistency and predictability in behavior.

The intent of the experimental work was not to perform a complete investigation of the behavior of all materials under all conditions. Rather, the purpose was to determine those factors that could influence the predictability and reliability in use. This report presents the data that has been

generated, describes how it was obtained, and points out those factors that appear most important for control. It is hoped that the data can also be used as a basis for further studies in the determination of limits of control required.

PARAMETERS

The processing of sheet material requires a number of functional steps or operations prior to use in the final microcircuit package. Those steps that can be classified as major are shown in Figure 1. Since each of these operations could have an effect upon the reliability of the final package, each operation was investigated to determine the controls required for consistency, hence reliability. It should be recognized, however, that those processes that may be required or good for one flat pack vendor may not be suitable for another vendor primarily because of materials selected or product requirements.

INTERDEPENDENCE OF PHASES

In order to study any process, materials must be carefully selected so that the limits of control can be more accurately defined to yield reliable results. For example, if soft glass is selected for metal sealing at the lead surface, both the degree of decarburization of the metal and its degree of oxidation prior to making the seal may be different than for hard glass. Likewise, in plating, the degree of cleanliness required for good solderability of the lead material after plating may be entirely different for plating with gold than with bright acid tin plating primarily because the tin bath itself can act as an excellent cleaner and surface activator. It is important, therefore, in attempting to describe an optimum process, that the process be defined in terms of both the materials to be used and the desired end results. The interdependence of the various processes also has an important bearing on the care needed and the control limits imposed.

PHASE I - OXIDATION

MATERIALS

Many different vendor materials, all of about the same composition, fall within the ASTM-F15 specification. These vendor materials differ in amounts of residuals, inclusions and methods of manufacture. An earlier survey of 12 different flat packs acquired from eight different vendors revealed that 11 of these flat packs had leads made from ASTM-F15 alloy; the remaining lead alloy was 42 alloy. Thus, the decision was made to investigate the ASTM-F15 materials. To do this, six different lots of material

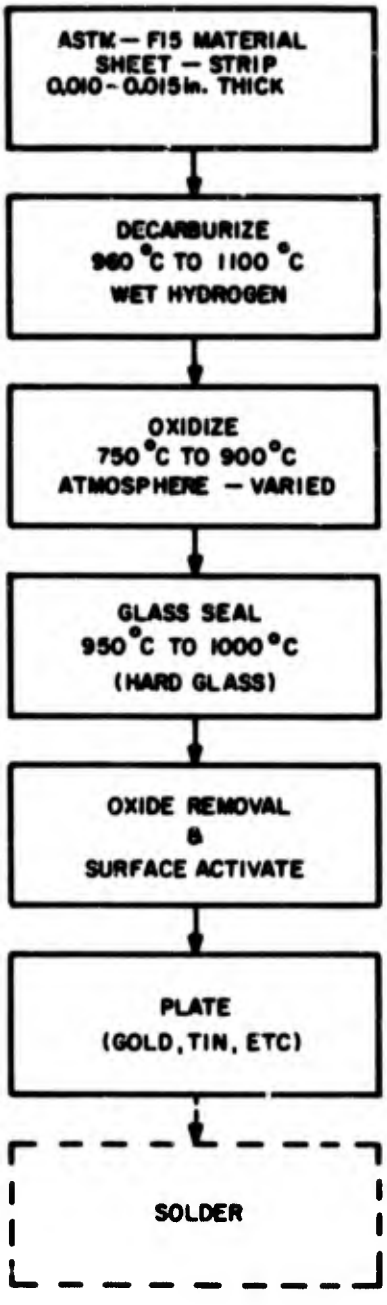

Figure 1. Steps in Preparing ASTM-F15 Material for Use in Flat Pack Leads

(two lots from one vendor) were obtained for the investigation*. Analyses of these materials are shown in Table 1. Analyses of the minor elements were made by emission spectographic techniques; some of the residuals were analyzed by atomic absorption; carbon and sulphur determinations were made on a LECO apparatus. Although not recorded, it should be noted that zirconium was present in all samples in the 0.01 to 0.05% range and 0.005% of beryllium was found in Vendor E material. Analysis of two other alloys, not of the ASTM-F15 type, which were secured for but not used in the investigation, are also included. The ASTM-F15 material specification requirements are shown for comparison.

Thicknesses of the different vendor materials varied from vendor to vendor, depending to some extent on whether the material was ultimately to be punched or etched. The thicknesses of the materials used in the experiment are shown in Table 2. All materials were used in the as-received condition.

TEST METHOD

Sample Preparation

For oxidation studies, samples 1 inch by 1 inch square were sheared from the sheet or strip material. Burrs were removed and the samples were cleaned in accordance with the schedule shown in Table 3, weighed, and immediately placed in the desired oxidizing atmosphere to insure that the surfaces to be oxidized remained clean and free of contaminants. All weighing was done on an Ainsworth analytical chain balance, to the nearest 0.0005 gram. The original samples of the 0.016-inch thick materials weighed approximately 2.0 grams each. For total surface area, the calculations included the edges of the sample as well as the edge in the hole used to suspend the sample during oxidation; however, because the rolled flat surface area is large when compared to the edges, the oxidation recorded is primarily that occurring on this surface. In order to insure uniform oxidation on all surfaces, samples were suspended from a 1/16th inch diameter quartz rod through an appropriate size hole drilled in the sample. The sample holder with the sample was placed in the constant temperature zone of a tube furnace.

---

*Five lots of material were obtained through the courtesy of the Bendix Corporation, Sidney, New York.

TABLE 1. ANALYSIS OF ASTM-F15 MATERIALS

Material (Vendor Lot)	Composition (Percent Weight) Ni	Co	Cr	Mn	Si	Cu	Al	Mg	Mo	Ti	C	S	Fe
A-1	30.58	17.52	0.012	0.454	0.050	0.020	0.00087	0.000063	0.016	-	0.018	0.010	Remainder
A-2			Nil	0.386	0.057	0.025	-	0.00012	-	-	0.018	0.010	
B-1	29.98	17.10	0.032	0.23	0.095	0.023	0.0022	0.00008	0.14	0.013	0.009	-	
B-2			0.052	0.27	0.065	0.017	0.0022	0.000065		0.02	0.015	0.005	
C-1	30.69	17.17	0.28	0.32	0.095	0.0092	-	0.00062	-	0.04	0.028	0.003	
D-1	30.04	17.05	0.012	0.408	0.095	0.01	0.0004	0.00011	-	-	0.009	0.012	
D-2			0.015	0.386	0.077	0.008	0.0004	0.00016	-	-	0.009	0.005	
E-1	31.52	14.9	Nil	0.05	Nil	0.01	Nil	Nil	Nil	Nil	0.01	0.01	
ASTM-F15 Specification Requirements	29.0	17.0	-	0.05	0.20	-	0.10	0.10	-	0.10	0.06	-	
Other Alloys Analyzed (for comparison only)													
Alloy 42		Nil	-	0.318	0.27	0.0077	0.0022				0.009	0.009	
Alloy 426		Nil	Nil	0.182	-	0.020	0.0004			-	0.044	0.005	Remainder

Note: - indicates not determined.

TABLE 2. SAMPLE MATERIAL THICKNESSES

Sample Material Vendor	Material Thickness (inches)
A	0.016
B	0.016
C	0.005
D	0.015
E	0.011

TABLE 3. PROCEDURE USED TO CLEAN SAMPLES FOR OXIDATION

Step	Cleaning Agent	Temperature	Time (Minutes)
1. Degrease	Trichloroethelene		
2. Alkaline Clean	Proprietary Solution	82°C (180° F)	5
3. Rinse	Running Tap Water	Room Temperature	2
4. Oxide Removal	Proprietary Solution	175°C (345° F)	2
5. Rinse	Isopropyl Alcohol	Room Temperature	1
6. Dry	Forced Cleaned Air		

Test Setup

The tube furnace contained three separate heating elements, each separately controlled. With proper adjustment, a five-inch constant temperature zone (±2°C) could be obtained for the temperatures and the gas flow rates desired. Both the temperature and the humidity were constantly monitored during oxidation. The dew point was measured using a Manufacturing Engineering and Equipment Corporation Electronic Water Analyzer which recorded the moisture content in parts per million of H_2O; this value was then converted to dew point. To obtain the oxidizing atmosphere, cleaned air flowing at a rate of 20 cubic feet per hour through both Dry Rite and Silica Gel driers yielded a constant dew point of -71°F (-57°C). This flow was sufficient to change the air in the furnace at a rate of approximately 20 times per hour. Opening the gas exit end of the furnace under these conditions and for the time required for sample insertion, showed no recorded change in either the temperature or the amount of moisture at the sample location. These are the conditions under which most of the samples were oxidized.

Figure 2 is a photograph showing the three zone tube furnace and control. Also shown are the water analyzer (left of photo) and the air drying tubes (right of photo). Both the thermocouple and the moisture monitor tube for temperature and humidity control were placed adjacent to the samples, near the center of the tube.

Surface Cleaning

As mentioned previously, all of the work on oxidation was done on the ASTM-F15 (Fe - 29% Ni - 17% Co) type alloy. Prior to measuring the rates of oxidation, the appearance and the adherence of the oxide with respect to prior surface treatments were investigated to determine consistency of performance. Samples from Vendor A material were selected and prepared by the following treatments:

a. Degrease only

b. Degrease and alkaline clean

c. Degrease, alkaline clean plus Kovar brightener (a mixture of acetic, nitric and hydrochloric acids)

d. Degrease, alkaline clean and treat in a proprietary solution

e. Degrease, alkaline clean and sand blast (50 μm grit)

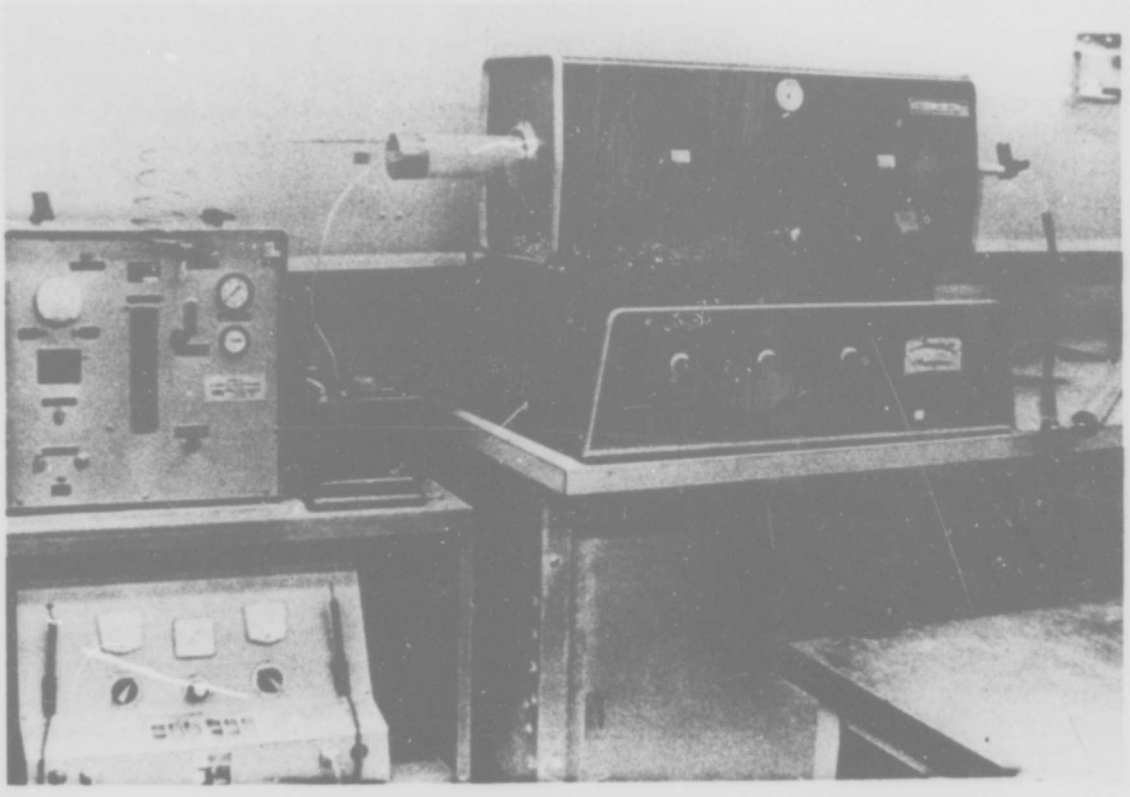

Figure 2. Tube Furnace Used for Oxidation

Samples treated by each of these methods were then exposed to temperatures of 750, 800, 850 and 900°C for times of 5, 10, 20 and 40 minutes. They were then examined visually with respect to appearance of oxide formed (dull matte black, shiny black, dull grey, etc.) and were rated for oxide adherence by bending the sample around a steel pin having a diameter of three times the thickness of the material. It was concluded that there were significant differences in both appearance and adherence, both with differences in time and temperatures of oxidation. The materials treated in the proprietary solution prior to oxidation gave the most consistent results. Except for surface roughness experiments which are described next, all samples for oxidation and glass sealing were prepared by this technique.

RESULTS

Effect of Surface Roughness

Having established the chemical cleaning treatment that gave the most consistent results, the possible surface roughness of the material as received or treated prior to oxidation for glass sealing was investigated for influence on the rate and adherence of the oxide. Since surface roughness is difficult to measure, except on a crude scale, roughness is defined here only by the techniques used to produce the surface condition. Samples of Vendor A material prepared by the previously described cleaning techniques yielded four different surface conditions and different oxidation rates as shown in Figure 3. The samples which had been degreased and those which had been both degreased and alkaline cleaned were of about the same in roughness since little or no attack by the alkali occurred. These samples showed about the same rate of oxidation. However, the etched and 50 micron blasted materials revealed increased oxidation at first, but then seemed to oxidize at the same rate after the initial stage. The curves drawn in Figure 3 have been smoothed and differ slightly from those in Figure 7; however, these differences appear to be explained by the differences in the roughening and oxidizing conditions in the two sets of data. Although the rates of oxidation show increased oxidation in the beginning stage, the rates of oxidation after a given time period (after obtaining a given thickness of oxide layer) appear uniform, thus indicating that the rate is diffusion controlled.

Experimental data of adherence of oxide obtained by oxidizing Vendor A material with two different surface finish conditions (as described under Surface Cleaning) at different temperatures and times is shown in Figure 4. For these data, all samples were oxidized in an atmosphere of about 40% relative humidity and evaluated by noting the degree of adherence after bending the specimen around a mandrel having a diameter of three times the thickness of the sheet. It is readily apparent that adherence is dependent

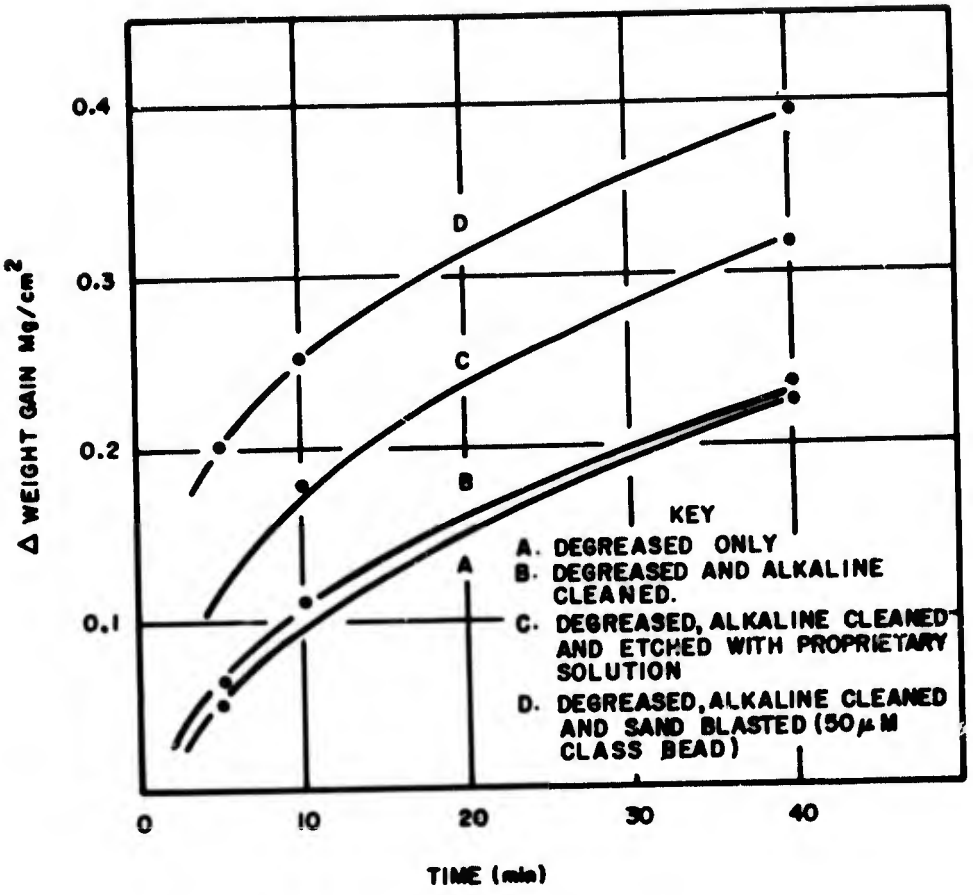

Figure 3. Effect of Surface Roughness (750° C, Still Air, Vendor A Material)

not only upon temperatures and time, but also upon the surface condition of the metal exposed. Although only limited experimental work was performed in this phase of the investigation, results do appear consistent within the sets of data and with diffusion of species or voids involved. It should be noted that although consistently adherent scales were produced by the degreased and alkaline cleaned specimens at 750° C for the shorter time (5 minutes), a small amount of descaling was observed on these samples and those which had been degreased only, for relatively higher temperatures and longer times. Since scaling is a surface reaction and, as observed above, consistency in adherence increases with an increase in degree of surface attack (except for the 50 micron grit blast), one obviously concludes that the surface is being conditioned in a way that is more conducive to the

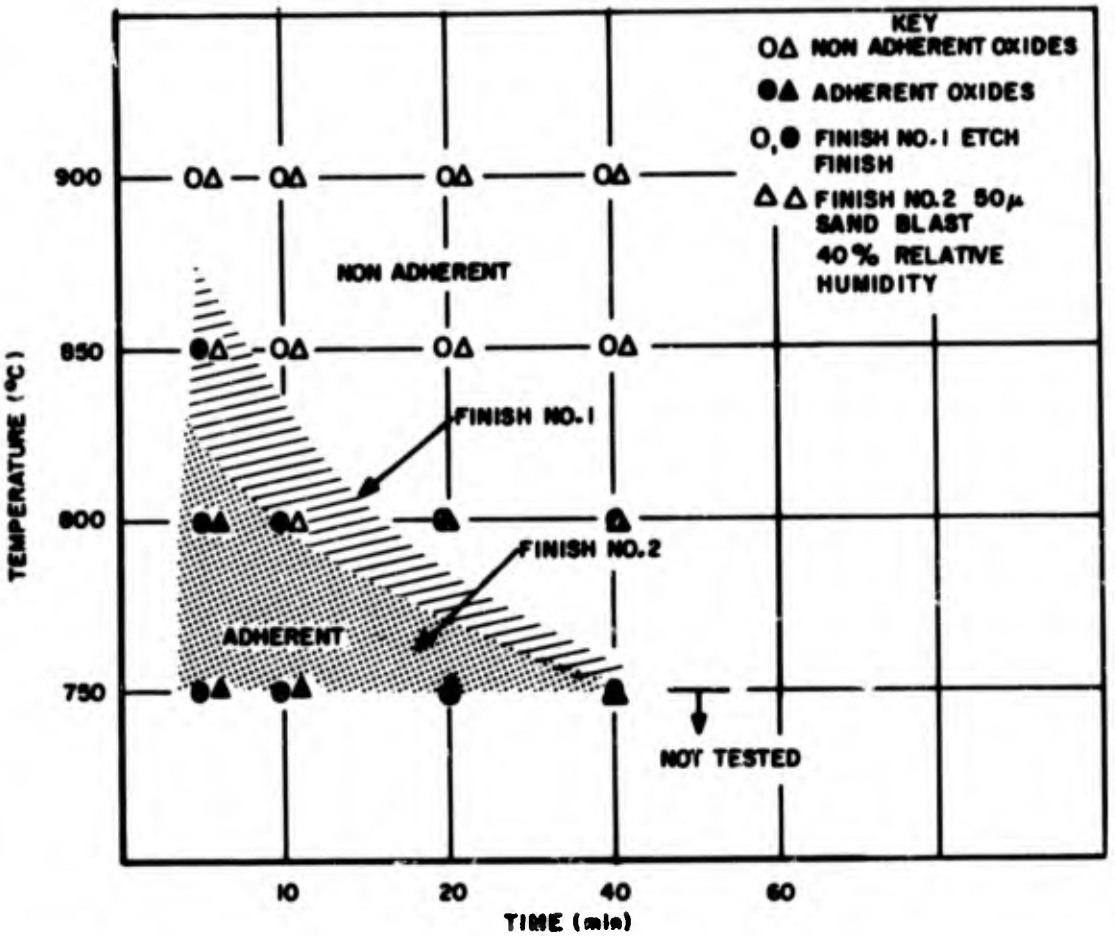

Figure 4. Effect of Time, Temperature and Surface Condition on Oxide Adherence (Vendor A Material, 40% Relative Humidity)

formation of FeO. Also, since the rate of oxidation is more rapid with the rough or coarse surface finishes than polished surfaces, one would expect a more rapid formation of the higher oxides. This perhaps is what is occurring with the 50 micron grit blasted surface and why a decrease in adherence is observed. It would appear, therefore, that there may be two opposing factors: (1) a conditioning of the surface by the removal of impurities, by cold work, or because of some other factor that favors the formation of FeO, and (2) if the conditioning roughens the surface, a decrease in factors favorable to FeO formation due to the higher rates of formation of Fe_3O_4 and Fe_2O_3. These results appear consistent with the findings of Carter[1] that hydrogen annealing was conducive to FeO formation.

[1]Carter, T.J., Wulf, G.L., and Wallwork, G.R., "Oxidation of Iron-1% Nickel Alloys", Corrosion Science, V9, N7, July 1969, pp.471-478.

Abendroth[2] on the other hand found FeO only on samples treated in a wet argon gas at 800 to 850°C; his samples were prepared by polishing with metallographic 4/0 paper.

Effect of Atmospheric Moisture

Because of its effect on processes such as the heat treatment of metals, the relationship of the dew point of the atmosphere in contact with the metal at heat treating temperatures upon reactions at the metal surface is common in the literature. Most of the information, however, pertains either to the oxidation of pure metals or to alloys of high tonnage production. Curves relating to the oxidation of iron, for example, showing the types of oxides formed at different dew points and temperatures, have been published in texts and references on heat treating practices.

A careful distinction must be made between the phenomena involved during the first stages of oxidation and those that apply after a certain film thickness has been reached. This difference is often a source of confusion to those who are not familiar with the different processes involved during thickening of oxide film. Wagner's theory of parabolic oxidation, which covers the later stages of growth, is a diffusion controlled process. The basic postulate of Wagner's theory is to the effect that the rate determining factor in oxidation is the diffusion of ions in the oxide lattice; the oxide lattice is known to contain defects and concentration gradients down which the ions can migrate.

It now appears that the consensus of opinion of various writers is that the adherence of the oxide film is related to the number of vacancy sites in the lattice; the number of sites increases with increases in the self-diffusion rate of iron and hence, with temperature. One of the early postulates was that adherence was obtained when the oxide grew outward, hence the metal ion diffused through the oxide scale to combine with oxygen on the outside surface. Under these conditions, a layer of FeO would most likely exist adjacent to the base metal.

Several oxide layers can be present on a metal whenever conditions are suitable for the metal to form stable compounds with the gas. The compound with the higher metal content will be nearest the metal surface. The relative thickness of the separate layers will depend mainly upon the diffusion rates through the layers and on the differences of chemical potentials

---

[2] Abendroth, R.P., "Oxide Formation and Adherence on an Iron-Cobalt-Nickel Glass Sealing Alloy," Materials Research and Standards, September 1965, pp 459-466.

at the interfaces. The relative rules of growth of the different layers, the mechanisms by which they grow, their volume relationships and their ranges of stability have to be taken into consideration. For example, it has been shown that FeO, which is unstable below 1060°F (571°C) in the bulk phase can be detected down to 750°F (399°C) when present as a thin film on iron.

Curves have been developed showing the equilibrium of Fe, FeO, and Fe_3O_4 on pure iron in atmospheres of different ratios of H_2O and H_2 with respect to temperature. These curves are shown in Figure 5. Curves with different values for the amount of moisture would be expected for changes in conditions such as for an H_2O-air atmosphere or for a base metal with nickel and cobalt present. In experiments using a pure binary iron - one percent nickel alloy, Carter et al[1] oxidized these alloys in dry oxygen and in a mixture of dry oxygen and nitrogen atmospheres after different pretreatments. Scales formed at 800°C were found to be predominantly nonadherent and were composed of the higher oxides Fe_3O_4 and Fe_2O_3 except where prior hydrogen annealing pretreatments were used. In the latter cases significant quantities of wüstite (FeO) were present in the adhering scale.

Rates of oxidation of metals generally increase with an increase in moisture content of the oxidizing atmosphere. How moisture might affect the rate of oxidation of this alloy was determined by measuring the rate of oxidation of the alloy for three different dew points. The curves obtained are shown in Figure 6. With atmospheres highly enriched with water vapor, the rate of oxidation of this alloy appears to remain relatively constant but the rate of oxidation decreases nonlinearly with a decrease in dew point. Adherent oxides were produced more readily with the lower dew point and spalling of the oxide would occur (also partly depending upon other factors) if the dew point accidentally or intentionally was increased. Because of the relative sensitivity of adherence to the dew point, the life of the driers at measured flow rates was determined and driers were rejuvenated much prior to depletion, even though the system was continually monitored.

Effect of Temperature

With the establishment of cleaning, surface finishing, and humidity controls for obtaining relatively reliable adherent oxides, the customary weight gain versus time curves were obtained for Vendor A material for different temperatures. These curves are shown in Figure 7. Each point on the curve represents an average of the weight gain for a minimum of at least three samples at the temperature and time involved. All samples were cleaned, immediately inserted into the hot zone of the furnace and then cooled in the same atmosphere before exposure to the ambient atmosphere. Ideally one would like to heat the sample in a vacuum or inert atmosphere, weigh the sample, subject it to the atmosphere desired and record the

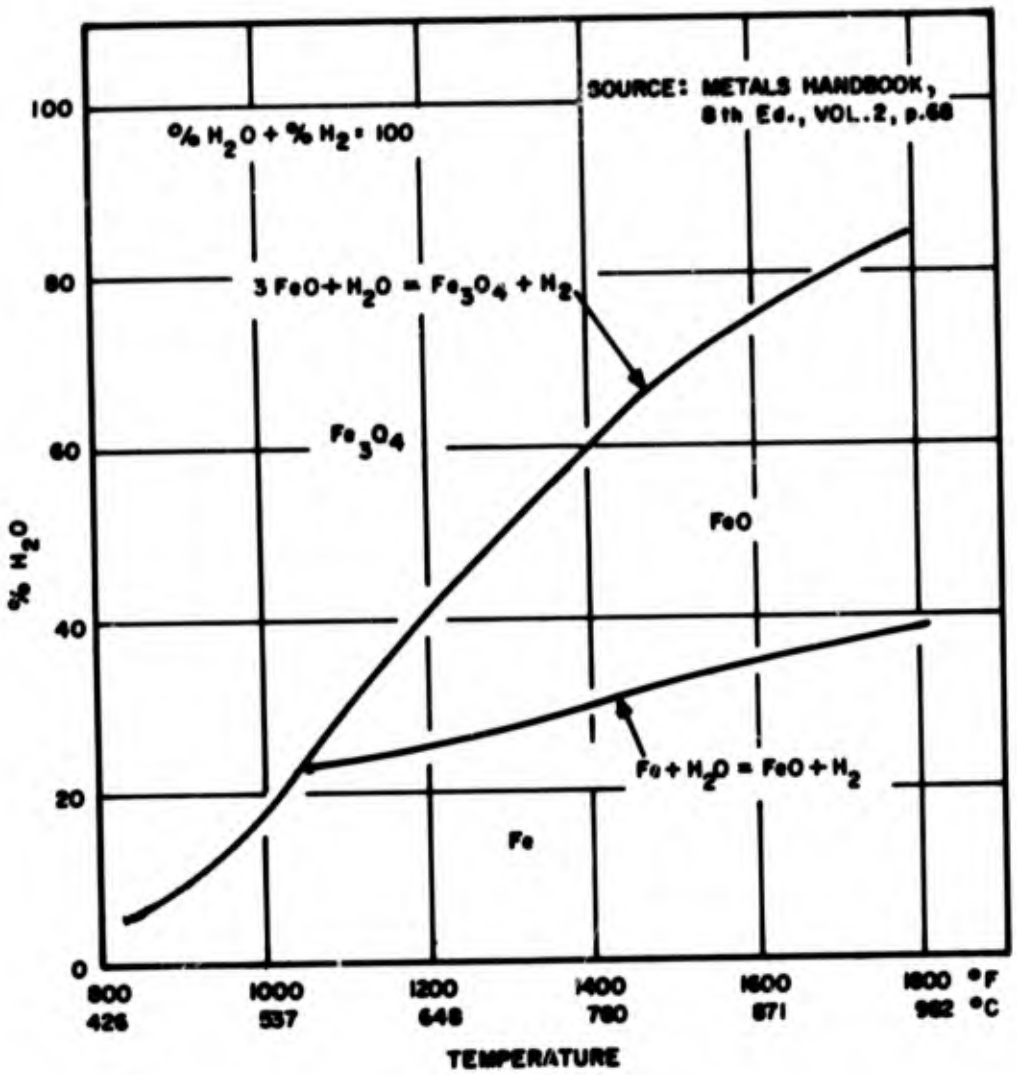

Figure 5. Effect of Ratio of H_2O and H_2 with Respect to Temperature

continuous weight gain during exposure. However, equipment to accomplish this was not available; thus the equipment shown in Figure 2 was used. Since the weight gain curves were obtained primarily to predetermine temperatures and time required for attaining given thicknesses or weights of oxides on samples for glass sealing experiments, no further analyses of these rates were made. The curves do show, however, the characteristic parabolic shape, especially at the higher temperatures; at the lower temperature the curve is almost exponential.

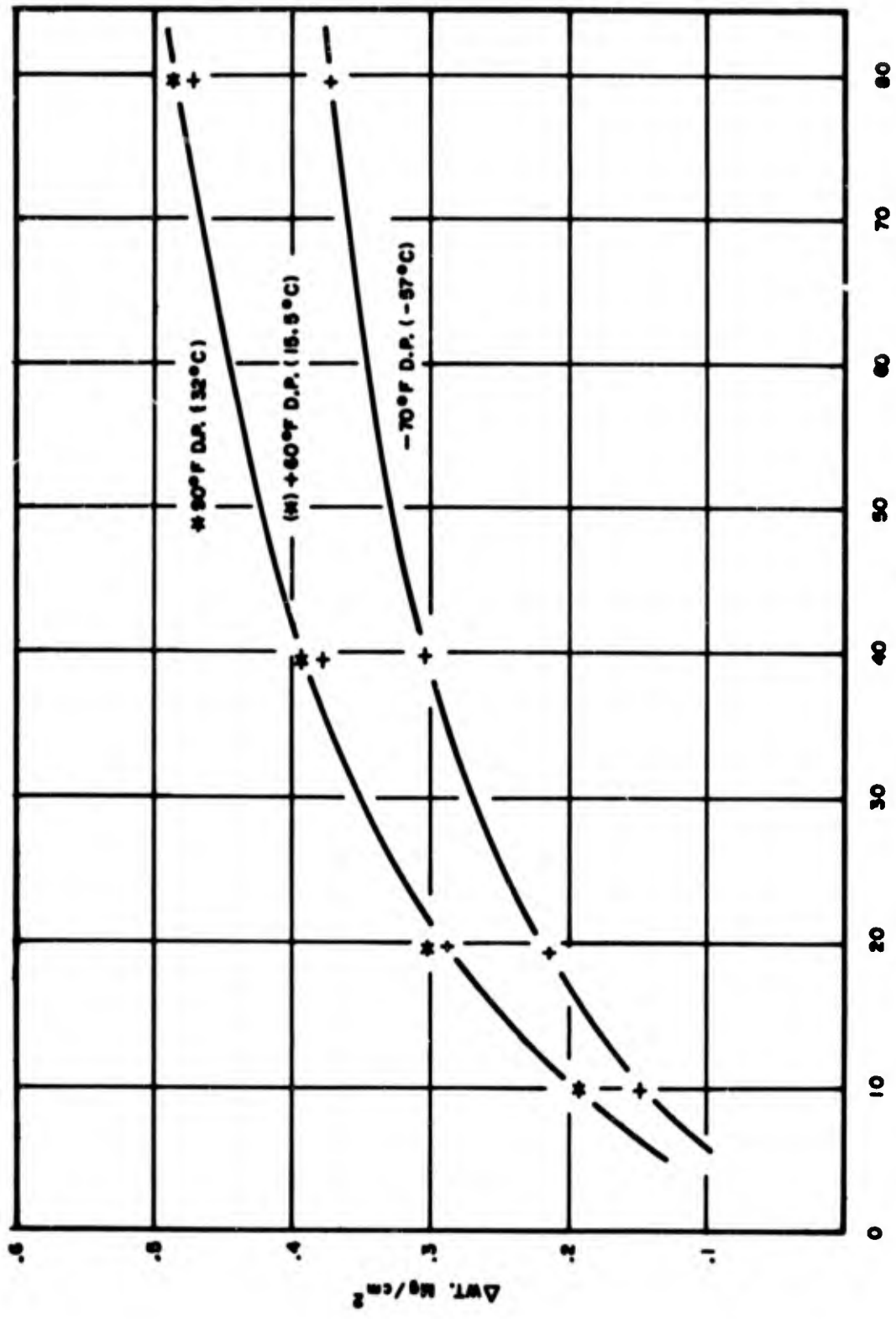

Figure 6. Effect of Atmosphere (Vendor A Material, 750° C, 1380° F)

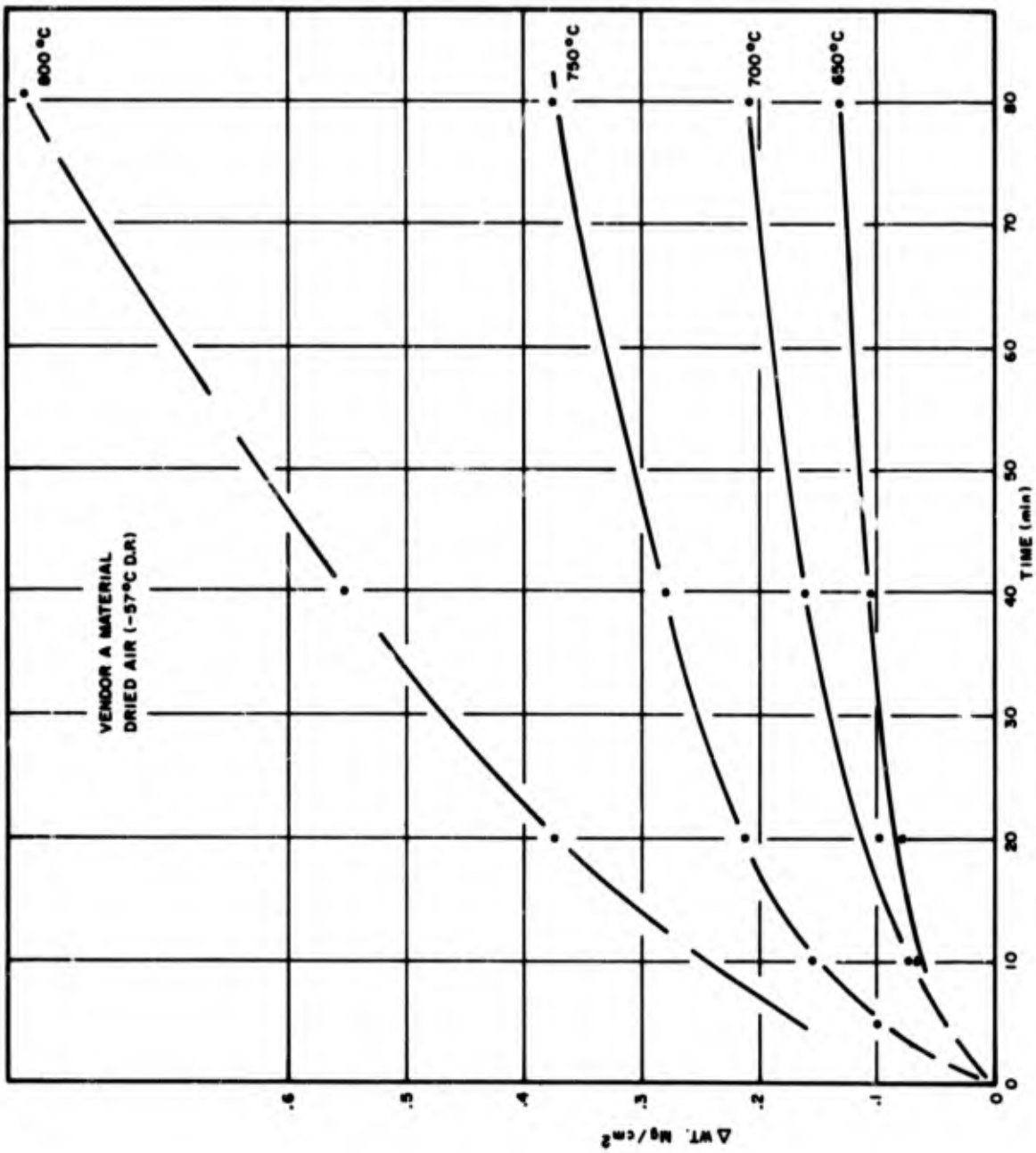

Figure 7. Weight Gain versus Time for Vendor A Material

In order to help understand the nature of the oxidation process, cross sections of oxidized samples were prepared for microscopic examination. Because the oxides were relatively thin, the samples were sliced at an angle of approximately 15 degrees to the flat surface. This procedure gives better detail of the metal-oxide interface and amplifies the oxide thickness. However, since the angle is acute, the thicknesses shown cannot be compared one to another because a slight change of angle will indicate a change in apparent thickness. The nature of the oxide formed on Vendor A material in both low and relatively high humidities at three different temperatures and two different times, is shown in Figures 8 and 9. Remembering that the thickness of the oxide should be discounted because of the acute angle of the section, it can be observed that at the lowest temperature (650°C) the oxide appears to be almost a single phase structure, and that at the more elevated temperatures a filigree develops and becomes increasingly prominent the higher the temperature. Lengthening the time of oxidation also appears to thicken this structure slightly. It seems reasonable to conclude from these observations that this structure develops from a different type of oxide formation at the grain boundaries. Because the oxidation product of the grain boundaries extends beyond the normal surface of the oxide, it would appear that some element(s) is diffusing toward the boundary and is oxidizing at a rate greater than that of the bulk material.

Scanning Electron Microscope photographs of the metal-oxide-air interfaces are shown in Figure 10. Nickel and cobalt element scans, shown on these same photographs, indicate that only a relatively small quantity of nickel, compared to the original alloy, is present in the oxide layer; cobalt, although very low in the grain boundary oxide, is present in the bulk material to about the same extent as in the original alloy. Additional SEM scans of this grain boundary oxide show this material to be primarily iron oxide, and presumably it is one of the higher oxides of iron. Photographs of an x-ray fluorescence exposure of this same area, Figure 11, confirm the general distribution of nickel, cobalt and iron; both cobalt and iron are widely distributed through both the metal and oxide, whereas the metal-oxide boundary is quite distinct for nickel. Additional analyses on the types of oxides formed, the distribution of the types of oxides and the elements in these oxides with variations of temperature, time and atmospheric conditions should be both interesting and fruitful especially if the results are related to efficiencies in the making of glass seals.

Use of Different Vendor Alloys

As stated previously, alloys of different trade names, all falling within the chemical specifications of ASTM-F15, are made and sold on the market

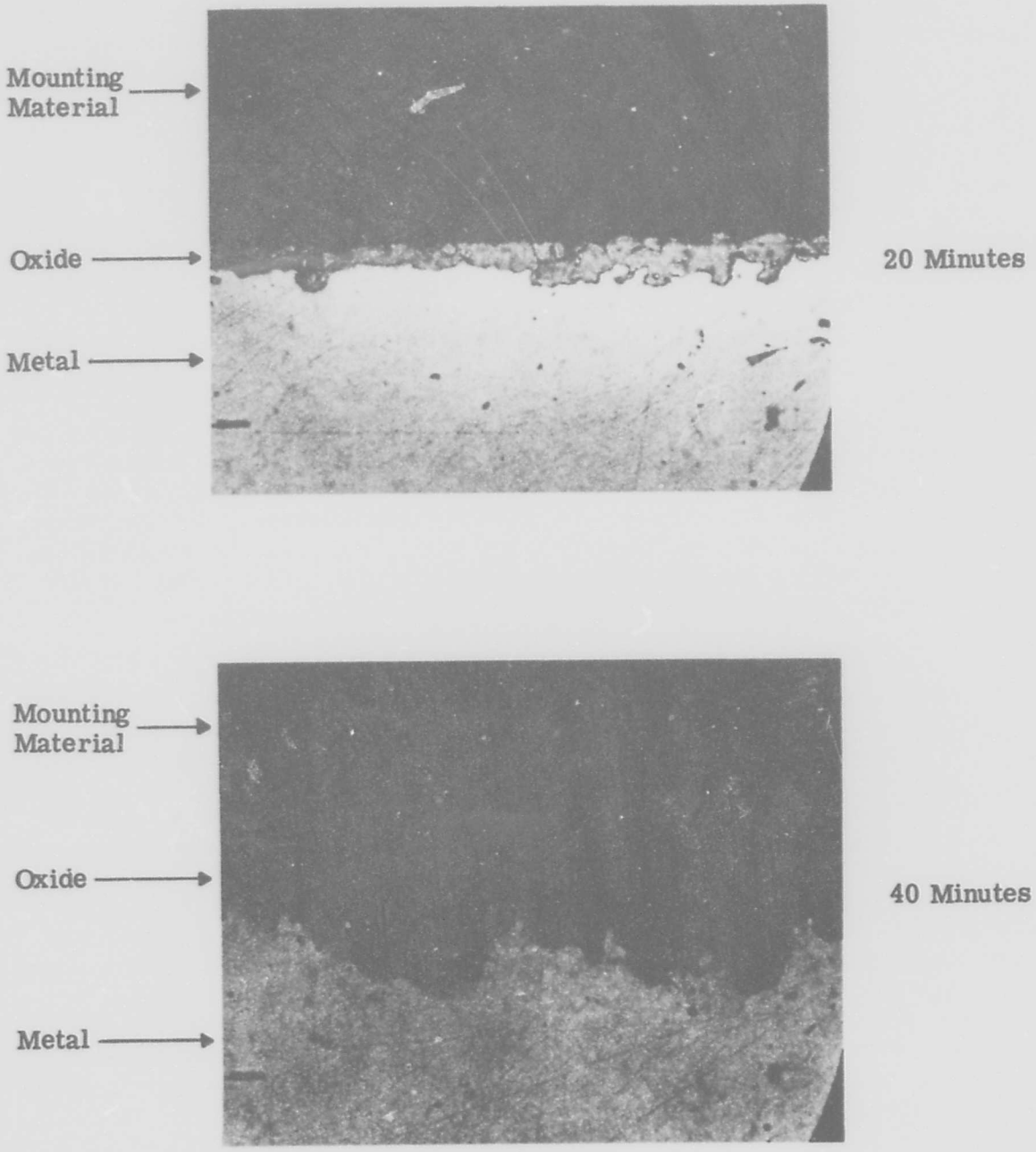

Figure 8. Vendor A Material Oxidized at Three Different Temperatures (20 CFH Dried Air, -56°C Dew Point, Mag. 350X) (Sheet 1 of 3 Sheets)

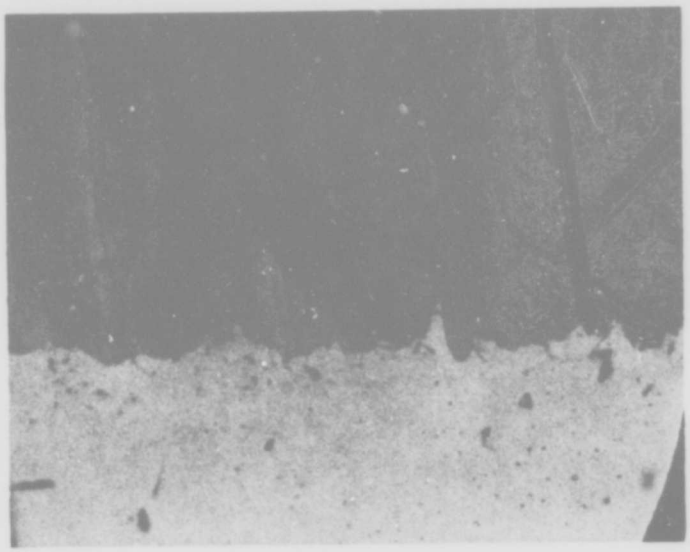

20 Minutes

40 Minutes

700°C

Figure 8. Vendor A Material Oxidized at Three Different Temperatures (20 CFH Dried Air, -56°C Dew Point, Mag. 350X) (Sheet 2 of 3 Sheets)

20 Minutes

40 Minutes

750°C

Figure 8. Vendor A Material Oxidized at Three Different Temperatures (20 CFH Dried Air, -56°C Dew Point, Mag. 350X) (Sheet 3 of 3 Sheets)

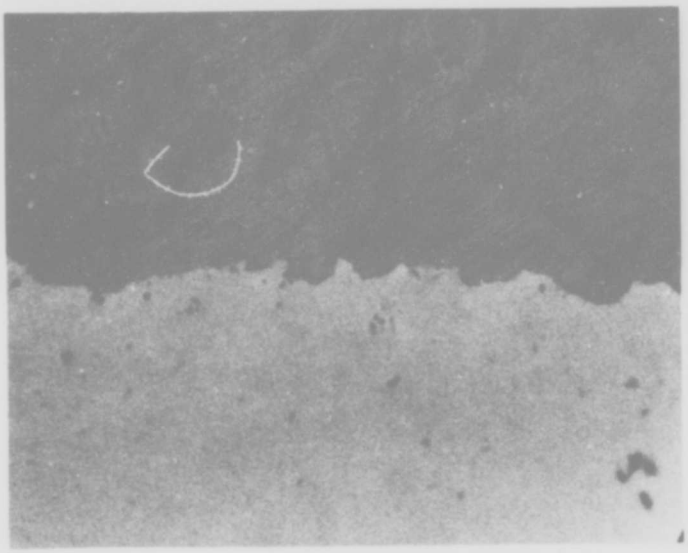

20 Minutes

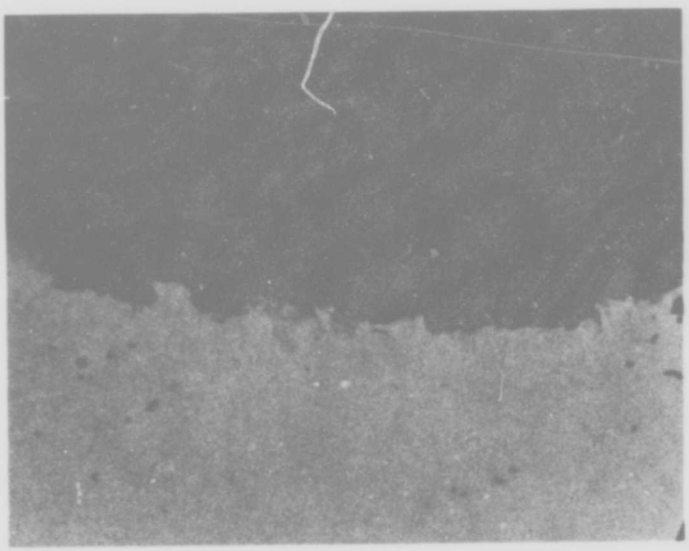

40 Minutes

650°C

Figure 9. Vendor A Material Oxidized at Three Different Temperatures
(Still Air, +15°C Dew Point, Mag. 350X)
(Sheet 1 of 3 Sheets)

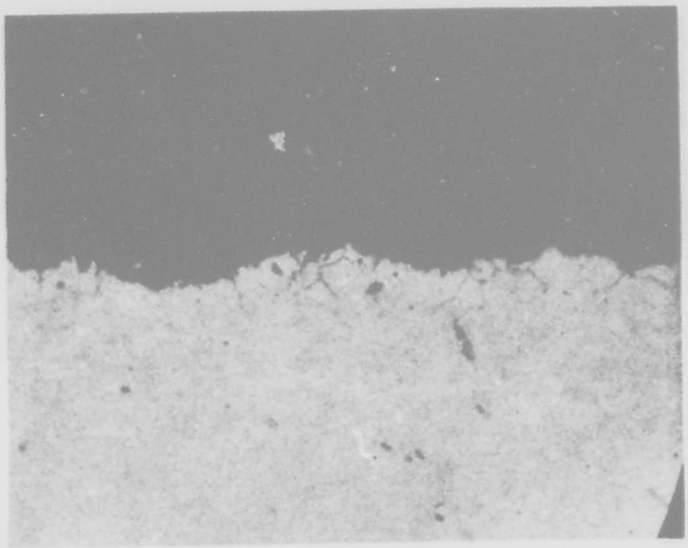

20 Minutes

40 Minutes

750°C

Figure 9. Vendor A Material Oxidized at Three Different Temperatures
(Still Air, +15°C Dew Point, Mag. 350X)
(Sheet 2 of 3 Sheets)

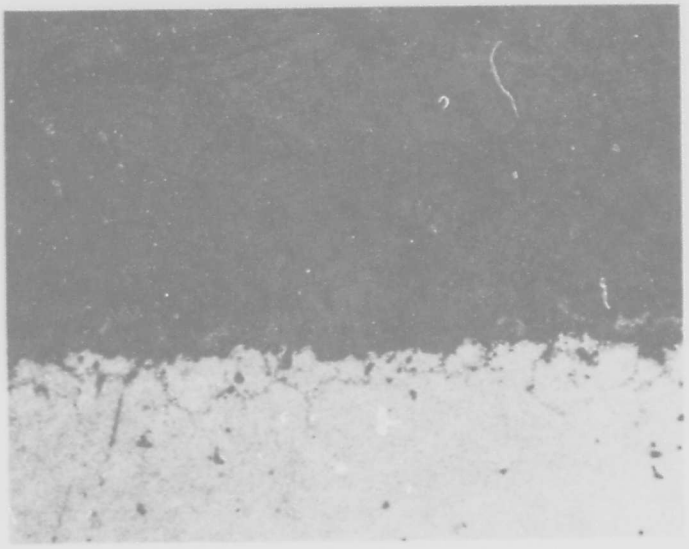

20 Minutes

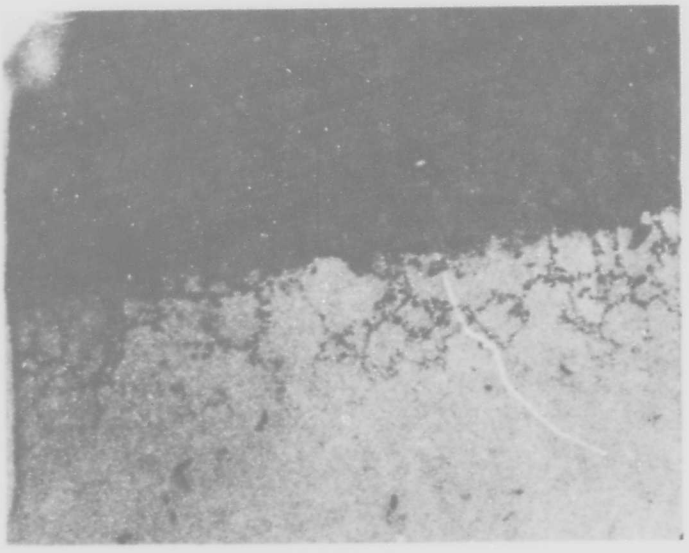

40 Minutes

800°C

Figure 9. Vendor A Material Oxidized at Three Different Temperatures (Still Air, +15°C Dew Point, Mag. 350X) (Sheet 3 of 3 Sheets)

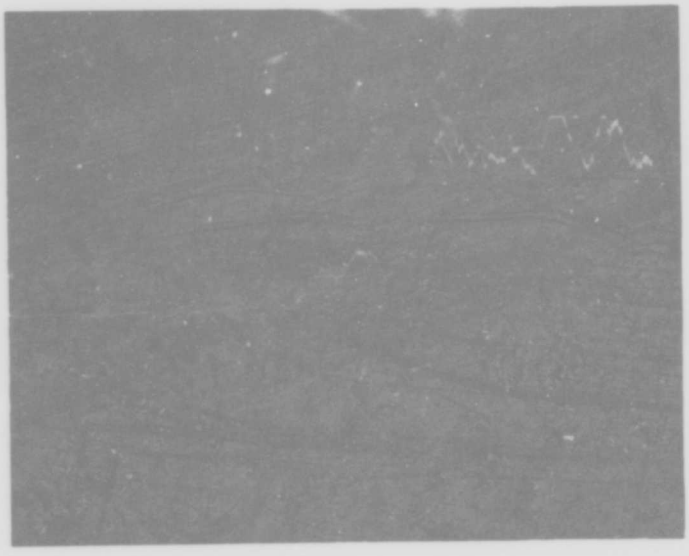

Nickel Scan

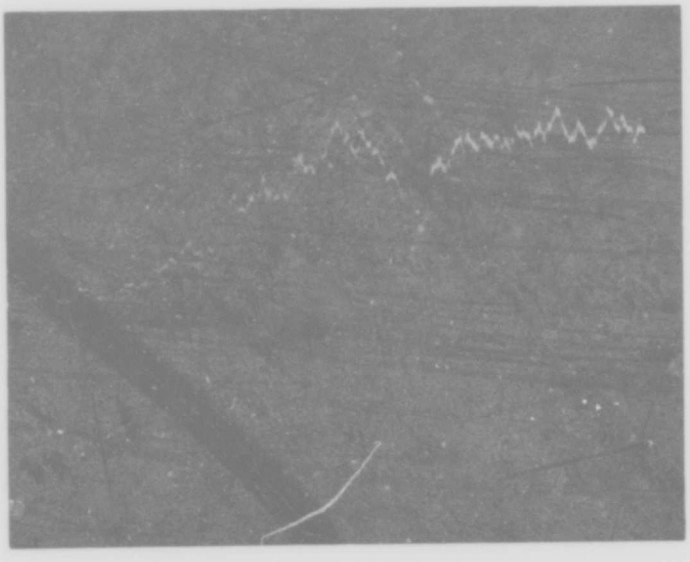

Analysis Line

Scan Line

Cobalt Scan

Figure 10. Scanning Electron Microscope Photographs of Vendor A Material Oxidized at 750°C for 40 Minutes in Still Air (Mag. 1000X)

Original Material

Nickel Element Map

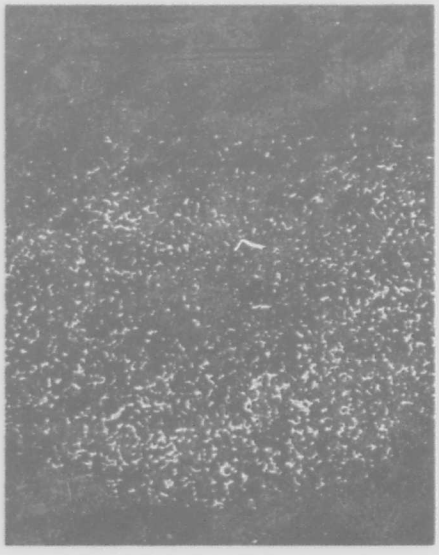

Cobalt Element Map

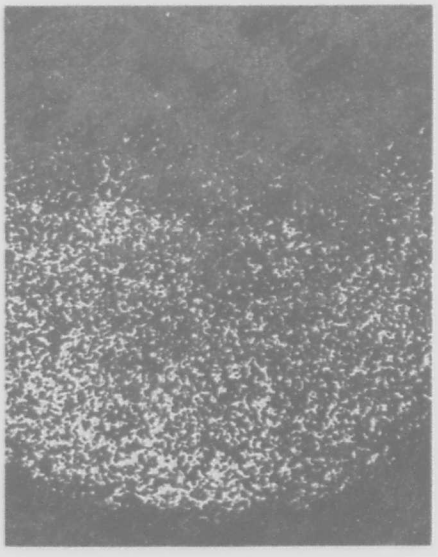

Iron Element Map

Figure 11. X-Ray Fluorescence of Vendor A Material Oxidized at 750°C, 40 Minutes, Still Air (Mag. 1000X)

for glass-to-metal seals. Five different vendor alloys and two lots of material from one vendor were oxidized at 750°C at a dew point of -70.6° F (-57° C) for times up to 80 minutes. The data obtained are shown in the form of curves in Figure 12. It is at once obvious that a flat pack vendor oxidizing Vendor A material under constant conditions for optimum glass sealing results could conceivably experience difficulties if Vendor E material were received even though they both were purchased to the same specification. As shown in the curves, the material from Vendor E oxidizes at a much more rapid rate and could have 50 to 100% more oxide on the surface than a Vendor A material for a given set of oxidizing conditions. Although one would not expect a perfect duplication of curves from lot to lot from a single vendor, the two lots of material from Vendor B indicate that better control of the manufacture of this material is desirable. All points shown in Figure 12 are an average of a minimum of weight gains for three samples; the variations of weight of different samples for the same datum point were relatively small.

Similar to the studies previously reported on the effect of temperature, photomicrographs were taken of cross sections of oxidized samples; these sections also were cut at acute angles to the major oxidized surface. The photographs, shown in Figures 13 and 14, reveal significant amounts of grain boundary oxides in those vendor alloys showing the more rapid rate of oxidation. This comparison of oxidation of grain boundary versus grain material probably can better be seen in Figure 15, where the surface of the oxide layer is photographed rather than in cross section. These photographs exhibit the relative amount of the two different types of oxides formed. Although the grain boundary oxidation appears to be more rapid in those alloys showing the greater rates, thus producing thicker boundaries, the greater difference apparently is in the number of grain boundaries present. Hence, grain size would seem to play a prominent role in rate studies.

Since all of these alloys were oxidized in the as-received state, except for the slight etch used to clean the surface prior to oxidation, and previous experiments had shown that the roughness of the surface did affect the rate of oxidation, samples of the slowest and most rapidly oxidizing alloys were abraded in a similar manner and oxidized. A comparison of oxidation curves of these two alloys in the abraded and unabraded condition is shown in Figure 16. Although these results do not clarify whether roughness of surface, grain size, or some other factor is responsible for increased oxidation rates of Vendor E material, the data appears to show that the material having the lower rate of oxidation is much more sensitive to surface roughness conditions (abrasion).

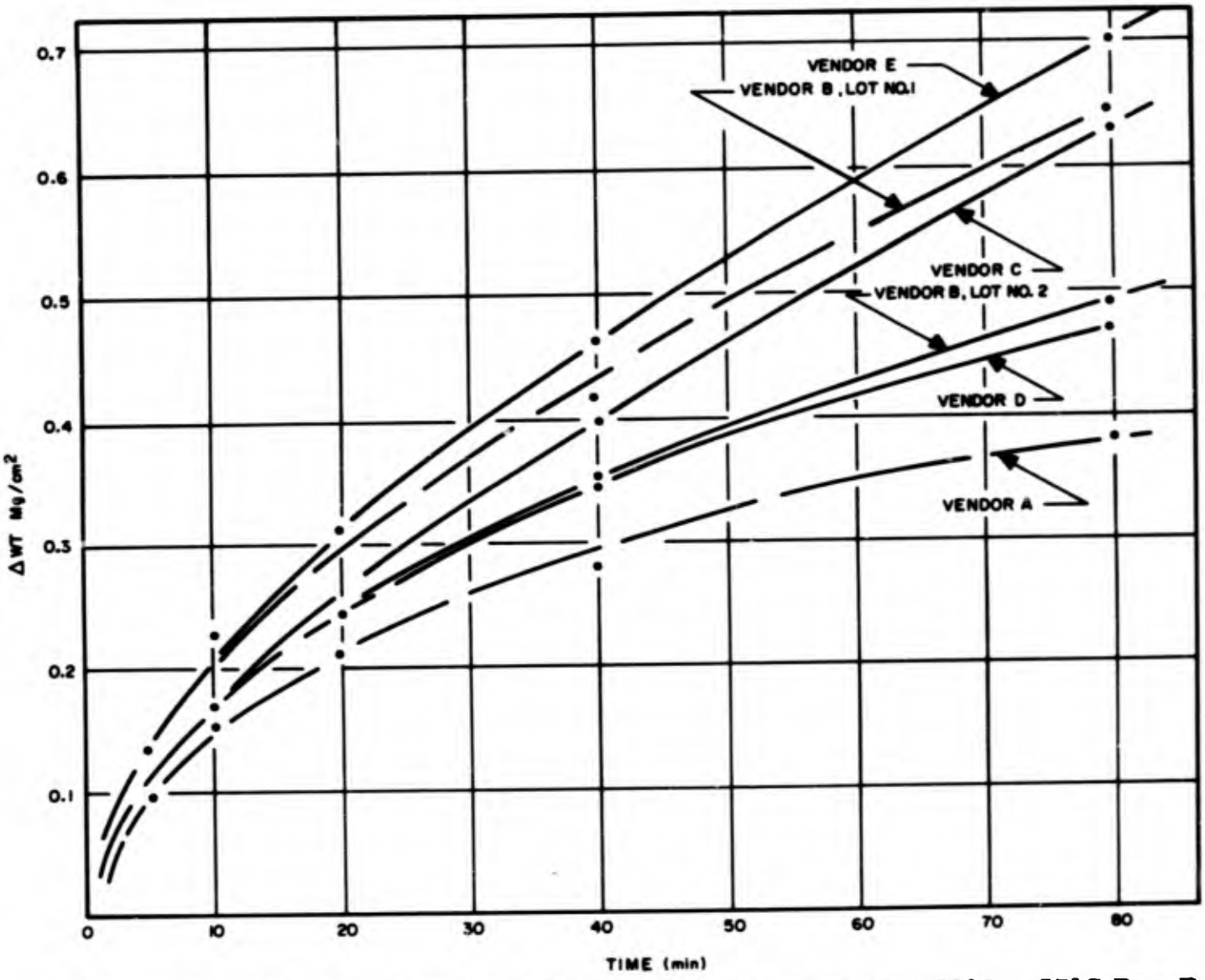

Figure 12. Oxide Growth with Time for Different Vendor Materials at 750°C, -57°C Dew Point

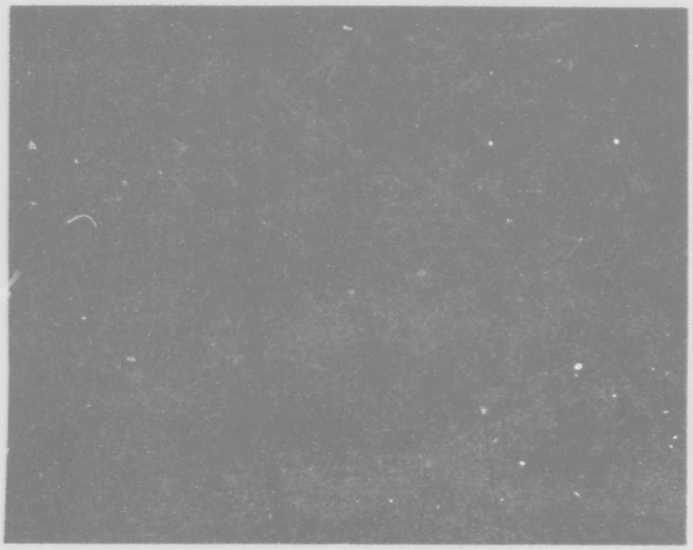

40 Minutes

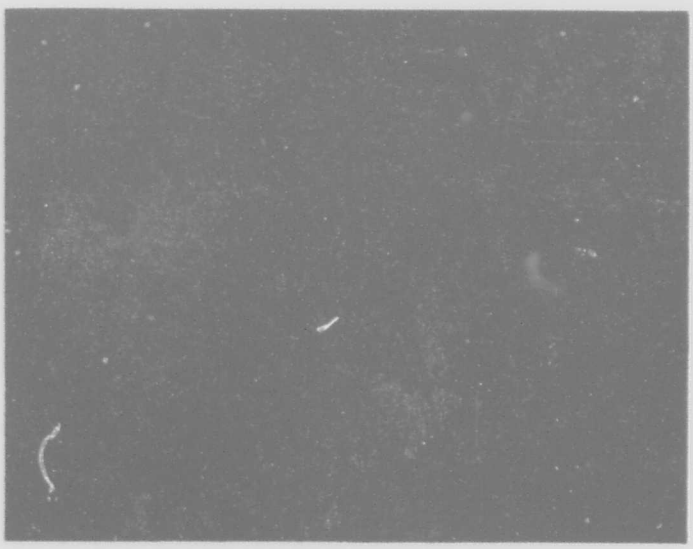

80 Minutes

Figure 13. Cross Section of Vendor B Material Oxidized at 750°C, 20 CFH Dried Air, -56°C Dew Point (Mag. 350X)

40 Minutes
Mag. 350X

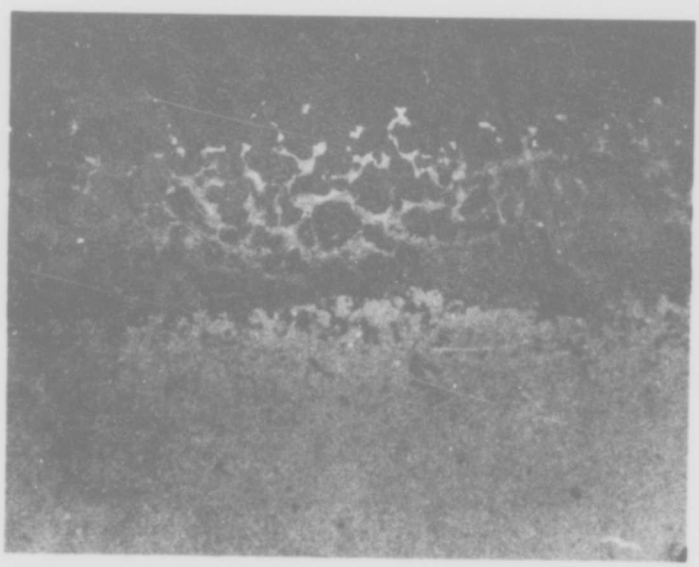

80 Minutes
Mag. 150X

Figure 14. Cross Section of Vendor D Material Oxidized at 750°C, 20 CFH Dried Air, -56°C Dew Point

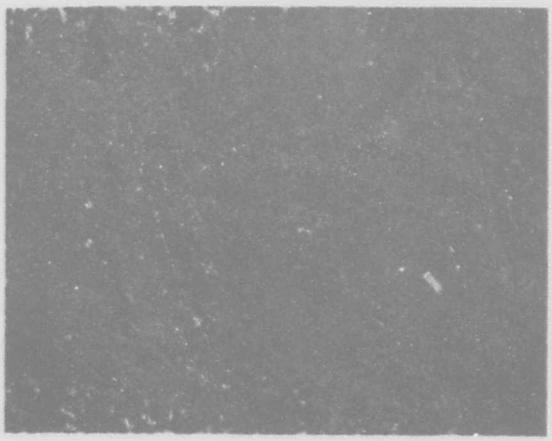

Vendor A Material

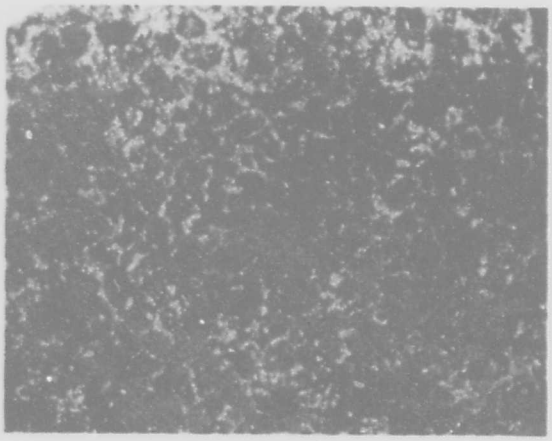

Vendor B Lot #1 Material

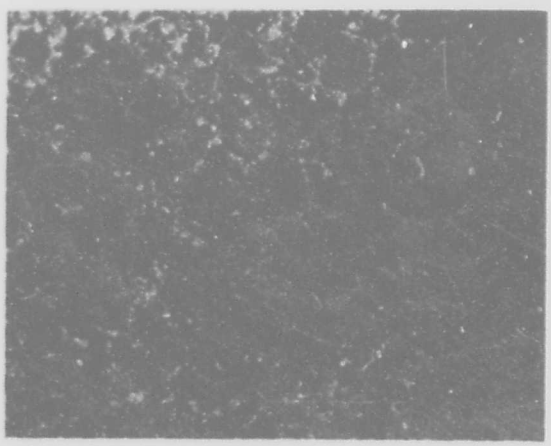

Vendor D Material

Figure 15. Surface of Three Different Vendor Materials Oxidized at 750°C for 80 Minutes, 20 CFH Dried Air, -56°C Dew Point, Mag. 350X

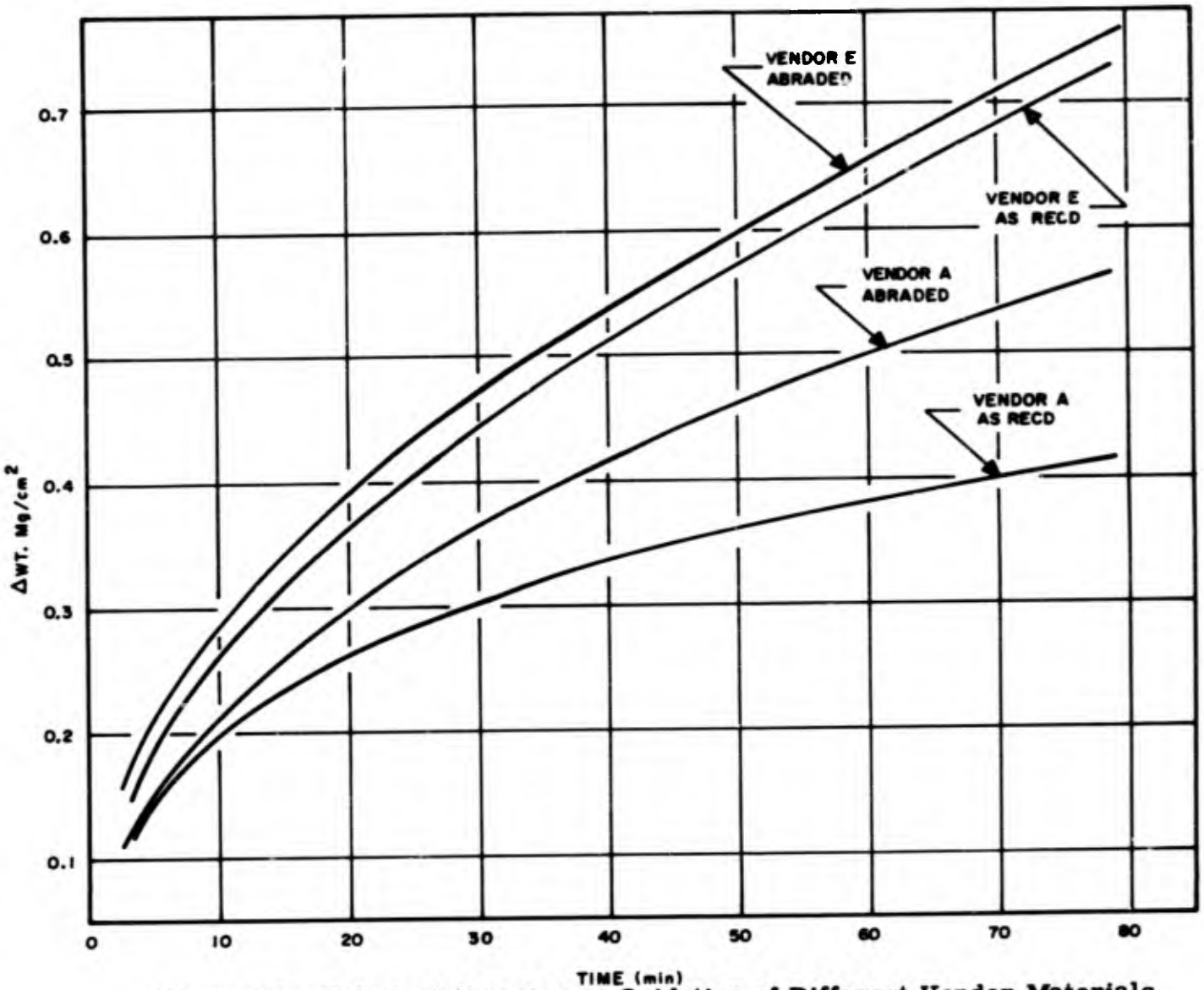

Figure 16. Effect of Abrasion on Oxidation of Different Vendor Materials

Grain Size and Grain Growth

Decarburization of the ASTM-F15 alloy prior to oxidation is an established procedure in a number of quality flat pack vendor houses. Because decarburization is carried out at a temperature much in excess of that of oxidation, samples of different vendor alloys were sealed in vacuum and heated to decarburizing temperatures to determine what changes in structures might occur. Since no decarburization or other chemical changes should take place, this treatment should indicate the effect of temperature alone on microstructure. Alloys of three vendors, A, B and E, were chosen; these alloys were heated to 1000, 1050, and 1100°C for 1/2, 1 and 2 hours. Samples were examined for grain growth both on the surface of the sample and in cross sections. No differences in the microstructures could be observed between the surface and either the cross section or sections taken at the midplane of the sample (see Figure 17), hence, all grain size measurements were taken on the surface of the sheet; this surface presented the larger number of grains for better averaging. The grain sizes obtained are shown in Table 4. Grain size appearance for the temperatures, times and each of the vendor alloys studied is shown in Figures 18, 19 and 20.

Figure 21 is a photograph of the surface of Vendor A material, showing the widely scattered off orientation grains. These grains are identified by the darker than usual grain boundaries and are believed to be those grains that grow at the expense of the surrounding matrix. The three photographs in Figures 22, 23 and 24 show the large grains of Vendor A material, the mixed grain size of Vendor B material and the relatively small size grains of material from Vendor E. That the large grains outlined are single grains is confirmed by the large twin bands extending to the boundaries. Upon close observation, one can see outlines of the smaller grains of the original material.

One can observe from Table 4 that, although some discrepancies exist in the grain size values (because of the limited number of measurements taken), Vendor A material shows visible growth with each increment of increased temperature and time for all values. Vendor B material exhibits little growth below 1050°C or at times below one hour, but does show a mixed growth at times and temperatures exceeding these values. Vendor E material exhibits little growth under any of the conditions imposed.

The differences observed in the high temperature growth of grains in these materials can be the result of any one or a combination of several conditions. Quite frequently when abnormal grain growth is observed, as in the case of aluminum oxides for control of grain size in iron and the inhibiting effect of iron-manganese sulphides in silicon ferrites, impurities play a prominent role in the stabilization of grain boundaries. An inspection of the

TABLE 4. GRAIN GROWTH OF VENDORS A, B AND E MATERIALS

Temperature (° C)	Material: Vendor A Average Grain Size (mm)	%	Vendor B Average Grain Size (mm)	%	Vendor E Average Grain Size (mm)	%
			1/2 Hour			
As Received	0.0183		0.0166	75	0.0306	50
			0.0037	25	0.0096	50
1000	0.0363	40	0.0215	50	0.0352	30
	0.0166	60	0.0096	50	0.0135	70
1050	0.0616	80	0.0200	50	0.0223	60
	0.0235	20	0.0100	50	0.0120	40
1100	0.0304	85	0.0169	65	0.0402	70
	0.0106	15	0.0077	35	0.0129	30
			1 Hour			
1000	0.0304	40	0.0215	40	0.0370	20
	0.0136	60	0.0067	60	0.0192	80
1050	0.0898	70	-		0.0276	70
	0.0295	30	-		0.0118	30
1100	0.0545	85	0.0616	60	0.0261	75
	0.0169	15	0.0124	40	0.0113	25
			2 Hours			
1000	0.0769	80	0.0215	30	0.0334	15
	0.0203	20	0.0083	70	0.0159	85
1050	0.1312	75	0.0542	60	0.0252	55
	0.0503	25	0.0183	40	0.0135	45
1100	0.0909	85	0.0660	75	0.0320	75
	0.0276	15	0.0186	25	0.0113	25

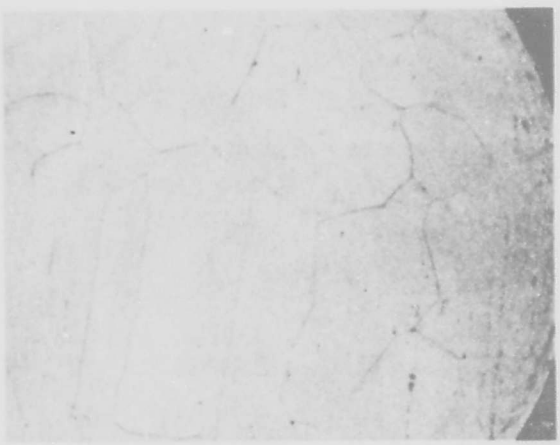

Vendor A Material, Below Surface of Sheet, Mag. 375X

Vendor A Material, Cross Section, Mag. 190X

Vendor B Material, Below Surface of Sheet, Mag. 375X

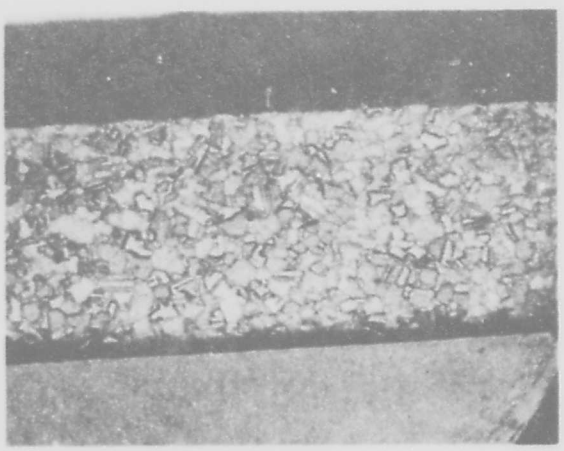

Vendor E Material, Cross Section, Mag. 190X

Figure 17. Alloys of Different Vendors Heated to Decarburizing Temperature (1100°C) for Two Hours

As Received

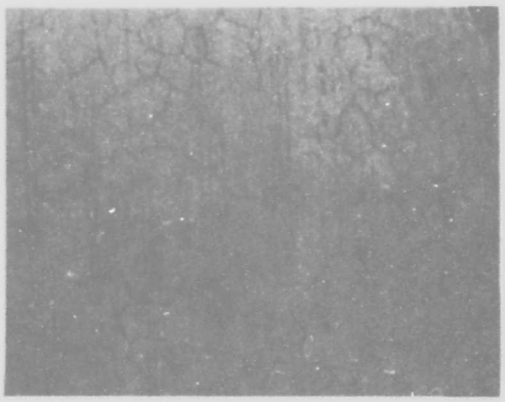

1000°C, 30 Minutes

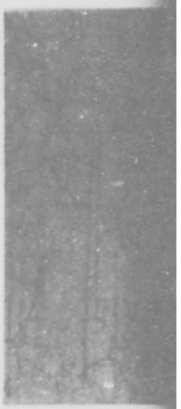

1050

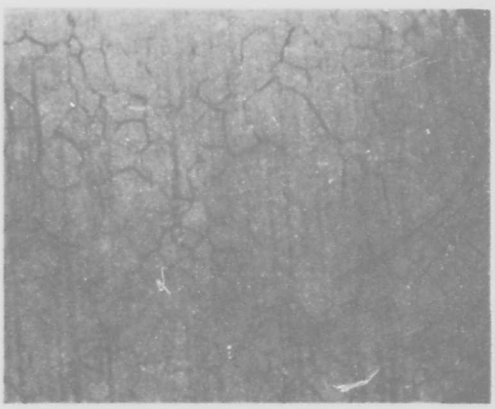

1000°C, 1 Hour

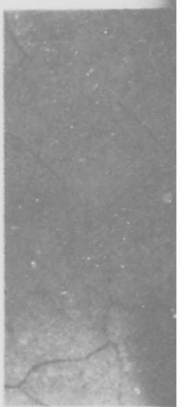

10

NOTE

MAGNIFICATION: 375X

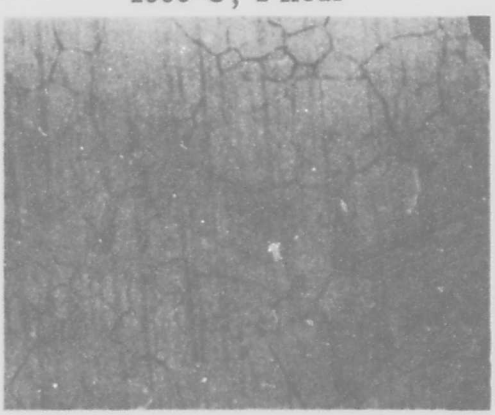

1000°C, 2 Hours

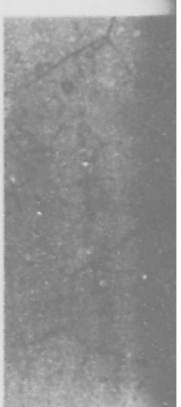

10

Figure

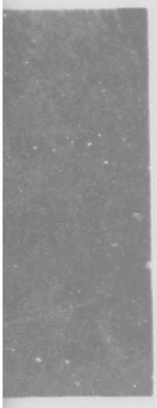

es

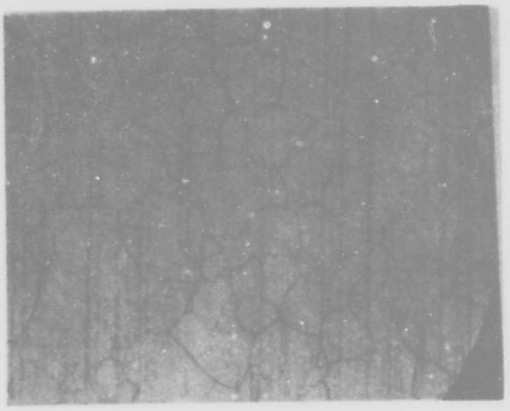

1050°C, 30 Minutes

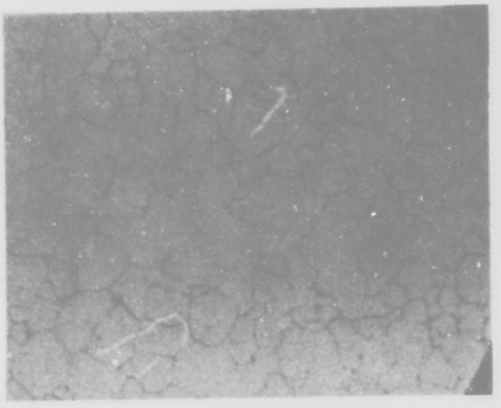

1100°C, 30 Minutes

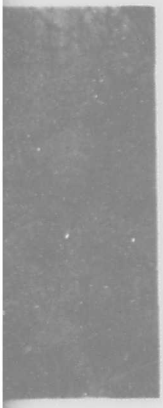

r

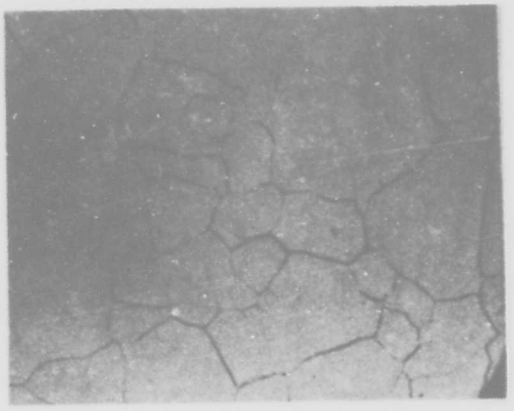

1050° C, 1 Hour

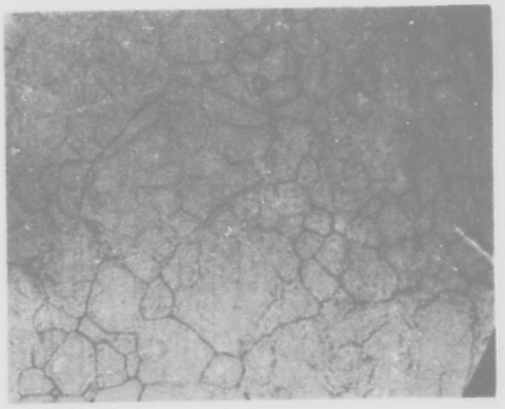

1100°C, 1 Hour

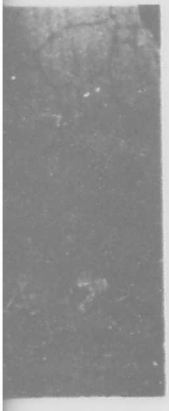

rs

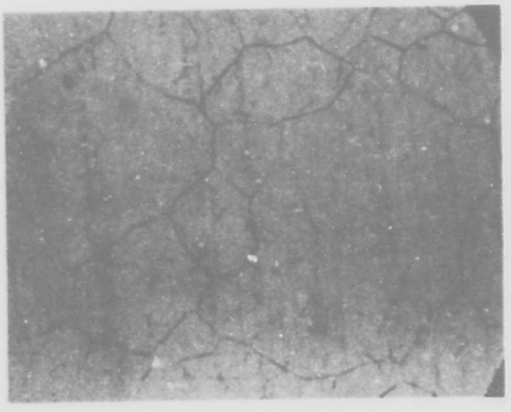

1050°C, 2 Hours

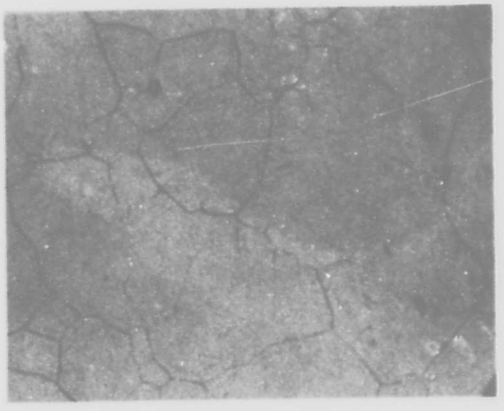

1100°C, 2 Hours

Figure 18. Grain Growth with Temperature and Time (Vendor A Material)

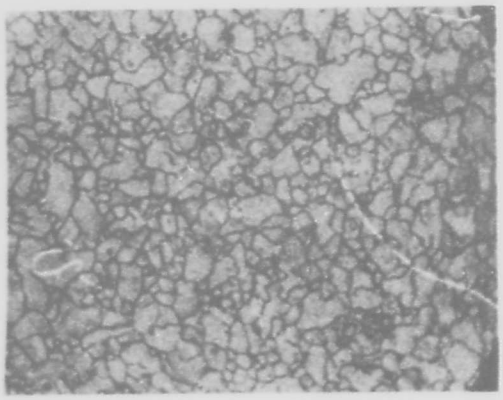

As Received

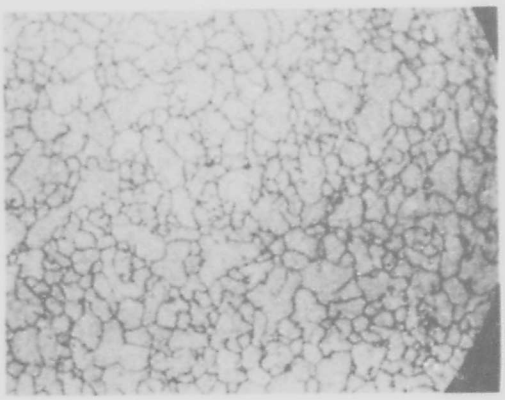

1000°C, 30 Minutes

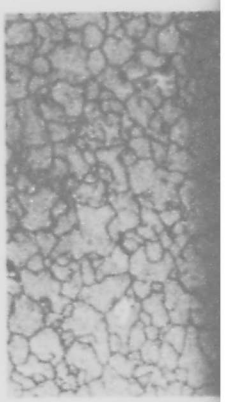

1050°C

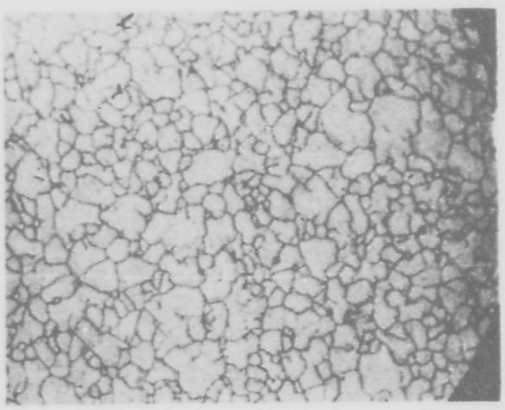

1000°C, 1 Hour

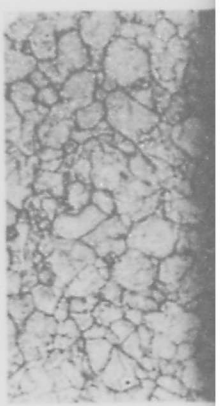

1050°

NOTE

MAGNIFICATION: 375X

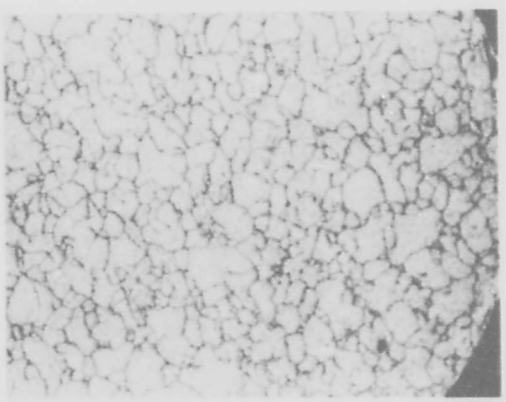

1000°C, 2 Hours

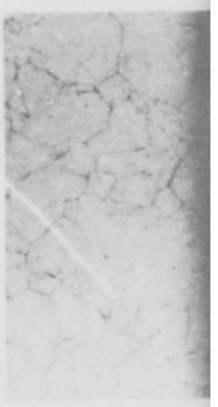

1050

Figure 1

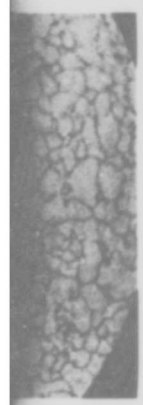

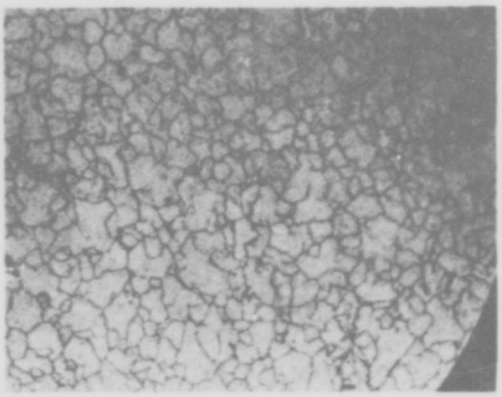

1050°C, 30 Minutes

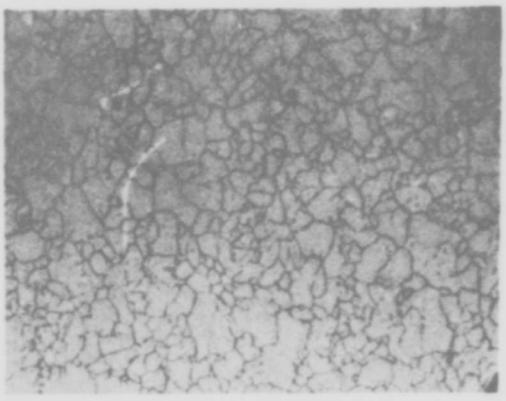

1100°C, 30 Minutes

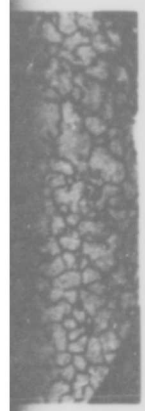

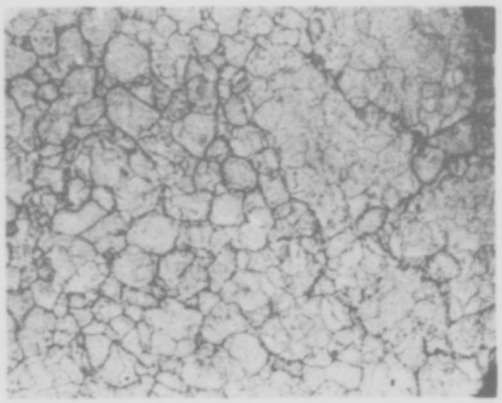

1050° C, 1 Hour

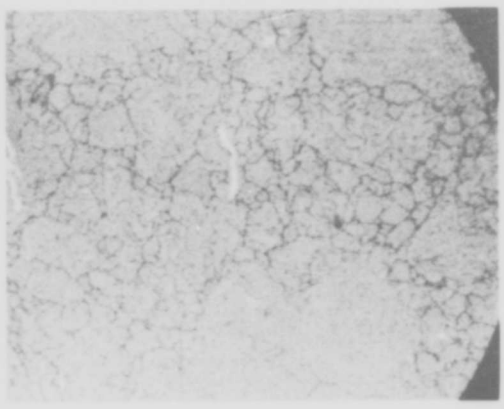

1100°C, 1 Hour

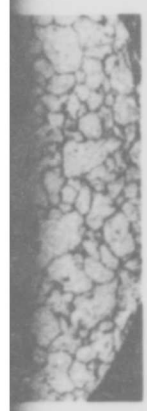

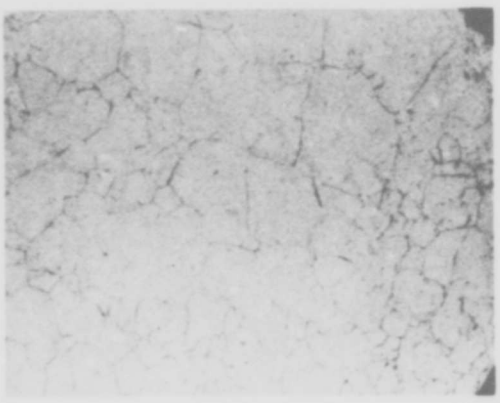

1050°C, 2 Hours

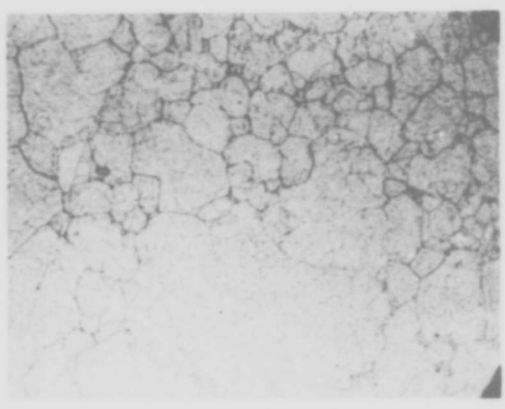

1100°C, 2 Hours

Figure 19. Grain Growth with Temperature and Time (Vendor B Material)

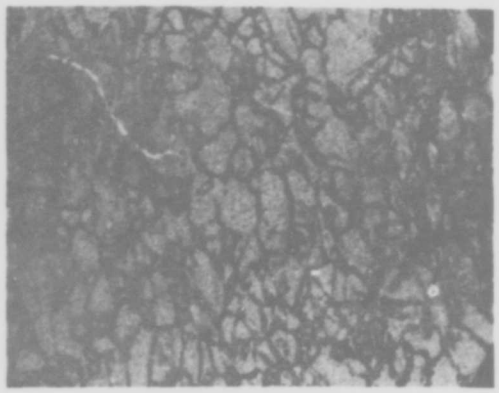

As Received

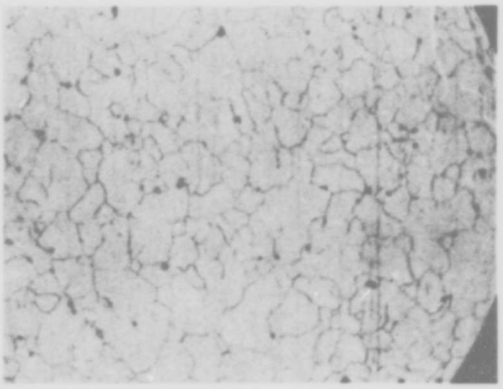

1000°C, 30 Minutes

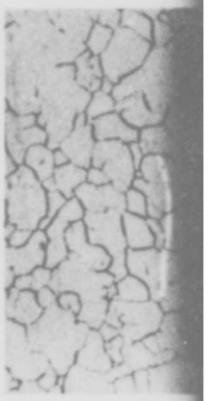

1050°

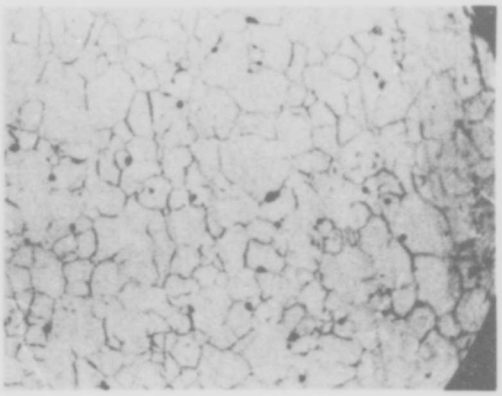

1000°C, 1 Hour

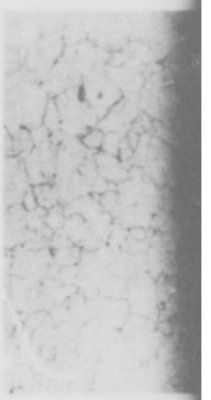

105

NOTE

MAGNIFICATION: 375X

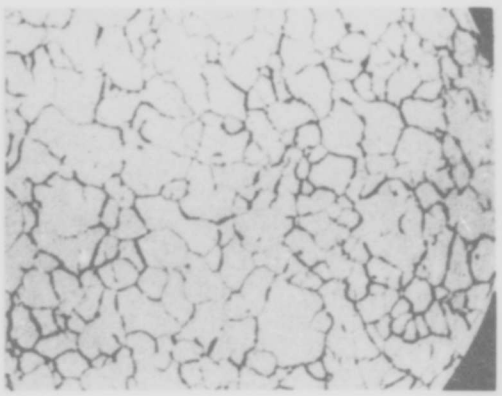

1000°C, 2 Hours

105

Figure 2

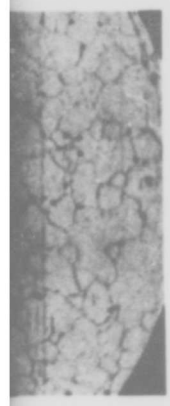

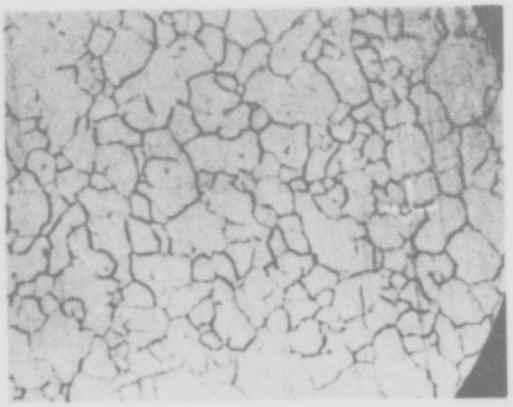

1050°C, 30 Minutes

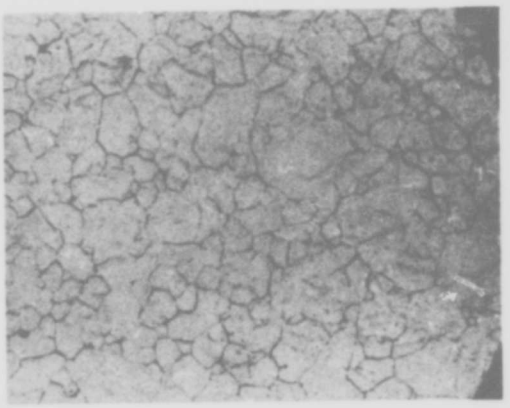

1100°C, 30 Minutes

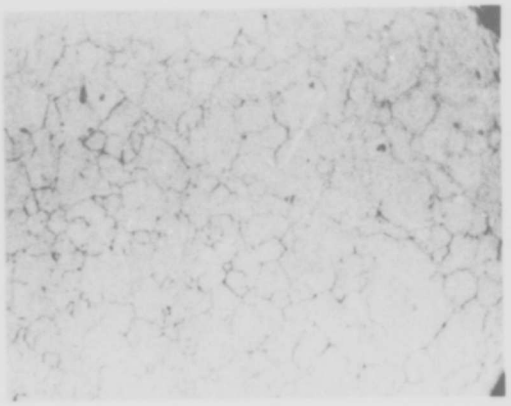

1050° C, 1 Hour

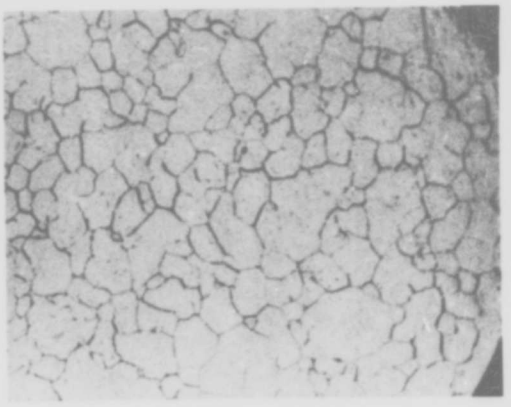

1100°C, 1 Hour

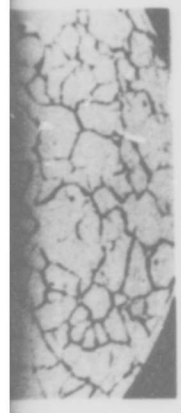

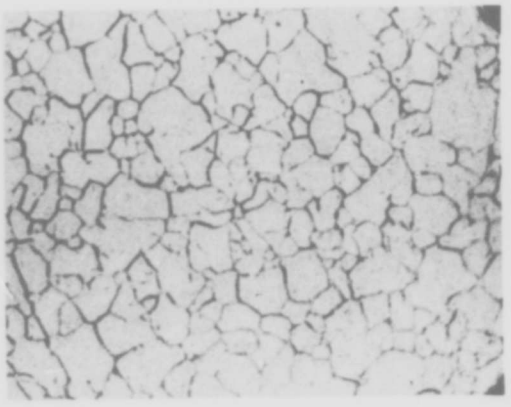

1050°C, 2 Hours

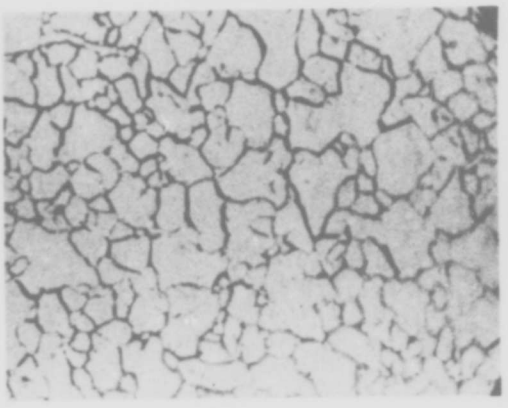

1100°C, 2 Hours

Figure 20. Grain Growth with Temperature and Time (Vendor E Material)

Figure 21. Vendor A Material as Received, Mag. 375X

Figure 22. Vendor A Material Heat Treated for Two Hours at 1050°C (Heat Tinted), Mag. 375X

Figure 23. Vendor B Material Heat Treated for Two Hours at 1050°C (Heat Tinted), Mag. 375X

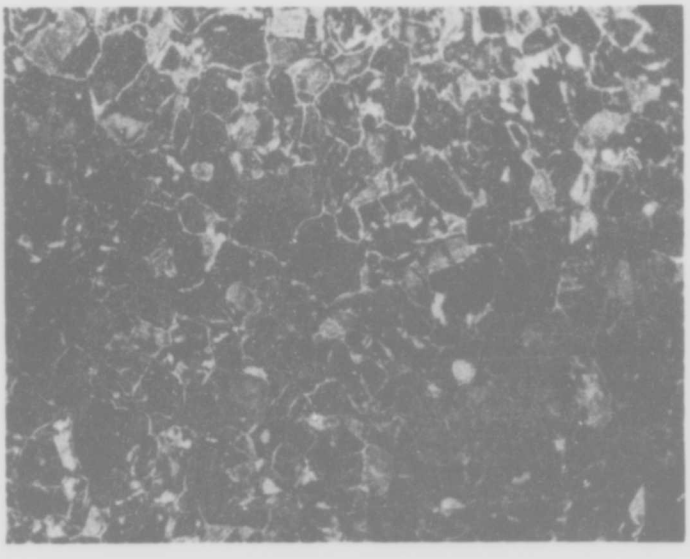

Figure 24. Vendor E Material Heat Treated for Two Hours at 1050°C (Heat Tinted), Mag. 375X

impurity content of the different materials, as shown in Table 1, reveals no significant differences except that Vendor E material contains beryllium in small quantities, and the microstructures do not reveal any unusual quantities of impurities at the grain boundaries. A second factor that may give rise to the type of growth observed is the crystal orientation of grains in the as-received material. Orientations determined on as-received materials[3] by X-ray diffraction show that Vendor A material has a mixed structure, whereas Vendor B material shows a preferred [200] and Vendor E a preferred [220] orientation. All of these materials show a preferred [200] after annealing at elevated temperatures. That these structures, in fact, do have a preferred structure in the as-received condition can be observed in the microstructures shown in Figures 18, 19 and 20. Areas of the photographs showing little grain boundary resolution are grains having approximately the same or near similar orientations.

Internal (Grain Boundary) Oxidation

Earlier in the discussion on the oxidation rates of Vendor A material as well as in the discussion of differences among different vendor materials, it was noted that the oxidation of the grain boundary occurred at a rate different from the bulk of the grain and that the composition of the resultant oxide also differed from that of the grain mass. This behavior is observed as an extension of grain boundary material beyond the normal scale surface. It seems reasonable to attribute this structure to a relatively rapid movement of some element, presumably iron, outward along these more rapid diffusion paths. Not only does the iron diffuse outward more rapidly, but oxygen atoms appear to diffuse inward along the grain boundaries at a more rapid rate, giving rise to oxide particle formation in the grain boundaries and below the metal-oxide scale interface. Because this subsurface oxide formation at grain boundaries has been observed in products from various flat pack vendors, and because this phenomenon has been thought to contribute to lead breakage in forming or use,[4] observations were made on the relative rates of external (scale) formation to the rates of internal (subsurface or grain boundary) oxidation.

Thicknesses of the external scale and depth of penetration of the grain boundary oxidation were measured on samples of Vendor A material oxidized at 750, 800, 850 and 900°C for times of 5, 10, 20 and 40 minutes each. Ten different measurements were made on each metallographically prepared

[3]Private Communication, C. A. Johnson, Bendix Corp., Sidney, N. Y.

[4]Zakraysek, L., "Glass Sealed Leads on Metal Components," IEEE Trans. on Parts, Hybrids and Packaging, Vol. PHP-8 No. 4, December 1972, pp. 45-48.

cross section of the oxidized samples. Although a large number of measurements were made, the irregularities of the scale-to-air and metal-to-scale boundaries as well as the lack of resolution of the innermost penetration of the oxygen along the grain boundary prevented consistent measurements to be made. Both scale and internal oxidation layers show a parabolic type curve of layer thickness versus time. The curves obtained can be said to be consistent with weight gain versus time curves shown earlier. The real interest here is whether there is a time-temperature-atmosphere relationship where the internal oxidation process is slower than scale formation and one could obtain the thickness of scale desired with a minimum of presumed detrimental grain boundary oxidation. Although the data are scattered, it would appear (see Figure 25), that the rate of oxygen diffusion along the grain boundaries increases with temperature at a rate greater than the rate of scale formation. After the initial stages of oxidation, one would expect these two rates to reach an equilibrium condition and be relatively constant, however, the low dew point of the oxidizing atmosphere may partly be responsible for the lower ratio at the higher temperatures. It would be interesting to see if measurements of the ratio over a wider span of temperatures, as well as a study of the effect of atmospheric moisture content, would show that the ratio becomes constant.

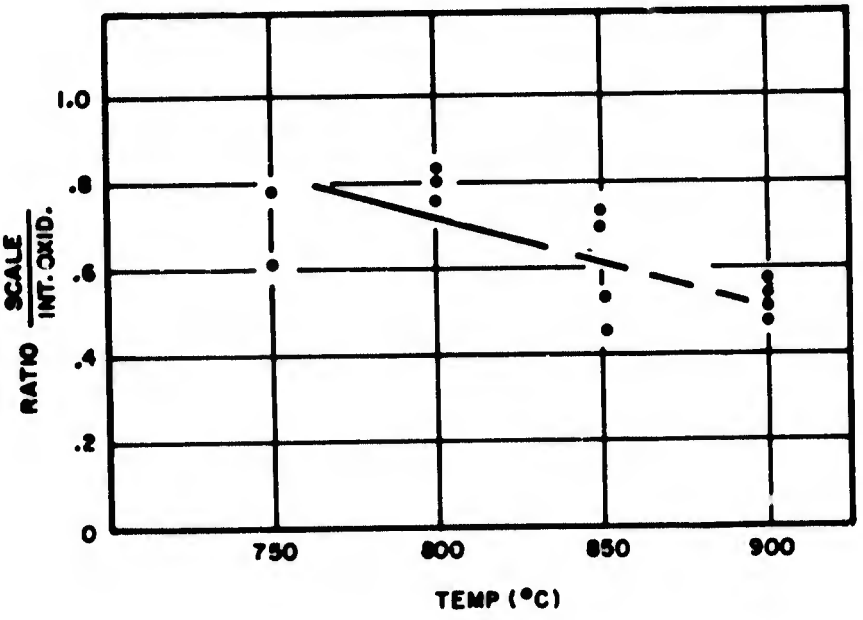

Figure 25. Ratio of Oxide Scale to Internal Oxidation for Vendor A Material

DISCUSSION

F15 material is oxidized only for the purpose of providing a surface required for glass sealing; oxidation serves no other purpose in the fabrication of the flat pack. In fact, except for undergoing a thorough cleaning for plating to obtain and retain a good solderable surface, these materials might better be used in the as-received condition. Since this oxidation process has but one function, an understanding of how best to achieve a desirable and optimum oxide seems fundamental. Primary to this are the type, quantity and limits of control of the oxide necessary to produce a good seal. This part of the problem is discussed in the following section. The remaining part of the problem lies in the type of material to be oxidized and the oxidizing conditions required to consistently obtain the oxide desired.

Prior discussions of the effects of abrading or roughening the surface, and the change of humidity, temperature and time have shown that these factors do have an effect upon the rate of oxidation. Most fabricators, who are concerned with these operations, and with whom we have discussed the processing of these materials, do maintain controls, to different degrees, over most of these variables through fixed processing routines. Although most houses appear to process only material from one vendor, the control that is exercised to insure that only one vendor's material is used appears quite variable. It has been shown that under constant oxidizing conditions, the amount of oxide and the types of oxides produced vary considerably, probably depending upon the mill processing schedules used by the vendors. It has been shown that the oxidation of F15 materials secured from different vendors proceeds at different rates and that even two different lots of material secured from a single vendor may show significant differences in the rate of oxidation.

Whether these rate differences are controlled by physical or chemical properties of the material is not well defined at this time. However, the differences in oxidation rates do appear to be related in some way to grain size and grain growth. It has been noted that the growth of the oxide is more rapid at the grain boundaries. Hence, the smaller the grain size the higher the rate. Furthermore, since it also has been shown that these oxides are almost pure iron oxide, the type of oxide scale on the surface of a fine grained sample must differ in overall analysis from those samples having a coarser grain. Grain growth has been shown to be practically non-existent in one material (Vendor E) but extremely great (enlarged by a factor of about 7 after two hours at 1050° C) in another material (Vendor A). Decarburization of these two materials (at the same temperatures but not for such extended periods of time) followed by oxidation should produce radically different results in the amount and type of oxide present. Whether the differences in grain growth between the two materials can be attributed to differences in

degree and/or type of grain orientation or differences in impurity levels and distribution of inclusions (grain growth inhibitors) is difficult to distinguish at this stage, although orientation does appear to be a major factor. It probably can be assumed that this material is somewhat similar to other materials, e.g., copper, silicon-ferrite, etc., where enlarged grain growth at elevated temperatures is dependent upon an orientation factor which in turn is dependent upon deformation and heat treating schedules (as well as types, number and distribution of inclusions) prior to the final product.

The work done here is not sufficient to make categorical statements on controls of materials at this time. No determinations have been made on the effect of nickel and cobalt contents and further work also is required to determine whether the carbon content or other impurities, or inclusions such as SiO_2, Al_2O_3 etc., though small in number, are in the range to be critical to the behaviors observed.

PHASE II - GLASS SEALING

The housings for semiconductors commonly are ceramic, plastic, or metal envelopes which contain an atmosphere required for the successful operation of the internal components. Whatever the pressure, vacuum or otherwise, a common requirement is that the envelope be provided with electrical leads which are hermetically sealed. These hermetic seals may be between dissimilar glasses, glass and ceramic or, as in the work to be reported here, glass and metal.

MATERIALS AND EQUIPMENT

A range of thicknesses of oxide was selected and the metal parts to be glass sealed were oxidized at the temperatures and times required as determined by the curves given previously (Figure 7). Three different glasses were used; however, most of the work reported herein is on the Corning 9119 hard glass.* The equipment used was essentially the same as described under the studies on oxidation except that dried argon gas was used as an atmosphere to surround the samples during sealing in order to prevent further oxidation of the sample during processing.

*Preforms of this glass were generously furnished by Mr. W. Simpson of the Corning Glass Works.

TEST PROCEDURE

Two preforms of hard glass were placed upon a previously oxidized metal part and then a similarly oxidized metal part was placed upon the glass preforms to make a sandwich-like construction as shown in Figure 26. This assembly was mounted on top of a small slice of fire brick; this combination was then pushed directly into the hot zone of the tube furnace. The argon gas flow was continuous and was adjusted so there would be no cooling of the sample parts, yet the gas in the tube would be replaced approximately once per minute.

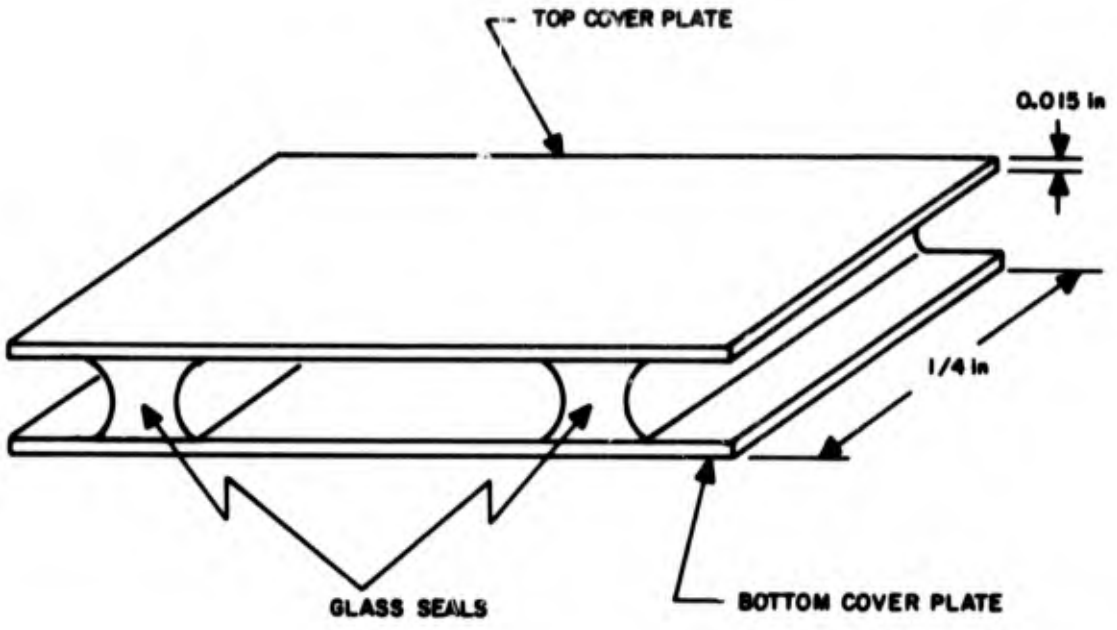

Figure 26. Glass Sealing Sample

After the sample had been held at temperature for the desired time, it was partly withdrawn and held in the argon for approximately 5 minutes at 500°C and then further withdrawn to cool to about room temperature, about 5 minutes, still in the argon atmosphere. At this time, the sample was completely removed from the furnace and set aside for fracture and evaluation. Samples were fractured by inserting a small wedge midway between the glass seals. The fractures were examined microscopically to determine the percentage of fracture through the glass and the oxide metal interface.

INTERNAL STRESSES

Glass-to-metal seals have been used in the microelectronics industry for some time and the stresses developed during sealing are highly dependent upon the seal configuration and the production process. This section of the report considers only those stresses which develop in this sealing sample configuration, which does not duplicate the configuration of a microelectronics package.

The goal of this study is to test for the relative strengths of the glass and the oxide interface. Stress can develop in the samples during glass sealing due to the differential thermal expansion of the metal and glass. These stresses, if tensile and sufficiently large, will exhibit themselves by causing cracks in the glass seals. Stress also develops during cooling of the samples due to temperature gradients and these can have the effect of raising or lowering the stresses due to differential expansion depending upon the relative magnitudes of the expansion coefficients and the temperature distribution within the sample. In this case, where the magnitude of the expansion coefficient of glass is higher than that of the metal and the temperature distribution during cooling is such that the glass is hotter than the metal, the tensile stresses in the glass will be lower during cooling than they would be if the sample were cooled at a uniform temperature.

In succeeding paragraphs, a calculation of the stresses developed in the sample as a result of the restrained free expansion after complete cooling is presented first, followed by an approximation to the order of magnitude of the tensile stresses developed in the sample as a result of a temperature gradient within the sample during cooling.

Final Stress Configuration

In glass sealing, the contraction of the glass that is of interest is the average differential contraction from the setting point of the glass down to room temperature. This setting point is the temperature at which the glass becomes so viscous that to all intents and purposes it can be considered rigid. The setting point, which generally is used in the sealing industry, lies somewhere near the midpoint of the annealing range. For this analysis the setting point of the hard glass shall be taken to be 450°C. For this temperature range, expansion information can be obtained for both the glass and metal. The expansion coefficients obtained from vendor data for both the glass and metal are as follows:

Expansion Coefficient (30°C - 450°C)*

Hard Glass - 5.9 in./in./°C x 10^{-6}

Metal (Vendor A) - 5.3 in./in./°C x 10^{-6}

*Setting Point = 450°C; Room Temperature = 30°C

The setting point configuration and the free contraction room temperature configuration are illustrated in Figure 27.

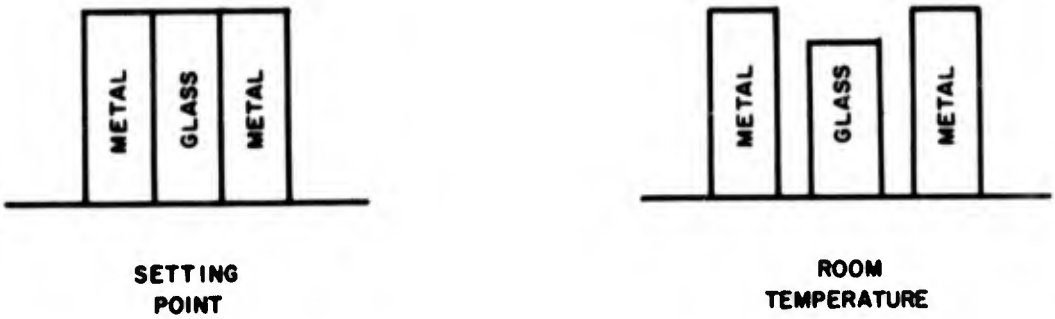

Figure 27. Setting Point and Room Temperature Configuration

In the free body diagram, Figure 28, let:

P = Force between the glass and metal

L_1 = Setting point length of both glass and metal

L_2 = Final, room temperature, length of glass, and metal

δ_K = Contraction of metal due to temperature change ΔT

δ_G = Contraction of glass due to temperature change ΔT

δ_{K1} = Change in length of metal due to force $P/2$

δ_{G1} = Change in length of glass due to force P

T_1 = Setting Point Temperature

T_2 = Room Temperature

$\Delta T = T_1 - T_2$

L_1 = Length at T_1

L_2 = Length at T_2

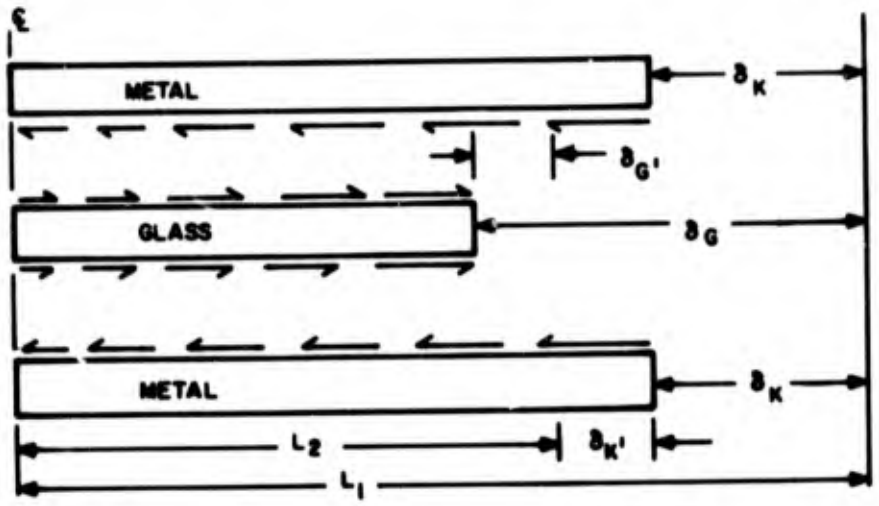

Figure 28. Free Body Diagram

Free Expansion

$$\delta_K = L_1 \delta_K \Delta T$$

$$\delta_G = L_1 \delta_G \Delta T$$

Change in length due to Force P

$$\delta_{K1} = \frac{(P/2)(L_1 - \delta_K)}{A_K E_K}, \quad \delta_{G1} = \frac{P(L_1 - \delta_G)}{A_G E_G}$$

Note:

$$L_1 - \delta_G \approx L_1 - \delta_K \approx L_1 \quad \text{First Order Approximation}$$

$$\therefore \delta_{K1} = \frac{P L_1}{2 A_K E_K}, \quad \delta_{G1} = \frac{P L_1}{A_G E_G}$$

In the Room Temperature configuration,

$$L_1 - \delta_K - \delta_{K'} = L_1 - \delta_G + \delta_{G'}$$

$$L_1 \alpha_K \Delta T + \frac{P L_1}{2A_K E_K} = L_1 \alpha_G \Delta T - \frac{P L_1}{A_G E_G}$$

$$(\alpha_G - \alpha_K) \Delta T = P\left(\frac{1}{2A_K E_K} + \frac{1}{A_G E_G}\right)$$

Let $a = E_K/E_G$ and $b = A_K/A_G$

Then the above equation becomes

$$P = (\alpha_G - \alpha_K) \Delta T \; A_G E_G \left(\frac{2ab}{1 + 2ab}\right) \qquad (1)$$

From cross sections of glass seals it was found that for glass sealing at 950°C the glass thickness is equal to the cover plate thickness.

950°C Sealing Temperature

Using equation (1) and

Metal thickness = 0.015 inch

Glass thickness = 0.015 inch

E (Glass) = $E_G = 8.2 \times 10^6$ psi

E (Metal) = $E_K = 20 \times 10^6$ psi

The stress in the glass

$\sigma_G = P/A_G$

= 1715 psi

990°C Sealing Temperature

Metal thickness = 0.015 inch

Glass thickness = 0.0075 inch

σ_G = 1860 psi

Cooling Stress Configuration

Stresses develop in a body, as a result of temperature gradients within the body, when the free expansion of each volume element cannot occur. Here again, as shown in the previous analysis, the factor that leads to stresses is the restraint of free expansion. The glass sealing samples are allowed to cool in the oven tube out of the heating zone near the end of the tube. The maximum velocity of argon through this tube approaches 0.5 ft/sec, assuming that the argon enters the oven at 25°C and is heated to about 500°C before it passes over the heating zone. At the exit end of the tube, where the sample is being cooled from sealing temperature, the argon will be cooling and hence the velocity will be lower. Any cooling at the exit end of the tube will be due to a combination of natural convection and radiation. The natural or free convection coefficient in this area of the tube would be equal to h_c = 2 Btu/Hr ft^2 °F. The properties of argon in this area of the oven were evaluated at an average temperature of 110°C. For free convection over a flat plate[5]

$$h_c = 0.71 \frac{K}{L} (a L^3 \Delta T)^{1/4}$$

where for argon at 110°C,

$$a = 0.59 \times 10^6/ft^3 \, °F$$

$$K = 12.44 \text{ Btu ft/Hr sq ft } °F$$

For the radiation coefficient, one may obtain an approximation for the maximum coefficient by obtaining the unit thermal conductance for radiation, h_r, as

$$h_r = \frac{\sigma F \epsilon (T_1^4 - T_2^4)}{T_1 - T_2'}$$

[5]Brown, A. I. and Marco, S. M., Introduction to Heat Transfer, 3rd ed., New York: McGraw-Hill, 1958.

where

σ = Stefan-Boltzmann constant

= 0.1714×10^{-8} Btu/Hr sq ft R^4

F = Radiation Form Factor, in this case = 1

ϵ = Emissivity of Radiating Body, assume = 1

T_1 = Maximum Body Temperature = 500°C

T_2 = Temperature of surface radiated to = 30°C

T_2' = Convection from gas temperature = 110°C

h_r = 7.4 Btu/Hr sq ft °F

Using this maximum radiation coefficient one may calculate the order of magnitude of the heat transferred from the sample. Assuming a constant rate of heat transfer from one side of the sample, the rate of heat transferred from the sample at an average temperature of 280°C to a temperature of 30°C can be determined from the equation:

$$q = (h_q + h_r)\, A\Delta T$$

One also knows that the change in temperature of the sample is:

$$q = C_p\, m\, \frac{dT}{d\theta}$$

where

q = rate of heat transfer from the body

C_p = is the specific heat of the glass

m = the mass of the sample

θ = time

then

$$\frac{dT}{d\theta} = \frac{(h_c + h_r)\, A\Delta T}{C_p\, m}$$

$$\frac{dT}{d\theta} = 3.83\ ^\circ C/sec$$

Therefore, the time required to change from an average temperature of 280°C at a constant rate of heat transfer of 7.3 Btu/Hr is:

$$\theta = 1.2 \text{ minutes.}$$

This value seems to be in good agreement with that observed during cooling of the sample.

The maximum tensile stress on the surface of a sample cooled at a constant rate of heat transfer[6] is equal to:

$$\sigma = \frac{E\alpha}{1-\mu} \frac{\phi r^2}{3K/\rho C_p}$$

For glass, assume the following properties:

$\rho = 2.4 \text{ gm/cm}^3$

$E = 8.2 \times 10^6 \text{ psi}$

$\alpha = 6.0 \times 10^{-6} \text{ in./in./°C}$

$\mu = 0.22$

$K = 0.006 \text{ cal/sec/cm}^2/\text{°C/Cm}$

$C_p = 0.130 \text{ Btu/lb°F}$

$r = 0.045$ inch (sample cooling from one side only)

$\phi = 3.83 \text{ °C/sec}$

$\sigma = 55 \text{ psi}$

It should be noted that the properties of glass were assumed for the entire sample. If the properties of the metal had been used in the analysis, the stresses would be about half of that shown above. In reality the stresses should lie somewhere between these two values.

These analyses show that the stresses developed during cooling can be considered negligible.

---

[6]Kingery, W. D., Introduction to Ceramics, J. Wiley and Sons, 1967.

RESULTS

Effects of Temperature, Time, and Oxide Thickness

Having established that the stresses in the glass due to different coefficients of contraction and thermal gradients were reasonably low, and further, that the rest times of the samples at the annealing temperature and cooling position of the tube were more than sufficient to reach equilibrium, metal-glass sandwiches were made to determine the degree of adherence of the glass-metal oxide-metal with variations in sealing conditions. Metal parts were selectively oxidized to give very light and relatively heavy oxide coatings; the heaviest oxide coating was approximately nine times that of the lightest oxidized sample. Sandwich structures using different weights of oxide on the surface and sealed at different temperatures and times indicated that a 975°C sealing temperature was somewhat near optimum. A 15-minute sealing time was selected to determine the effect of oxide thickness; similar data were then obtained for sealing temperatures 25°C on either side of the apparent optimum, i.e., at 950°C and 1000°C. The effect of temperature and oxide weight for a 15-minute seal is shown in Figure 29. As previously noted, the fractured samples were examined microscopically. Areas where the glass lifted the oxide from the metal surface were readily discernible. In Figure 29 these areas are depicted percentage-wise as black. Conversely, those samples showing complete fracture through the glass are shown as open circles. Since Figure 29 represents but one time slice through the limited glass sealing temperature range, similar data were obtained for one-half and twice this time value to determine the effect of time at these sealing temperatures. These data are shown in Figures 30 and 31. It is apparent that for short sealing times, the temperature of sealing is much more important than for longer sealing times. Reasonably good seals were obtained only with the lighter oxides at the minimum times and temperatures whereas good seals could be obtained over a relatively broad band of oxide thicknesses at the highest sealing temperature used. For the longest time used for sealing (30 minutes), the width of the band of oxide thickness appears to be almost insensitive to temperature, except at the highest temperature where thin oxide scales showed poor adherence.

Since time at temperature is readily converted into energy, a combined time-temperature plot or energy input versus oxide weight gain correlation is shown in Figure 32. Here the energy is defined as the difference in temperature between the sealing temperature and the setting temperature ($T_S - T_{SP}$) multiplied by the time at the sealing temperature. The setting temperature is defined here as the midpoint between the annealing and strain point temperatures; for Corning 9119 glass, this value is

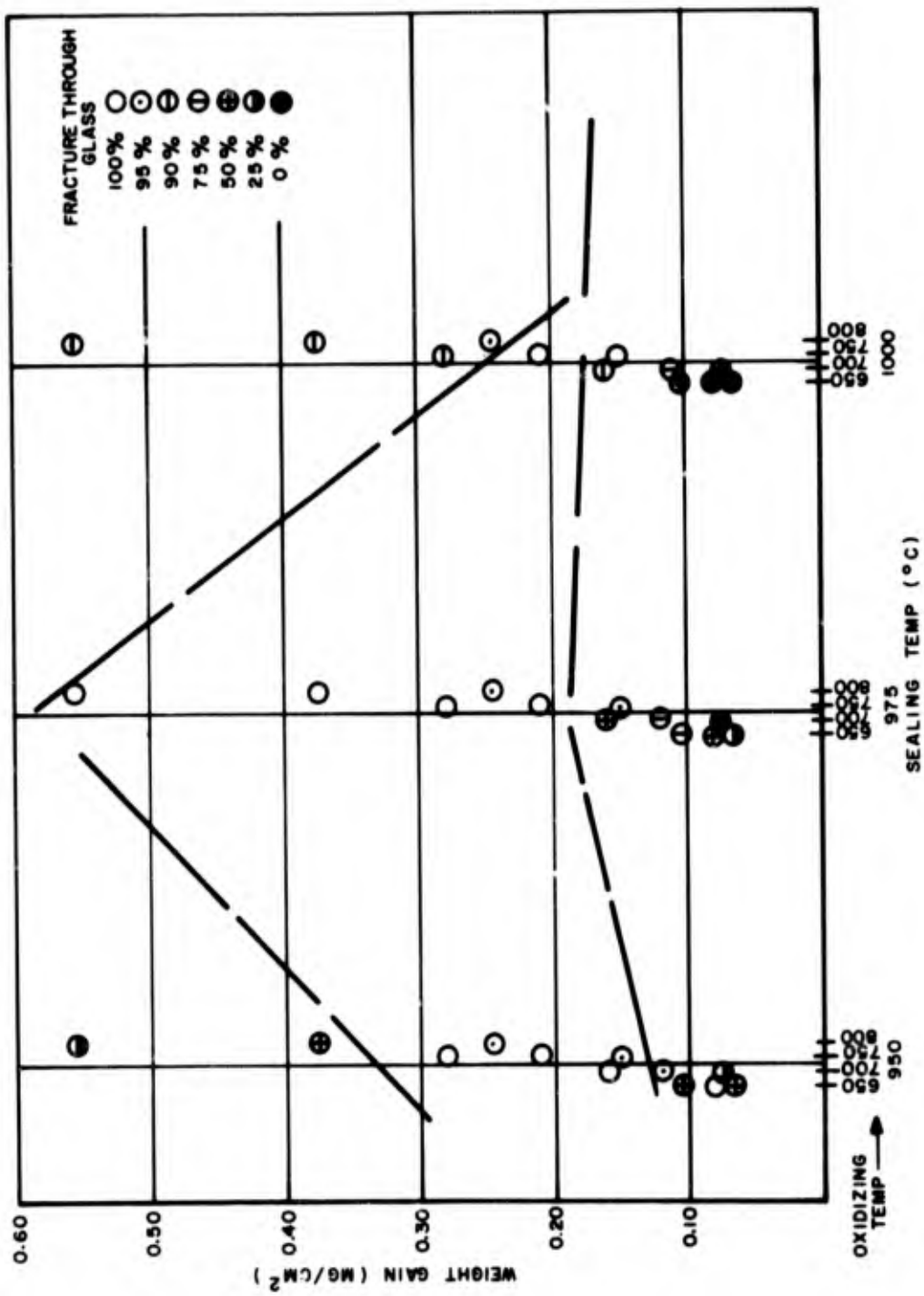

Figure 29. Effect of Temperature and Oxide Weight for a 15-Minute Seal (Vendor A Material and Corning 9119 Glass)

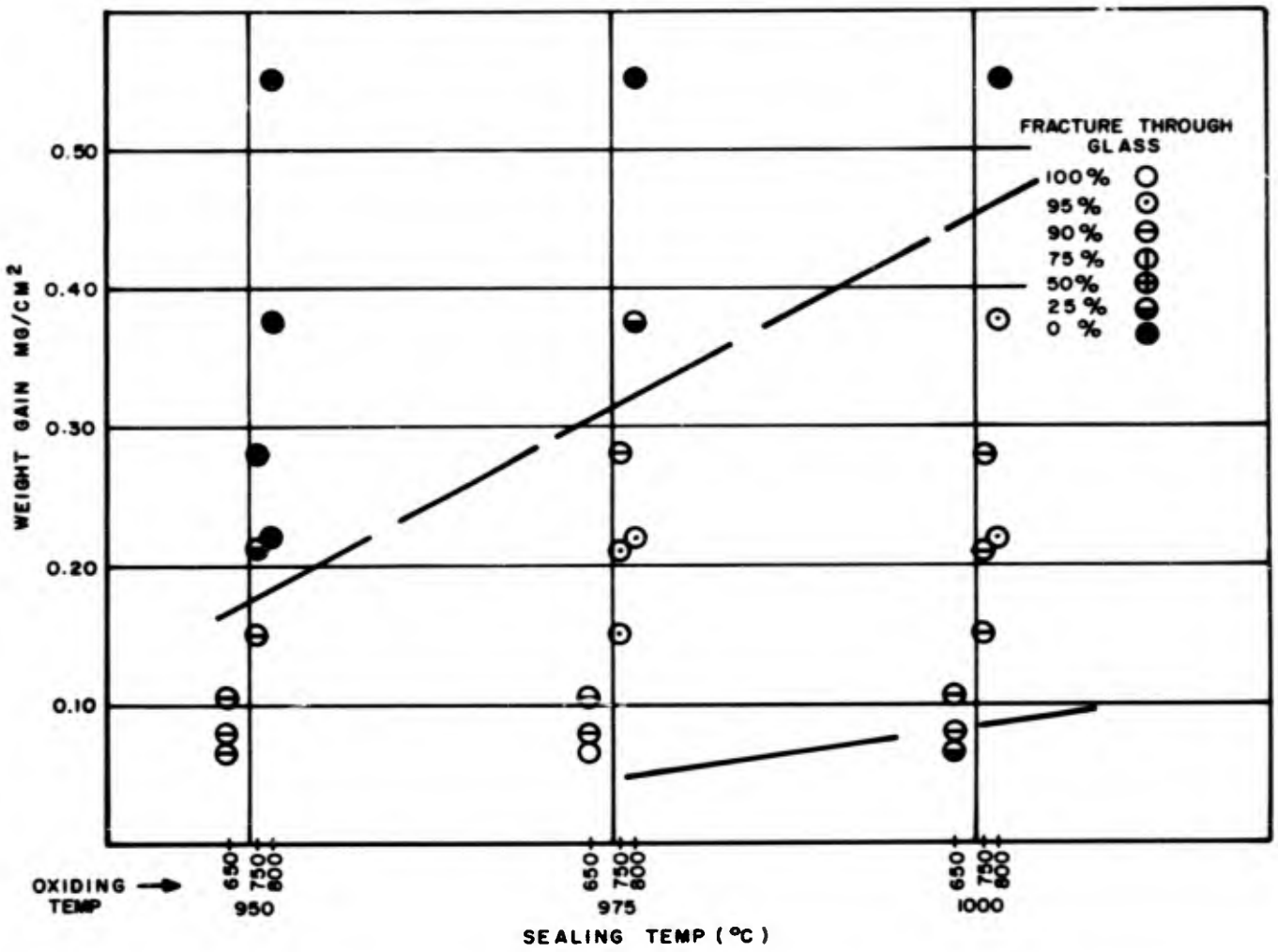

Figure 30. Effect of Temperature and Oxide Weight for a 7.5-Minute Seal (Vendor A Material and Corning 9119 Glass)

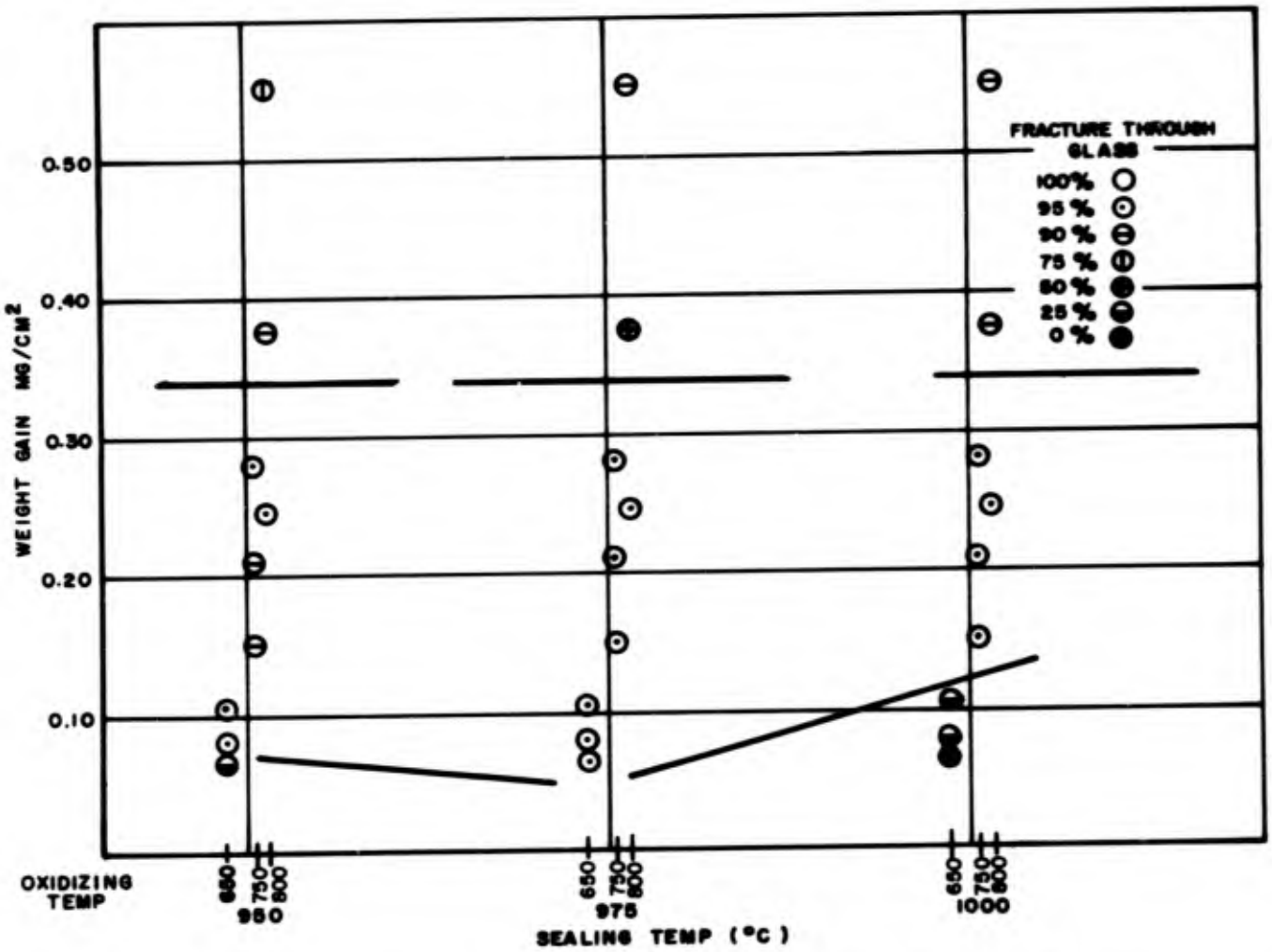

Figure 31. Effect of Temperature and Oxide Weight for a 30-Minute Seal Time (Vendor A Material and Corning 9119 Glass)

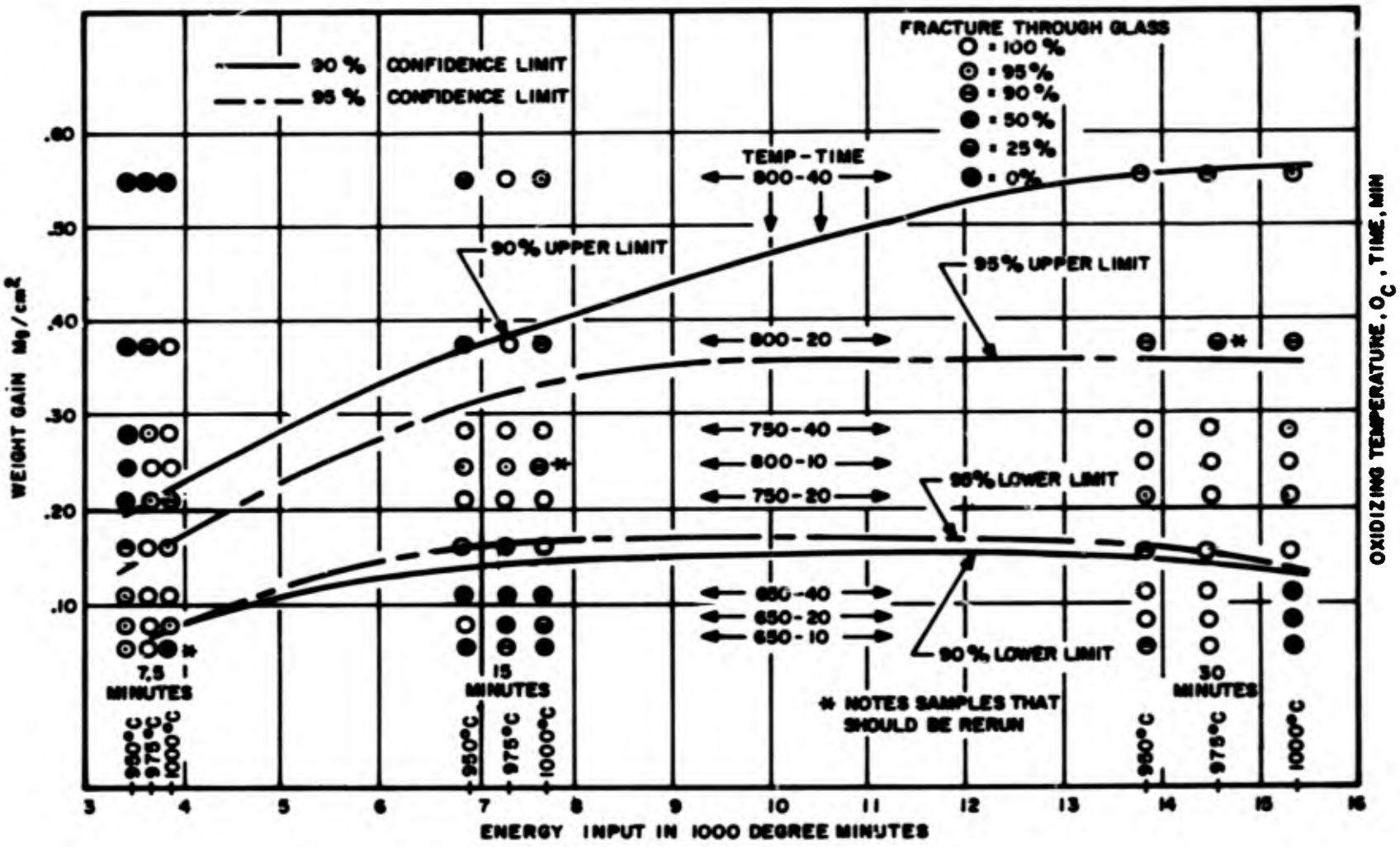

Figure 32. Glass Sealing Energy Input versus Oxide Weight Gain During Oxidization Showing % Fracture through Glass for Corning 9119 Glass and Vendor A Material

computed to be 488.5°C. It is readily apparent that the higher energy input used in the sealing operation allows much more freedom in selecting the oxide thickness for glass sealing. (Since the points in these figures are single evaluations, they should not be taken as absolute values.) Furthermore, the base material is from a single vendor (Vendor A) and the glass is but one vendor's glass, Corning 9119. Other vendors' base metals or other glasses may show similar curves, but they may shift in absolute value depending upon the adherence of the oxide and the type of glass used. Abendroth, in his study on oxide adherence using EN-1 glass and an unidentified F15 material, concluded that a minimum thickness of about 0.65 mg/cm^2 has to be exceeded before adherence is developed.[2]

Some concern was felt early in the program regarding the effect of bubble formation in the glass affecting the distribution of glass fracture versus oxide fracture values. Limited observations were made of those seals containing bubbles and within the confines of the experiment, no correlation was observed with either sealing temperature or oxide thickness. Fracture through the glass occurred in both bubbled and unbubbled glass; likewise, fracture through the oxide-metal interface occurred in both types of samples. Thus, it was concluded that bubble formation was not interfering with results of adherence studies and further work on this aspect of sealing was not pursued. M. R. Notis[7] in a study of the effect of decarburization of this alloy on bubble formation with Corning 7052 glass concluded that bubble formation was related to decarburization and that the decarburization temperature should be higher than the glass-to-metal sealing temperature if bubbles were to be avoided. He also concluded that grain size of the Fe-Ni-Co alloy has no effect on glass-to-metal seals. More will be said on this subject later in the report.

Previous data have shown that the best glass-to-metal seals (i.e., a glass fracture) is obtained when the oxide on the alloy, prior to sealing, is within a defined thickness range, the range being dependent upon the sealing temperature. Furthermore, previous investigations on adherence of the oxide to metal have shown that adherence is dependent upon the formation of a layer of FeO adjacent to the metal. To better understand the differences between good and poor seals, a series of photomicrographs of both kinds of seals, sealing at different temperatures, and with thick and thin oxide

---

[7] Notis, M. R., "Decarburization of an Iron-Nickel-Cobalt Glass Sealing Alloy," Journal of the American Ceramic Society, Vol. 45, No. 9, 1962, pp. 412-416.

coatings were examined and compared for differences at the glass-to-metal interface. No firm conclusions could be drawn from these examinations except that where the oxide coating was thin and the sealing temperature (and energy input) high, no oxide could be observed at the interface (Figure 33(a)); hence lifting occurred. On the satisfactory samples (all glass fracture) a small amount of oxide was visible at this interface (Figure 33(b)); however, the differences between these and other unsatisfactory samples could not be discerned. Reaction products in the form of cubic and needle structures (Figure 34 (a) and (b)) could be observed in some good seals; however, these structures were not identified and much work remains to understand these interface reactions.

Meniscus Shape

Photomacrographs of cross sections of glass sealed samples can show the shape of the meniscus formed by the glass seals between the metal plates. An attempt was made to characterize this meniscus shape by use of the dihedral angle formed between the glass and metal and to determine whether this angle changes with a change of sealing temperature and amount of oxide in the sample. The dihedral angle as was measured on the photomacrographs is shown in Figure 35.

The samples used covered the full range of the oxidation times and temperatures shown in Figure 7. Oxidation of Vendor A material at 650°C for 10 minutes shows a weight gain of about 0.06 mg/cm^2 and those at 800°C for 40 minutes show weight gain of about 0.55 mg/cm^2, approximately a 1:10 ratio. It was felt that any differences in the meniscus shape could be observed in the cross sections of these samples sealed at 950°C and 1000°C. Table 5 presents the dihedral angle data, as measured, for both 950°C and 1000°C sealing temperature for 15 minutes.

TABLE 5. DIHEDRAL ANGLE FOR GIVEN SEALING TIME AND TEMPERATURE VERSUS OXIDATION TIME AND TEMPERATURE

Oxidation Temperature (°C)	Oxidation Time (minutes)	Dihedral Angle (θ_1, θ_2, θ_3, θ_4) Sealing Conditions	
		950°C - 15 min.	1000°C - 15 min
650	10	18, 20, 13, 18	-----
800	10	13, 15, 8, 10	35, 16, 13, 17
800	40	17, 13, 17, 21	23, 20, 23, 25

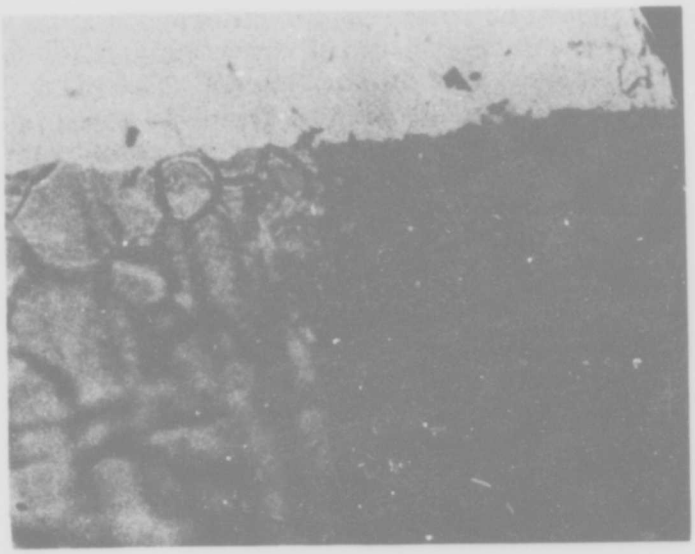

(a) Poor Seal -- Oxidized at 650°C, Dried Air, 10 Minutes, -56°C D.P., Sealed at 950°C, 15 Minutes, Mag. 600X

(b) Good Seal -- Oxized at 750°C, Dried Air, 40 Minutes, -56°C D.P., Sealed at 950°C, 15 Minutes, Mag. 350X

Figure 33. Photomicrographs of Good and Bad Seals

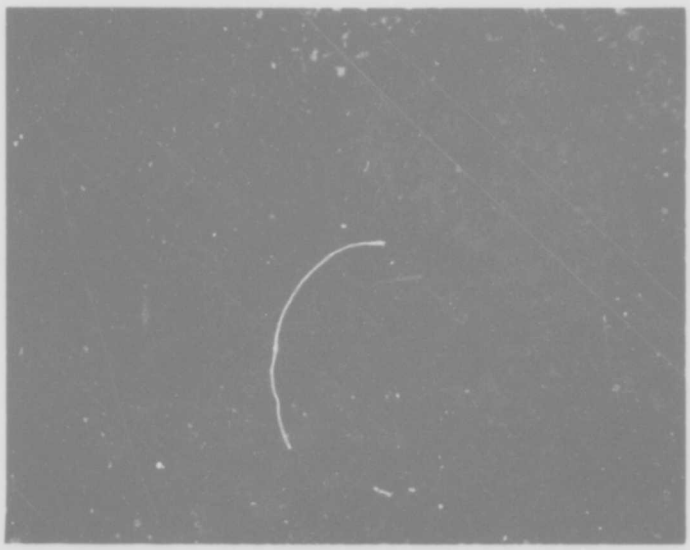

(a) Oxidized at 650°C, 10 Minutes; Sealed at 975°C, 30 Minutes; Mag. 150X

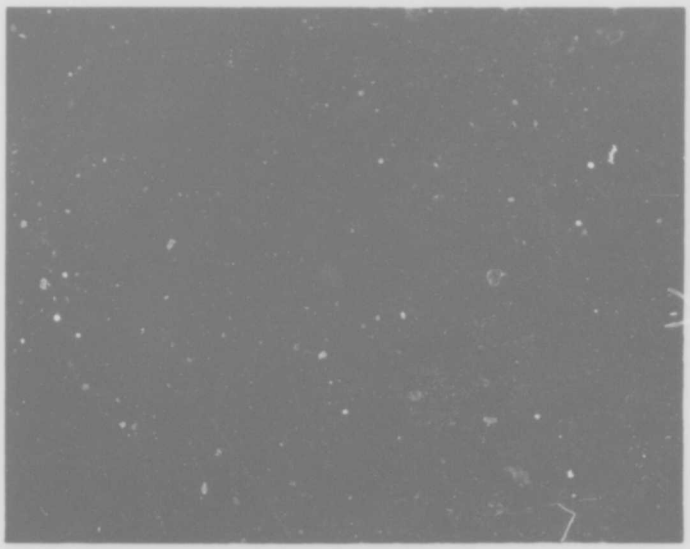

(b) Oxidized at 650°C, 10 Minutes; Sealed at 975°C, 30 Minutes; Mag. 350X (Higher Magnification of Sample in (a) Above)

Figure 34. Good Seals Exhibiting Reaction Products in Form of Cubic and Needle Structures

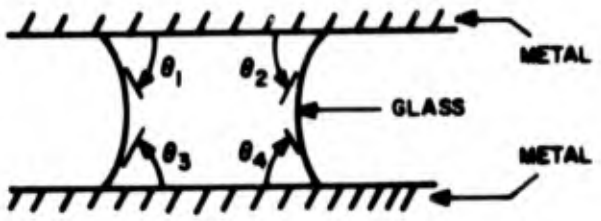

Figure 35. Meniscus Dihedral Angle

Correlations were attempted with respect to the angle made with the faster cooling cover plate and the slower cooling cover plate; no trend was found. Most of the sets of data have a standard deviation of about 3°. The correlation of the dihedral angle with sealing temperature, oxidation time and temperature was recognized to be limited by the relatively small number of samples taken. A further limitation occurred when it was recognized that the angle varied along the length of the glass seal and the angle measured depended upon where the cross section was taken. The angles varied and the cross sections were taken randomly. Cross sectional area measurements of the amount of glass in the seal found the quantity of glass in the seal to vary by only about 2.4%. This small variation was attributed to the use of glass preforms.

Although a general trend noted was that the average dihedral angle of the samples sealed at 950°C was lower than those sealed at 1000°C, no good correlations were found. It was concluded, therefore, that the amount of work required to find a correlation by this technique, if one exists, was prohibitive.

Use of Other Glasses

In addition to the glass used to make glass-to-metal seals previously discussed, a second lot of glass, similar in composition but with a particle size held to narrow limits, was used to make seals. A limited number of samples were used to compare with data points on the curves previously obtained. To eliminate the possibility of slight differences in the oxidation of the samples as well as unknown differences that might occur on the sealing conditions, the glass-to-metal sandwiches were made using one piece of the first lot of glass and one piece of the second lot. A comparison was then

made of the two different fractures from the one sandwich. Experimental results revealed a decrease in the range of oxide thickness for the glass with the more closely controlled particle size. These results differed from what was expected; however, additional work is required to draw any firm conclusion. The differences observed may be a result of a difference in the kinetics of reaction causing differences in time to reach equilibrium conditions.

A third glass, one of the soft glass types, a Dow Corning 00130 (SG 7), also was used for limited experimental work. The glass obtained was in powder form rather than a preform, as used previously. For consistency and to permit comparisons among the glasses used, attempts were made to obtain preforms of the same size and shape as the preforms of hard glass used in the previous experiments. After many unsuccessful attempts using a wide variety of materials for die blocks, it was not until the extreme sensitivity of this glass to the carbon impurities in the die blocks became known that success was achieved in making uncontaminated preforms. With the earlier preforms, the erratic results, plus a slight but noticeable change in the color of the preform as well as the glass in the final seal over seals made not using preforms, were strong clues to these compositional changes. Most of the effort using this glass was spent in learning of the characteristics of the glass. Insufficient data are available to make comparisons of sealing efficiencies and characteristics of the three glasses.

DISCUSSION

Considerable work is reported in the literature on the making of glass seals and glass-to-glass, ceramic-to-glass, and porcelain-to-metal bondings appear to be relatively well understood; however, the glass-to-metal seal is somewhat more complex and less understood. In the present studies attempts were made to determine if the amount of oxide dissolve in the glass, as well as the sealing temperature and time, could be related to the meniscus shape in cooled samples. No correlation was evident over the range of oxide thickness, temperatures, and times selected. The thickness of the glass in the seal, using constant thickness preforms, is dependent upon the sealing temperature and presumably will also be dependent upon the weight supported by the glass at sealing temperatures. The meniscus shape does not appear to be very sensitive to temperature change, but the flow of glass in the seal would appear to be important to physical characteristics of the package. One of the principal effects of temperature is upon adherence. Before adherence can be developed, however, wetting of the metal by the glass must occur. The same principle that applies to wetting of the metal by solder (described under Solderability) applies also to the wetting of metal by glass. In the case of molten glasses and solid metals, the wetting of the metal by the glass depends upon the glass composition with the degree of wetting reaching a maximum

value when the glass becomes saturated with a low valence oxide of the substrate metal.[8] Good wetting conditions have also been associated with improved adherence between the glass and the metal.[9] As is shown in the curves of Figure 32, the method of making the seal is a kinetic process which requires that the time-temperature relationships be controlled.

As the oxide is dissolved by the glass, the saturation concentration is immediately established at the interface and is maintained only as long as some undissolved oxide is present. The dissolved oxide becomes an integral part of the glass structure. When the last bit of discrete oxide is dissolved, continuing diffusion begins to drop the substrate oxide concentration in the glass at the interface to values lower than the saturation concentration and the quality of adherence also begins to drop. The most desirable situation seems to be to dissolve all of the discrete oxide and have a saturated glass composition directly in contact with the clean metal surface.

Since this process is kinetic in nature, it is dependent not only on temperature and time but also upon the composition and structure of the glass and substrate material. Not only the rate at which saturation is reached but also the degree of solubility required to reach saturation can be changed with a change in substrate specie. It has already been noted that the nature and perhaps the ratios and type of oxide on the surface of the F15 alloy can be altered by changes in orientation and grain growth; consistency or inconsistencies in glass mixes should also have an effect upon rates and degrees of solubility to reach saturation. The physical nature of the metal substrate oxide also will affect the diffusion rate. Although Notis concluded that grain size of the Fe-Ni-Co alloy has no effect on glass-to-metal seals, a conclusion reached after observing consistent seals in both small and large grain material, the variation of grain size in his material ranged from 0.015 to 0.15 min. in diameter; however, his material presumably was from one vendor and oxidation was carried out after wet hydrogen decarburization. It was previously noted that Carter concluded that hydrogen annealing pretreatments gave significant quantities of FeO and adhering scales. Certainly in this work, rates of oxidation and types of oxides obtained differ from grain boundary to grain mass and, if the type of oxide or the surface has any influence upon wetting and adherence by the glass, noticeable differences in these characteristics should occur if there is a

---

[8] Adams, R. B. and Pask, J. A., "Fundamentals of Glass-to-Metal Bonding," Journal of the American Ceramic Society, Vol. 44, No. 9, 1961.

[9] Pask, J. A. and Fulrath, R. M., "Fundamentals of Glass-to-Metal Bonding, VIII -- The Nature of Wetting and Adherence," Journal of the American Ceramic Society, Vol. 45, No. 12, 1962.

significant difference in grain size during the oxidation process. Vendor A material consistently produced adhering scales when properly prepared and oxidized even without a hydrogen annealing pretreatment, but Vendor E material was equally consistent in producing nonadherent oxides. These differences were explained on the basis of grain size; however, additional factors need investigation. It becomes imperative, therefore, that controls of composition and fabrication of the metal substrate be established to be able to produce the consistency of oxide required for good seals with defined time-temperature-atmosphere parameters, and with a defined and controlled glass composition. Energy curves for different lots of glass also may need to be determined to resolve if there are requirements for the control of composition or physical characteristics of the glass.

PHASE III - PLATING

OBJECTIVES

An electroplated finish on IC package leads serves several purposes. Some of these stem from flat pack manufacturing needs, others are due to assembly requirements and still others are governed by the application. Some of the most significant requirements include corrosion protection during manufacture, bondability and weldability during assembly, and solderability and corrosion protection during the useful lifetime of the package.

Although numerous variations have been attempted, most systems now utilize gold or tin and tin alloy electroplated finishes with or without underplating. The objective of the study described in this report was to evaluate the effectiveness of plated finishes now being used by the industry, with special emphasis on those used in military electronics applications. Because of the nature of problems most commonly encountered in the use of electroplated components, particular attention was given to the preparation of the base material as well as to the deposited product. The compositions of the electro deposit and the plating baths were monitored, and the effect of single and duplex deposits on mechanical and physical properties was evaluated through the use of bend, peel and corrosion tests. Other studies were made in regard to aluminum and gold flying-lead bondability as well as to the solderability of finishes on external leads.

SELECTION OF MATERIALS

A survey of eight suppliers of flat packs showed that, for all of the available types of packages, a gold plated finish is standard on eight flat packs

and optional on two. Tin plate is standard on five flat packs with no supplier offering tin plate as an option. Solder (hot dip) is optional on ten types of flat packs. A nickel-under-gold finish is provided on only one flat pack from one supplier.

Seldom is the purity of the gold plate specified. For this reason, two types of gold deposits were selected for evaluation in this study, one a high purity, 99.9% minimum gold plate, and the other a 99.7% minimum gold plate.

Since a nickel underplate has been thought to provide additional corrosion protection to the assembly, this finish system was also evaluated, mainly in regard to the effectiveness in use. Based on the ductility and adherence results of preliminary tests on nickel deposited from Watts, sulphate and sulfamate electrolytic solutions, and of phosphorus and boron electroless nickel, the sulfamate process was selected for detailed study during this program.

Bright Acid Tin (BAT) and Bright Acid Solder (BAS) were used as representative of tin and solder finishes. These deposits were selected because of their superior corrosion resistance.

PROCESSES

The proper cleaning and activation of base metal surfaces are necessary to the successful deposition of electroplated finishes. Because of the inherent nature of the F15 (Ni-Co-Fe) type alloys and because of the effect of other processes (especially oxidation for glass sealing), the cleaning and activation of this alloy is somewhat more critical than for many other materials.

Cleaning

Procedures were developed for cleaning the F15 alloy in preparation for electroplating. The steps in the process used for cleaning the material in the nonoxidized condition were as follows:

(a) Trichloroethylene vapor decrease, two cycles.

(b) Electro clean in cleaner C3 (10 oz/gal) at 180°F, three minutes at 6 volts, parts cathodic.

(c) Rinse in cold, running distilled water at tap temperature.

(d) Immerse for two minutes in 50% HCl at room temperature.

(e) Rinse in cold, running distilled water at tap temperature.

(f) Immerse for two minutes in F15 activator, A2 electrolytic, operating at 175°F. Parts anodic at 6 volts.

(g) Rinse in cold, running distilled water at tap temperature.

(h) Plate immediately (gold, gold strike or BAS).

(i) For BAT (only), skip step (h) and immerse in 50% H_2SO_4 for two minutes at room temperature.

(j) Rinse in cold, running distilled water at room temperature.

(k) Plate BAT immediately.

(l) Rinse in cold, running distilled water.

(m) Immerse in isopropanol, remove and blow dry (oil free, filtered air).

When the F15 alloy is oxidized in preparation for glass-sealing, a heavily oxidized surface condition may result. The procedure used in this study for the removal of such an oxide was as follows:

(a) Immerse in 20% HCl at 140°F for 20 minutes.

(b) Rinse in running water at tap temperature.

(c) Immerse parts in cleaner C4 at 172-175°F for 15 minutes.

(d) Electro clean in cleaner C3 (10 oz/gal) at 180°F, parts cathodic at 6 volts for three minutes.

(e) Rinse in cold, running distilled water at tap temperature.

(f) Immerse in 50% HCl at room temperature for two minutes.

(g) Rinse in cold, running distilled water at tap temperature.

(h) Immerse in F15 activator, A2 electrolytic, at 175°F for two minutes. Parts anodic at 6 volts.

(i) Rinse in cold, running distilled water at tap temperature.

(j) Plate immediately (gold, gold strike or BAS).

(k) For BAT (only), skip step (j) and immerse parts for two minutes in 50% H_2SO_4 at room temperature.

(l) Rinse in cold, running distilled water.

(m) Plate BAT immediately.

(n) Rinse in cold, running distilled water.

(o) Immerse in isopropanol, remove and blow dry (oil-free, filtered air).

Plating Activators

In the development of cleaning procedures, a number of approaches were evaluated for surface activation. The selection of F15 surface activators was made on the basis of the receptiveness of the surface to solder after activation. For various reasons most of the tested activators could not be used to prepare the F15 alloy for plating. The results of the study of activators are, therefore, based upon the solderability of F15 alloy after activation treatment and before plating. This procedure has been found to be highly effective in determining the degree of activation as related to wettability by molten solder. The general conclusions in regard to activation are shown in Table 6.

As has been stated, the determination of an "active" surface condition was based on solderability. Other factors must also be considered before a particular activation process can be used on IC packages. Surfaces treated with activator A1, for example, were found to be very solderable, but not useable in treatment prior to plating. On the other hand, A2 (nonelectrolytic) and A3 did not improve solderability but do serve as activators for plating. A2 (electrolytic) produced more favorable results. A4 was used because of its ability to remove heavy oxides. Activators A5, A6 and A7 were not used because they were not very effective and involve a very long procedure. All the others were rejected for various other reasons: A8 because of its fluoride content, BAS as inappropriate under an electroplate, Hot HCl because of possible chloride contamination, A9 because it is a flux and not suitable for plating preparation, and BAT because it is not suitable under an electroplate. The BAS and BAT solutions serve as F15 activators, but both deposit soft finishes which will interfere with subsequent plating.

The qualitative results showed that the activators selected (A2, A3, A4) for use in the present project will satisfy the requirement for the preparation of F15 alloy for electroplating. The specific technique used for this

TABLE 6. F15 SURFACE ACTIVATION

Activator	Result	Remarks
A1	Not Acceptable	Deposits a layer of metallic lead. Although very solderable, this metallic layer would not be desirable in subsequent plating processes.
A2 (Nonelectrolytic)	Not Acceptable	F15 very passive, requires active flux.
A3	Not Acceptable	Same as A2
A4	Not Acceptable	Same as A2
A5	Not Acceptable	Limited wetting occurs
A6	Not Acceptable	Same as A5
A7	Not Acceptable	Same as A5
H_2SO_4 50% Solution at Room Temperature	Not Acceptable	Very poor activation
A8	Marginal	A less active surface is obtained with this solution/anode system than when lead anodes are used. The presence of fluorides may limit usage to certain glasses.
BAS	Marginal	Produces a good solderable surface similar to BAT. The high fluoride content of the bath limits usage to hard glass.
A2 (Electrolytic)	Marginal	Activation is obtained but solder appears spotty.
Hot HCl (50% Solution)	Acceptable	Produces a surface receptive to solder using a water white rosin flux. The time between HCl and flux/dip must be short.

TABLE 6. F15 SURFACE ACTIVATION (Continued)

Activator	Result	Remark
A9	Acceptable	This "cold" activator is removed prior to fluxing for solder dip. Very good activation with water white rosin.
BAT	Acceptable	Complete activation of F15 alloy, compatible with soft glasses, excellent activation.

determination (i.e., solderability) provides a positive indication for activator selection purposes, but the procedure does not, in itself, allow a complete judgment to be made. Therefore, a number of criteria must be, and were, considered for the final selection.

Plating Solutions and Control

A total of eight different plating solutions were evaluated during the course of this investigation. The following is a description of the makeup and control used in each instance.

(a) AuS - Gold strike used for Au1 only. Make up per supplier bulletin.

Operating Temperature	100° F
Specific Gravity	13° Baume′
Current Density	1.5 A/ft^2
pH	3.5
Anodes	Platinized Titanium

Mechanical solution agitation

Strike for 3 minutes at 1.5 A/ft^2

(b) Au1 - Gold plate to MIL-G-45204B Type 3 (99.9% Au). Make up per supplier's bulletin. All parts with initial gold strike per AuS.

Operating Temperature	130° F
Specific Gravity	18° Baume′ at 80° F

Current Density	2 A/ft^2
pH	7.0
Anodes	Platinized Titanium

To Plate	Time (minutes)	Current Density (A/ft^2)	(A/in.^{2})
200 x 10^{-6}	40	2	0.0138
150 x 10^{-6}	30	2	0.0138
50 x 10^{-6}	10	2	0.0138

(c) Au2 - Gold plate to MIL-G-45204B Type 1 (99.7% Au). Make up per supplier's bulletin.

Operating Temperature	110°F
Specific Gravity	15° Baume' at room temperature
Current Density	5 A/ft^2
pH	4.0
Anodes	Platinized Titanium

Mechanical solution agitation

Solution filtered daily after use

To Plate	Time (minutes)	Current Density (A/ft^2)	(A/in.^{2})
50 x 10^{-6}	7.2	5	0.0347
150 x 10^{-6}	14.4	5	0.0347

(d) NiS - Nickel plate according to supplier technical data sheet.

Temperature	120°F
Current Density	40 A/ft^2
pH	3.8
Anodes	CP cast nickel

Mechanical solution agitation

40 A/ft^2 for 9 minutes deposits 0.0003 in.

(e) BAT - Bright Acid Tin plate according to supplier bulletin.

Temperature	60°F
Current Density	15 A/ft^2 (Cathode)
Anodes	99.999% Sn

To Plate	Time (minutes)	Current Density (A/ft^2)	(A/in.^{2})
100 x 10^{-6}	3.5	15	0.1041
250 x 10^{-6}	8.75	15	0.1041

(f) BAS - Bright Acid Solder plate according to supplier bulletin.

Temperature	60°F
Current Density	15 A/ft^2 (Cathode)
Anodes	Cast 63/37 vac. melt solder

To Plate	Time (minutes)	Current Density (A/ft^2)	(A/in.^{2})
100 x 10^{-6}	3.5	15	0.1041
200 x 10^{-6}	7.0	15	0.1041
50 x 10^{-6}	1.75	15	0.1041

(g) ENiP and ENiB - The Phosphorous and Boron electroless nickel materials were eliminated from consideration due to poor results in bend tests and because of poor solderability.

Sample Racking and Solution Care

Sample panels were plated by attachment to stainless steel racks of a standard size. The F15 panels were spot welded to the stainless steel racks with an intermediate stainless steel wire loop for hanging. Sample panels were cut to one size; therefore the current density was standardized for a given number of samples (plus the rack). The gold and nickel baths were contained in pyrex beakers with continuous stirring while the samples were held stationary. The tin and solder baths were filtered and chilled in addition to the use of continuous stirring. Bath analyses were made by the supplier when solution usage ended.

Each of the electroplating baths was held strictly for the plating of the F15 samples. No other materials were processed in the baths until the F15 plating was completed, at which time a series of copper control samples were plated in the same solutions. It is possible that Sn/Pb may have been introduced into the gold bath at this time (from the solder used to attach hangers).

Selection of Thickness Plate

Plating thicknesses of from 50 microinches to 250 microinches were determined to be in the range of interest, covering the spread formed in normal usage, that required by the military specifications, and that which was decided to be of most value to the presently planned experiments. More recent industry trends indicate that still other thicknesses (especially in regard to duplex gold and gold substitutes) may prevail, but the ranges decided upon here seem to offer validity according to the present state-of-the-art in IC lead finishes.

MEASUREMENT OF THICKNESS

All measurements of gold plating (single deposit) were made by Beta Back Scatter techniques. The Betascope measurements were calibrated with a set of gold plated samples that were also measured by metallographic cross section. All tin, tin-lead and all duplex gold samples were measured by metallography. Table 7 shows the measured results on plated sample panels.

TESTING FOR POROSITY

Numerous methods are described in the literature for detecting porosity of plated parts. Experience in the laboratories indicates that these tests generally can be classified into one of two broad categories: (1) excessive metal attack where the corroding agent(s) far exceed the most severe environmental exposure, and (2) limited sensitivity where reproducibility often is lacking. In this latter case, initial trials show negative results but later tests may show increased quantities of porosity.

In this investigation, four basic porosity tests (with variations) were evaluated as shown in Table 8.

As noted above, the test selection was to be on the basis of consistency and reproducibility, which in turn depend upon the activity of the corroding agent and the method of application as well as the plate and substrate material to which it is applied. The Prussian blue test applied with a saturated then partially dried quantity of the developer on photographic paper appeared to

TABLE 7. PLATING THICKNESSES

Sample No.	Vendor Base Metal	Coating	Actual Thickness (10^{-6} in.)
1	A	BAT-100	110
2	A	BAT-250	262
3	A	BAS-100	120
4	A	Au1-50	57
5	A	Au1-200	179
6	A	Au2-50	53
7	A	Au2-150	114
8	A0	BAT-100	120
9	A0	BAT-250	262
10	A0	BAS-100	95
11	A0	Au1-50	52
12	A0	Au1-200	159
13	A0	Au2-50	42
14	A0	Au2-150	141
30	B	BAT-100	120
13	B	BAT-250	260
32	B	BAS-100	120
18	B	Au1-50	53
19	B	Au1-200	149
20	B	Au2-50	51
21	B	Au2-150	104
22	B0	BAT-100	110
23	B0	BAT-250	275
24	B0	BAS-100	130
25	B0	Au1-50	55
26	B0	Au1-200	146
27	B0	Au2-50	52

TABLE 7. PLATING THICKNESSES (Continued)

Sample No.	Vendor Base Metal	Coating	Actual Thickness (10^{-6} in.)
28	B0	Au2-150	121
29	A	Au1-100 over NiS-30	-
15	A	Au1-10 over Au2-40	49
16	A	Au2-40 over Au1-10	62
17	A	Au1-20 over Au2-80	90
33	A	Au2-80 over Au1-20	85
34	A0	Au1-100 over NiS-30	-
35	A0	Au1-10 over Au2-40	77
36	A0	Au2-40 over Au1-10	82
37	A0	Au1-20 over Au2-80	108
38	A0	Au2-80 over Au1-20	50
39	B	Au1-100 over NiS-30	-
40	B	Au1-10 over Au2-40	50
41	B	Au2-40 over Au1-10	75
42	B	Au1-20 over Au2-80	84
43	B	Au2-80 over Au1-20	82
44	B0	Au1-100 over NiS-30	-
45	B0	Au1-10 over Au2-40	70
46	B0	Au2-40 over Au1-10	65
47	B0	Au1-20 over Au2-80	123
48	B0	Au2-80 over Au1-20	75
49	Cu	BAT-100	-
50	Cu	BAT-250	-
51	Cu	BAS-100	-
52	Cu	Au1-50	-

TABLE 7. PLATING THICKNESSES (Continued)

Sample No.	Vendor Base Metal	Coating	Actual Thickness (10^{-6} in.)
53	Cu	Au1-200	-
54	Cu	Au2-50	-
55	Cu	Au2-150	-

Note:
1. Au1 and Au2 single coat measured by Betascope.
2. BAT and BAS by optical measurement.
3. #12 Meniscograph sample, and #12 MIL-STD-883 test sample examined for gold under solder - none found.
4. Duplex coatings measured optically.
5. Code "0" refers to oxidized metal (at rate of 0.25 mg/cm^2 by weight gain).
6. Au1 is 99.9% pure gold.
7. Au2 is 99.7% pure gold.

TABLE 8. EVALUATION OF POROSITY TESTS

Test	Evaluation
1. Mixed Acids Test (HNO_3 + HF; 3:1 ratio)	Gave impression of excessive porosity
2. Prussian Blue Test	
a) Blue regions developed on sample Reagent: Concentrated HNO_3 Developer: KCN + NaCl	Excessive bleeding
b) Blue regions developed on photographic paper Reagent: Concentrated HNO_3 Developer: KCN + NaCl (on photo paper)	Satisfactory
3. Electrolytic Test Reagent: $NaNO_3 + Na_2CO_3 + H_2O$ Indicator: Cupron	Requires fixturing Limited usage
4. Boiling Water Test Distilled water (boiling)	Poor resolution Pores difficult to detect

meet the qualities best. The results are shown in Figure 36. As expected, numerous pores can be seen in the gold plate having a nominal thickness of 5×10^{-6} inches, and this number decreases with an increase in the thickness of the plate. At 5×10^{-6} inch thickness of gold plate, only a few random pores can be observed. The effectiveness of this thickness of plate can also be observed in salt spray results and the results of solderability testing after exposure to ambient conditions.

BEND TEST

Samples were tested by manually bending them around a mandrel having a diameter three times the thickness of the sample. Each sample was

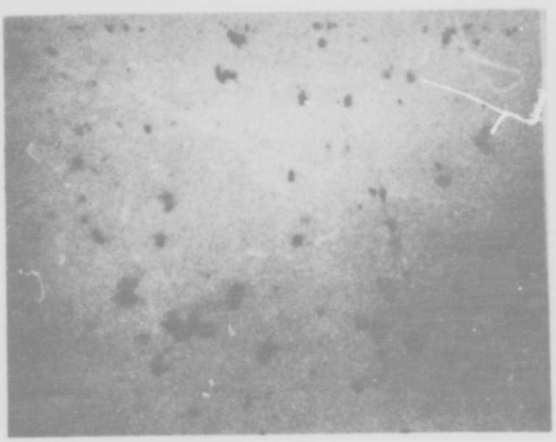

$5 \cdot 10^{-6}$ Inch Thickness

$10 \cdot 10^{-6}$ Inch Thickness

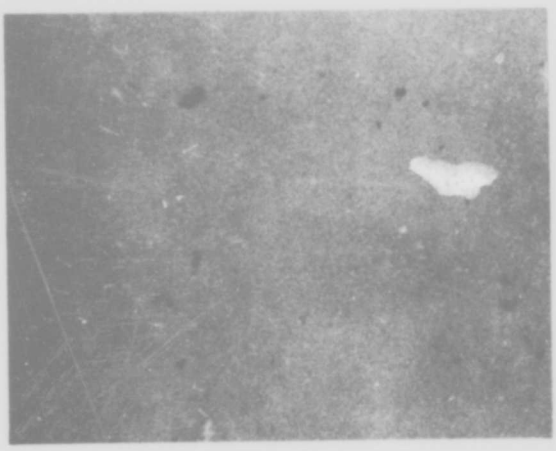

$25 \cdot 10^{-6}$ Inch Thickness

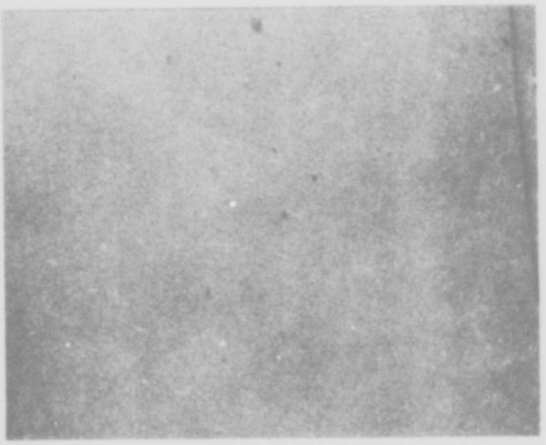

$50 \cdot 10^{-6}$ Inch Thickness

Figure 36. Porosity of Gold (Au1) Plate

bent to a 180° fold. The samples were then evaluated by use of a microscope at magnifications to 50X. Each sample that showed evidence of any visible cracking at 50X or below were labeled "cracked." Any separation of the plated deposit from the base metal at the same magnifications was designated as a "peeled" sample. All of the samples were held in vacuum at room temperature for about two weeks prior to the bend test. Table 9 gives the results of the bend and peel tests.

SALT FOG EXPOSURE

Samples were tested for salt fog exposure, and examined microscopically after 240 hours at 95°F in a 5% salt solution. Qualitative results and the final disposition are shown in Table 10. It should be noted that samples were classified as failed if, during the microscopic examination at 15X, any corrosion of the base metal was found or if the plate showed signs of pitting or corrosion products. For example, BAT samples when examined by eye appear excellent after the test, however, microscopic examination reveals some sacrificial corrosion of the tin especially in area of the bend. Close examination and critical evaluation also leads to some inconsistencies as in the case of Sample Number 11 where 50 x 10^{-6} of gold plate (Au1) is rated satisfactory in the bend but failed on the flat.

PHASE IV - SOLDERABILITY

INTRODUCTION

The electronics industry today is founded on the soldered joint. With the advent of high-reliability, solid-state devices attached to working circuits by solder joints, a minimum of two per device, the joint reliability becomes a significant factor in the equipment reliability. The relative ease with which the solder joining process can be automated, the decrease in size of microcircuits, and the subsequent increase in packaging densities make it imperative that the quality of the solder joint be designed into the manufacturing process. This quality must be designed in by choice of tested materials and process control rather than by inspection and rework of each and every minute solder joint. The performance characteristics of electrical components can be expressed in fairly precise quantitative terms, but the quality of the solder joint (solderability) has traditionally been specified in only rather vague terms. Disagreement between vendor and purchaser of microcircuit devices on the solderability of leads of these devices is common. There is ready agreement on device leads having excellent solderability or those having extremely poor solderability; however, large numbers of leads falling into the grey zone in between are subject to dispute. The aim

TABLE 9. BEND AND PEEL TESTS

Sample No.	Bend	Peel	Sample No.	Bend	Peel
1	Crack	No Peel	29	C	P
2	No Crack	-	30	N	-
3	N	-	31	C	-
4	N	-	32	N	-
5	N	-	33	N	-
6	N	-	34	N	-
7	C	N	35	N	-
8	C	N	36	N	-
9	C	N	37	N	-
10	C	N	38	C	-
11	N	-	39	N	-
12	N	-	40	N	-
13	N	-	41	C	N
14	C	Peel	42	N	-
15	C	-	43	N	-
16	N	-	44	C	P
17	N	-	45	N	-
18	N	-	46	C	-
19	N	-	47	C	-
20	C	N	48	N	-
21	C	N	49	C	-
22	N	-	50	N	-
23	N	-	51	C	-
24	N	-	52	N	-
25	N	-	53	N	-
26	N	-	54	N	-
27	N	-	55	N	-
28	C	N			

TABLE 10. RESULTS OF 240 HOUR SALT FOG EXPOSURE TEST

No.	Sample Finish	Base Metal	Flat (Surface)		Bend (Radius)	
			Pass	Fail	Pass	Fail
1	BAT-100	A		X		X
3	BAS-100	A		X		X
4	Au1-50	A		X		X
5	Au1-200	A	X		X	
6	Au2-50	A		X		X
7	Au2-150	A	X			X
8	BAT-100	A0		X		X
10	BAS-100	A0		X		X
11	Au1-50	A0		X	X	
13	Au2-50	A0		X		X
14	Au2-150	A0		X		X
30	BAT-100	B		X		X
32	BAS-100	B		X		X
18	Au1-50	B		X		X
20	Au2-50	B		X		X
21	Au2-150	B	X			X
22	BAT-100	B0		X		X
24	BAS-100	B0		X		X
25	Au1-50	B0		X		X
27	Au2-50	B0		X		X
28	Au2-150	B0	X			X
29	Au1-100 over NiS-30	A	X			X
15	Au1-10 over Au2-40	A		X		X
16	Au2-40 over Au1-10	A		X	X	
34	Au1-100 over NiS-30	A0	X			X

TABLE 10. RESULTS OF 240 HOUR SALT FOG EXPOSURE TEST
(Continued)

No.	Sample Finish	Base Metal	Flat (Surface) Pass	Flat (Surface) Fail	Bend (Radius) Pass	Bend (Radius) Fail
35	Au1-10 over Au2-40	A0		X		X
36	Au2-40 over Au1-10	A0		X		X
39	Au1-100 over NiS-30	B	X		X	
40	Au1-10 over Au2-40	B		X		X
41	Au2-40 over Au1-10	B		X		X
44	Au1-100 over NiS-30	B0		X		X
45	Au1-10 over Au2-40	B0		X		X
46	Au2-40 over Au1-10	B0		X		X
49	BAT-100	Cu		X		X
51	BAS-100	Cu		X		X
52	Au1-50	Cu	X			X
53	Au1-200	Cu	X			X
54	Au2-50	Cu		X		X
55	Au2-150	Cu	X			X

of this portion of the study was to attempt to define those characteristics of a lead and the preparation of a lead that will reliably yield excellent solderability, and further, to determine whether solderability can be measured quantitatively.

There are a number of methods used to measure the solderability of a component or surface, but these methods usually give a subjective measure of solderability. Some of these methods are discussed briefly below. Recent developments in methods to obtain a measure of quantitative solderability have been in the area of surface tension or wetting force testers. One such tool, the Meniscograph, also described below, was used in this study as one measure of solderability of the surface. Other methods such as

MIL-STD-883, Method 2003 and the Hot Iron Test, were used in this study for comparison with the results obtained from the Meniscograph.

The following definitions were used in this work:

(a) Solderability - A surface or component has been said to be solderable when a molten tin-lead solder will completely flow out in satisfactory time on the surface forming a continuous, permanent film, with a metallurgical bond at the interface, in the presence of an unactivated, water-white rosin-based flux. That is to say the surface is wetted and remains wetted by the solder.

(b) Wetting - has been defined as the formation of a smooth and continuous coating of solder on the surface of the metal forming a metallurgical bond at the interface between the metal and the solder. The surface or coating so formed should be of good lustre and have a minimum wetting angle as defined below.

(c) Wetting Angle - The dihedral angle formed by the original surface of the metal and the surface of the formed solder coating at the border of the solder coating.

(d) Dewetting - The drawing back of the formed solder coating into globules or ridges having fairly high wetting angles and leaving behind a thin coating of solder over the surface.

(e) Non-Wetting - The formation of open areas of exposed original base metal generally with solder ridges around the exposed areas with high wetting angle. Those areas bridged by the solder coating where no metallurgical bond has formed should also be called non-wet areas.

TESTING FOR SOLDERABILITY

Bead or Globule Test

This method measures the time required for a small premeasured ball of molten solder to wet around a wire or component lead as it is lowered into the ball. With later versions of this method, the time is measured electronically and gives a more accurate measure of the solderability. This method is used extensively in Europe but not in the United States.

Pessel Spread Factor Test

This test allows a specially prepared solder specimen to spread on the surface of the test specimen under controlled conditions of time and temperature. After cooling, the area of spread is measured and compared with an index which gives an indication of the solderability of the surface. The larger the spread, the better the solderability. Because of the time consumed in measuring the spread area, Pessel and others estimate the area by measuring the maximum height of the spread and calculating the spread factor as:

$$\text{spread factor } (\%) = 100\,(D-H)/D$$

where D equals the diameter of a sphere with a volume equal to the volume of the solder preform used and H equals the measured height. Pessel has defined a qualitative relationship of spread factor to solderability for copper and this would have to be redefined for nickel alloys.

Edge-Dip Test

The edge-dip test is specified in the following:

(a) MIL-STD-202, Method 208

(b) MIL-STD-883, Method 2003

(c) Institute for Printed Circuits (IPC) Test Method S-801

(d) Electronics Industries Association (EIA) Specifications:

RS-319 for Printed Wiring Boards
RS-178 for Component Leads

In all these specifications the edge-dip test is similar in that the test sample is dipped vertically into a pot of molten solder for a predetermined time, and then withdrawn. The conditions, such as temperature of the pot, time in the pot, immersion and withdrawal rates are all closely controlled. An automatic dipping device, as shown in MIL-STD-202, can be used to control the time and rate factors. The usual criteria for acceptable solderability are: minimum of 95% solder coverage of dipped surface, no concentration of small pin holes, no dewetted areas, no rough spots or non-wetted base metal. This assessment is made after the sample is removed from the bath and the solder has solidified.

Tin Research Institute (T.R.I.) Test

This test is a wetting time solderability test, usually employing flat specimens. This test determines the time required for complete wetting of the sample when immersed in solder. The action of the wave soldering machine is simulated and the time of the immersion can be measured electronically. This method usually is used on a Go/No Go basis where a wetting time is selected and the sample is required to wet in this length of time. Again, in this test, the assessment of the soldering surface is made after the solder coating has solidified.

Hot Iron Test

The purpose of this test is to determine the solderability of previously tinned samples. A determination is made as to the ability of the solder to flow and to be moved uniformly. The samples used in this test must be in a tinned condition and should require no additional solder. Tinned samples exhibiting a coating of solder are fluxed and heated with a well tinned iron. During the heating cycle the soldering iron is moved along the edges and surface of the sample while being observed microscopically at 10-15X magnification. Poorly wet, dewet or highly wettable materials are easily differentiated by proper application of this test method.

Meniscograph Test

The original idea for this type of equipment was presented by L. G. Earle in 1945. The Meniscograph or wetting force tester gives a graph of the vertical wetting force applied to a sample by the molten solder versus time; i.e , it measures the change in vertical wetting forces acting on a sample during the soldering by edge-dipping. This record of the wetting process may be used to obtain the following information about the wetting process:

(a) The time required to commence wetting

(b) The wetting rate

(c) The equilibrium wetting force

(d) The time required to reach equilibrium

SELECTION OF SOLDERABILITY TEST METHOD

The Meniscograph was selected for this study as one measure of the solderability of the sample surface. Many of the test methods described are limited to specific shaped samples. All methods, except for the Meniscograph

are somewhat subjective if not in the final results obtained, then because of an arbitrary end point, the significance of which is sometimes in doubt. The only process which gives a quantitative result of the soldering process versus time is the Meniscograph.

Many of the above methods, although useful in specific applications, do not provide a numerical measure of solderability, but rather require a visual and subjective interpretation of the results. The edge-dip test of MIL-STD-883 and the Hot Iron test previously described were run on some samples for comparison and correlation with the results obtained from the Meniscograph.

THE MENISCOGRAPH TEST OF SOLDERABILITY

Principles of the Meniscograph Test[10]

The basic phenomenon of wetting, as explained in classical texts, is shown in the state of equilibrium in Figure 37.

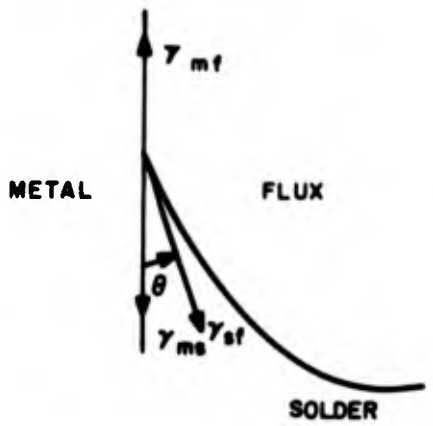

Figure 37. Equilibrium State of Wetting

In the presence of flux, γsf is the surface tension of the solder/flux interface, γmf is the surface tension of the metal/flux interface and γms is the surface tension of the metal/solder interface. In the state of equilibrium, the following equation holds:

$$\gamma mf = \gamma ms + \gamma sf \cos \theta$$

[10] Mayhew, A. T. and Wicks, G. A., Solderability and Contact Angle, Great Baddow Essex, U.K., Marconi Electronics Ltd.

where θ = contact angle at the line where all three phases of solder, metal and flux meet.

Changes in γmf and γms, which require large amounts of energy to change the surface area of the metal, are revealed by changes in their equilibrium with γsf. Hence, the solderable quality of the metal surface is revealed by changes in the shape of the solder meniscus formed in the equilibrium state. Thus, for a given solder alloy, flux and constant temperature, changes in the condition of the metal surface will be reflected in changes in the contact angle θ. Hence, the wetting force, F. measured by the Meniscograph will be resolved by the interfacial tension of the solder/flux holding the collar of solder above the surface of the solder pot.

$$F = \gamma mf - \gamma ms = \gamma sf \cos\theta$$

$$F = \gamma sf \cos \theta$$

Thus, changes in the surface condition of the metal, the solderability of the surface, are reflected by changes in the vertical wetting force, F.

Equipment Operation

The test sample is suspended vertically from the instrument weighing system. The solder bath is raised to meet the sample and is controlled so that the sample is immersed in the solder to a predetermined depth. This immersion of the sample produces an upward force on the sample before wetting occurs and this is equal to the weight of the solder displaced by the specimen plus the downward meniscus of the solder surface. As wetting commences, the solder runs up the surface of the test sample until it finally reaches an equilibrium with an upward meniscus plus the downward force equal to the weight of the solder collar held up around the sample minus the weight of the solder displaced by the sample below the surface of the solder.

The weighing system converts loads to electrical output and this output is fed to a strip-chart recorder where a continuous record of the wetting force versus time is obtained.

The Meniscograph Curve

Figure 38 is an idealized Meniscograph curve with the different stages of testing process indicated.

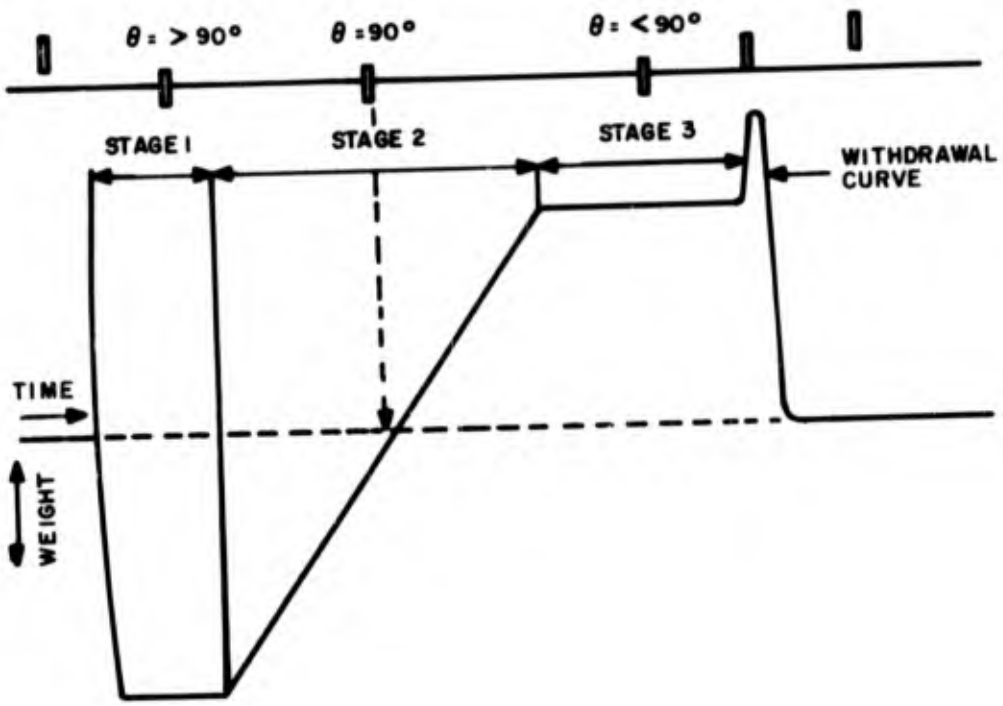

Figure 38. Idealized Meniscograph Curve

The three stages indicated in Figure 38 are as follows:

(a) Stage 1

The specimen is partially immersed in molten solder, and a downward meniscus is formed against the specimen surface while it remains unwetted. At this stage the specimen suffers a hydrostatic up thrust, or loss in weight equal to the weight of solder displaced.

(b) Stage 2

As wetting takes place, the contact angle decreases and solder moves up the sides of the specimen, producing a gradually increasing downward force.[11]

[11] Johnson, D. and Robinson, W., "Solderability Evaluation Instrument Description and Typical Curves," Raychem Pub., Aug. 2, 1971.

(c) Stage 3

Equilibrium stage.

Use of the X-Y Recorder

Although the Meniscograph is equipped with a strip-chart recorder, this study required a comparison of a number of Meniscograph curves. The overlaying of strip-chart curves on a light table or zerox copies proved very troublesome. Research in the area of quantitative solderability turned up investigators[11] who used an X-Y recorder instead of the normal strip-chart recorder. It was found that for this study the X-Y recorder proved very useful. The recorder was wired into the Meniscograph circuit in such a way that the recorder sweep was triggered when the Meniscograph was started. In this way, using either the X or Y axis as a sweep axis and the other axis as a recorder of the output of the weighing system of the Meniscograph gave a continuous record of wetting force versus time (at a known sweep rate).

Using samples of constant length causes triggering of the X-Y recorder at the same point in the test cycle, and hence, allows Meniscograph traces of different samples to be time indexed on the same sheet of graph paper. This equipment allows for a better presentation of results without retracing curves on a single sheet of paper.

The use of the Meniscograph in this study was aimed primarily at determining the effect of aging, both ambient and accelerated, of plated samples on the solderability of these surfaces. Since a selection of the flux used and temperature of the solder bath, as well as other variables in the soldering operation affect the shape and hence the numerical values of the Meniscograph curve, illustrations of some of these effects will precede the discussion of the Meniscograph curves.

Repeatability of Curves and Samples

In order to determine the reproducibility of the Meniscograph curve and the uniformity of samples plated in the baths, standard racks containing the usual six samples each were plated per schedule and were immediately tested on the Meniscograph. One such set of curves, one for each sample, for BAT plating is shown in Figure 39. Some variations observed are caused by slight differences in sample size, edge effects, placement of the sample in the Meniscograph holder, etc. For example, individual sample lines shown at the start of test when the sample is plunged into the solder bath differ slightly because the distance between the sample and solder bath differed at time zero.

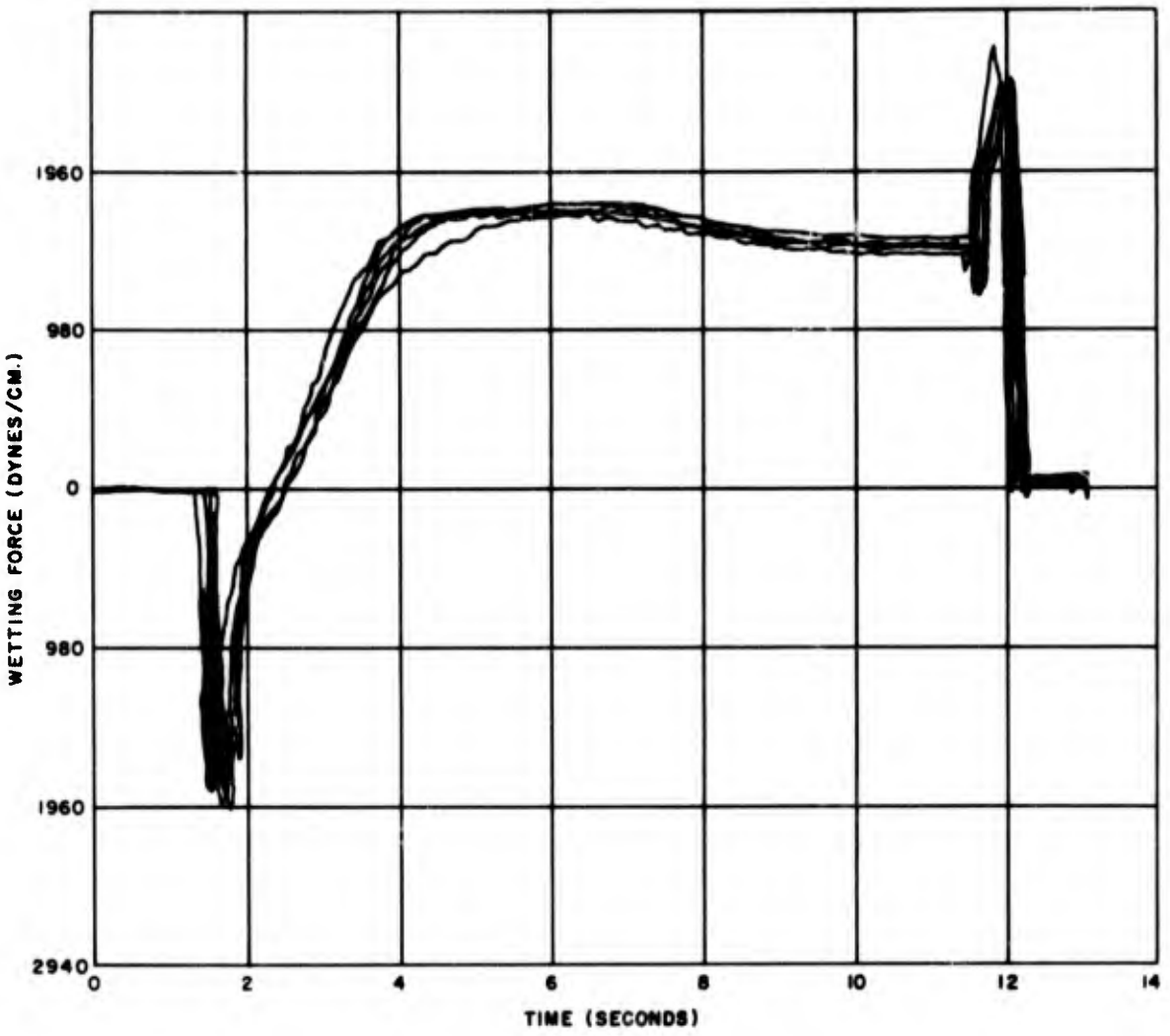

Vendor A Material
BAT Plated, 100 Microinches Thick
Flux: Water White Rosin
Solder Bath Temperature: 260° C

Figure 39. Six Sample Traces of Samples Plated Simultaneously

FLUX ACTIVITY

One of the advantageous features of the Meniscograph is its ability to measure the activities of different fluxes on the various surfaces of materials. Very simply stated, the function of a flux in a soldering operation is twofold; it reduces the surface tension of the solder and it cleans the surface to be soldered. For relatively clean surfaces, the distinction between differently activated fluxes should be small; for relatively dirty or oxidized surfaces, a clear distinction should be observed in the use of fluxes of different activities. These different activities can be observed in Table 11 where the time for the meniscus to reach a position of $\theta = 90°$ is taken from the Meniscograph curve as that value of time in seconds where the curve crosses the zero line of the wetting force ordinate.

TABLE 11. FLUX ACTIVITY OF DIFFERENTLY PREPARED COPPER SURFACES

Flux	Time for $\theta = 90°$ (seconds)			
	Degreased Only	3 Months at Room Temperature	Oven-Aged 1 Hr. 600°F	Chemically Cleaned
Water-White Rosin	>10.0	2.0	0.80	0.40
Mildly Activated Flux	0.80	0.25	0.40	0.25

Curves showing the rate of wetting of copper samples aged at room temperature for three months and fluxed with water-white rosin, mildly activated, and fully activated flux are shown in Figure 40.

EFFECT OF TEMPERATURE OF SOLDER BATH

Increases in the temperature of the solder bath not only increase the rate of reaction of the solder and the metal surface, but also decrease the surface tension of the solder and increase the rate of reaction of the flux on the metal surface. The sum total of these activities can be observed in Figure 41 for four identically prepared samples fluxed using two different fluxes, a water-white rosin and a mildly activated flux, and soldered at two different temperatures, 230°C and 260°C. Increases in temperature of the solder bath are much more effective in increasing the rates of reaction of the slower action fluxes.

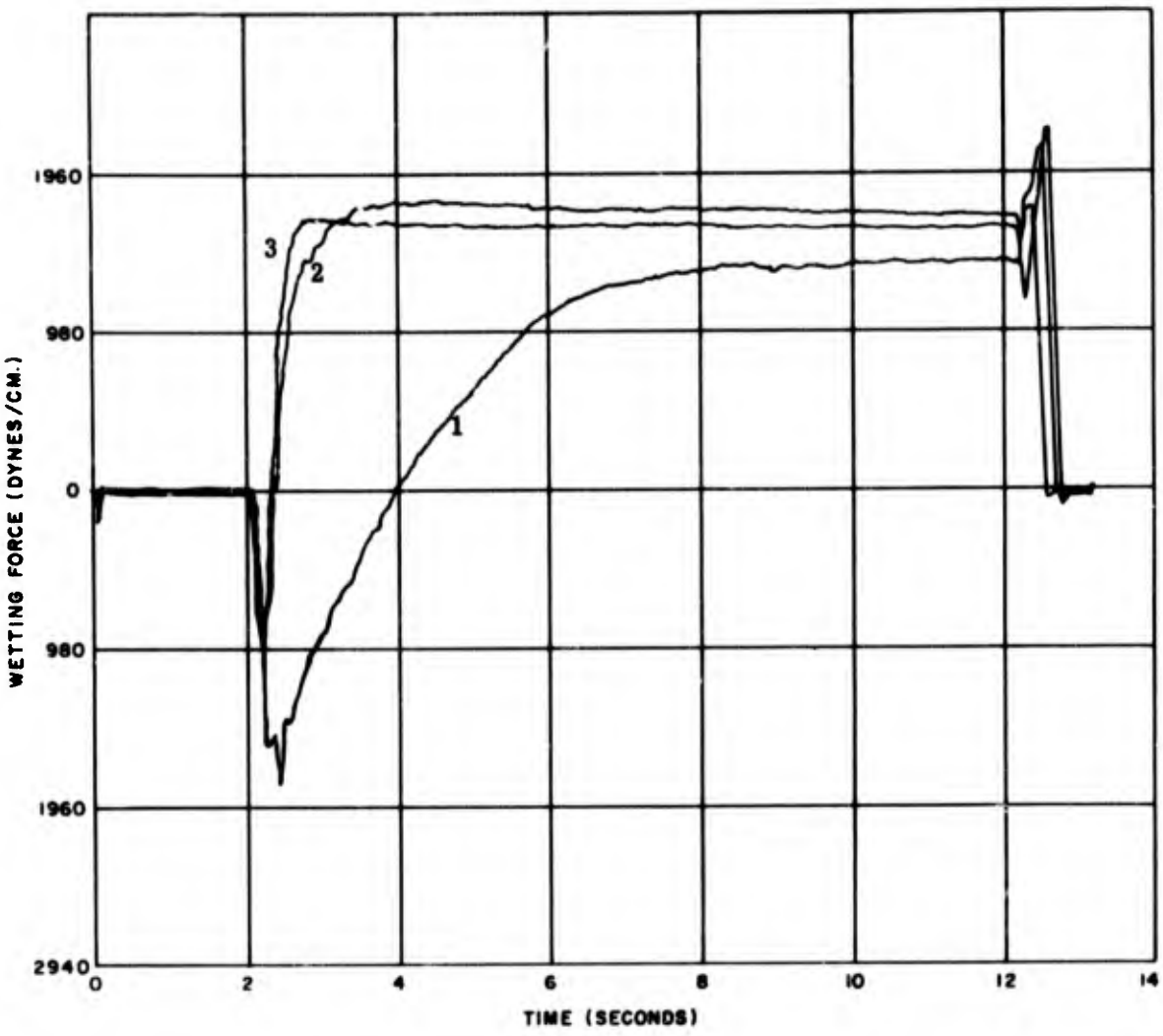

Base Material: Copper Oxidized 3 Months at Room Temperature
Solder Bath Temperature: 260°C
Curve 1: Water White Rosin
Curve 2: Mildly Activated Flux
Curve 3: Fully Activated Flux

Figure 40. Effect of Type of Flux on Oxidized Copper

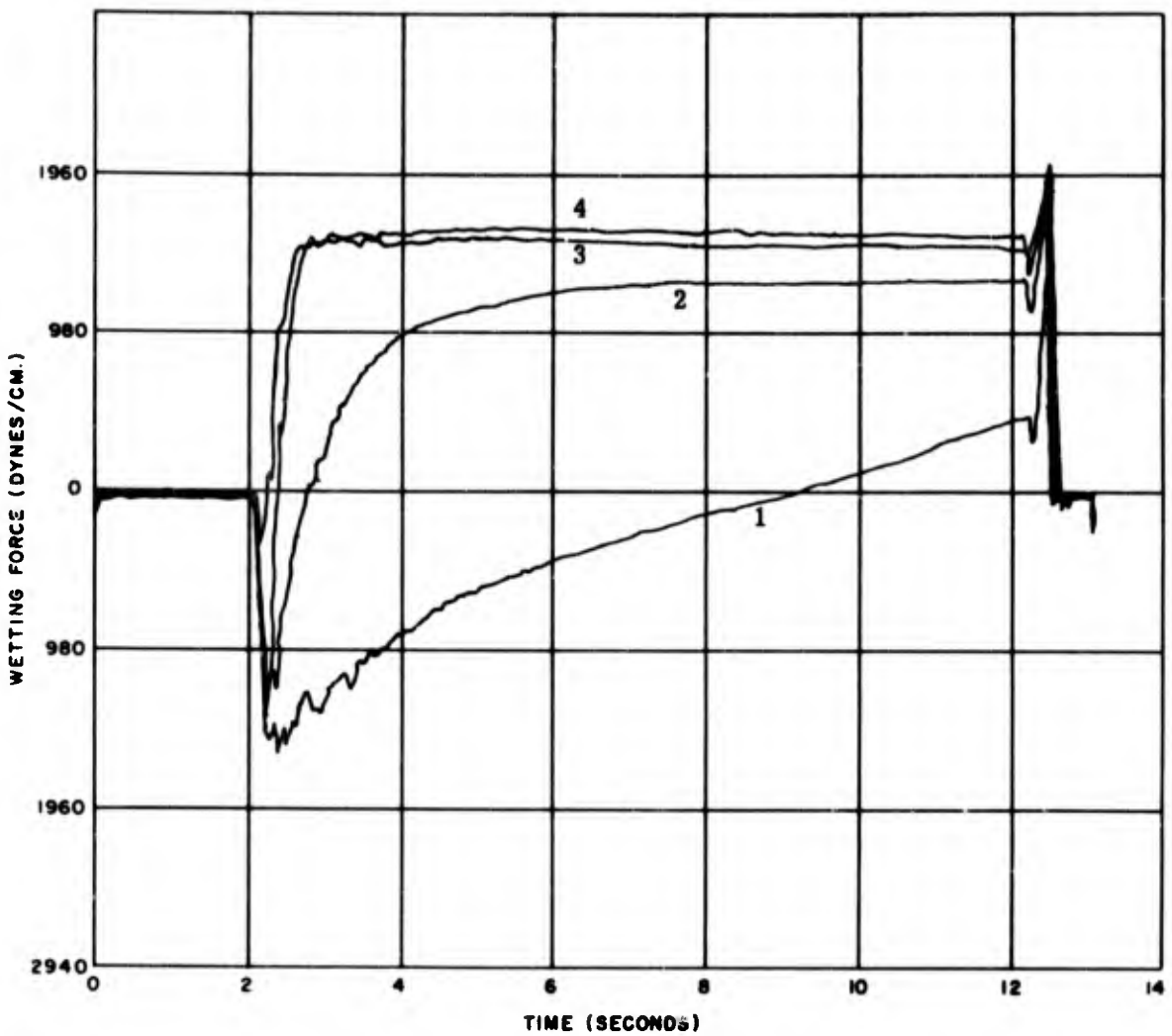

Base Material: 0.012 Inch Chemically Cleaned Copper
Curve 1: Water White Rosin Flux. Solder Bath Temperature: 230°C
Curve 2: Water White Rosin Flux. Solder Bath Temperature: 260°C
Curve 3: Mildly Activated Flux. Solder Bath Temperature: 230°C
Curve 4: Mildly Activated Flux. Solder Bath Temperature: 260°C

Figure 41. Effect of Temperature, Two Different Fluxes

EFFECT OF SAMPLE SIZE

The Meniscograph basically is a sensitive precision electronic balance capable of continuously reading weight changes. Although the weight range of the instrument is rather large, there are controlling factors that limit the sample size the instrument can accommodate, such as mechanical and electronic noise in the instrument and chart recorder as well as the capacity of the weighing mechanism.

Effects of sample size on the Meniscograph curve can be observed in Figure 42 where all other factors such as type of base metal, flux, solder temperature, depth of immersion, etc. were kept constant. The samples chosen were chemically cleaned copper, each 0.018 inch thick, but with widths of 1 inch, 1/2 inch and 1/4 inch. It can be observed that as the width of the sample decreased, the final height of the curve, i.e., the weight of the meniscus, decreases. Furthermore, the time to reach $\theta = 90°$ also decreases, presumably because of heat transfer not only in the sample itself but perhaps to a small degree, in the highly localized lowering of the solder bath temperature adjacent to the sample. Immersion depth appears not to, and should not, have any effect on the wetting force value.

EFFECT OF CLEANING

The importance of cleaning prior to soldering cannot be overemphasized. Cleaning prior to the application of flux is mandatory, since the measurement of degree and type of contamination is not only extremely difficult but time consuming. The effect of surface cleaning already has been illustrated in Table 11 and Figure 40 under the discussion of flux activity. Large differences in the degree of surface cleanliness can be illustrated by adjusting the activities of the fluxes used.

MENISCOGRAPH RESULTS OF PLATED SOLDERABILITY SAMPLES

In this section examples of Meniscograph curves will be presented for those platings described in the section on Phase III - Plating. For the "as plated" condition, comparisons of types of plating on copper and ASTM-F15 alloy will be made. The effect of the thickness of the plating, the type of plating, and the use of an underplating or overplating upon the Meniscograph curve will be shown. Also shown will be the effect of exposure of these samples to ambient atmospheres upontypical Meniscograph curves.

Comparison of Types of Coatings, As-Plated Samples

Figures 43 and 44 show the effect of wetting force versus time for the four basic types of platings on copper base material and ASTM-F15 alloy

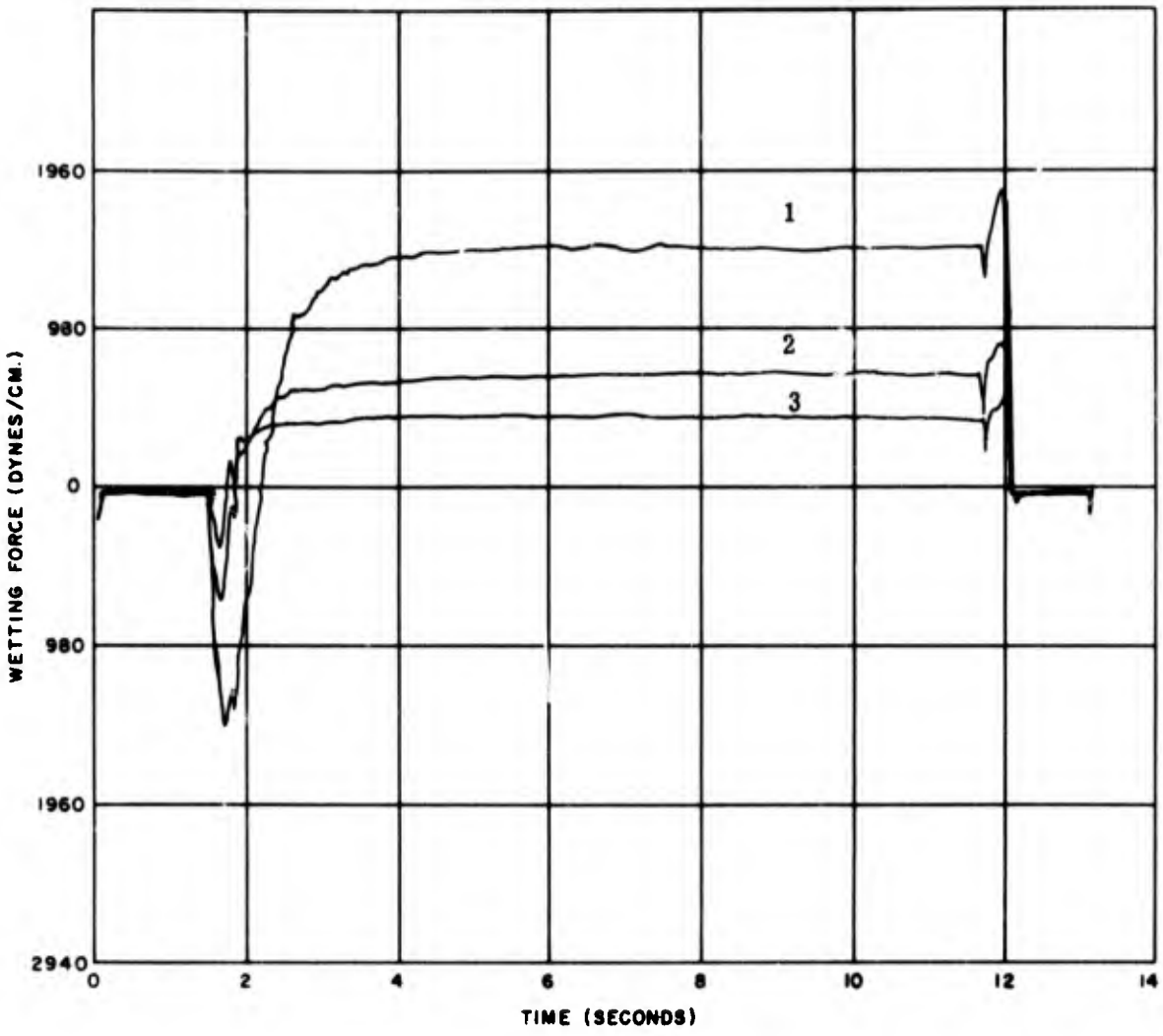

Base Material: Chemically Cleaned Copper
Solder Bath Temperature: 230°C

	Sample Size (inches)		
	L	W	Th.
Curve 1:	1 x	1 x	0.012
Curve 2:	1 x	0.50 x	0.012
Curve 3:	1 x	0.25 x	0.012

Figure 42. Effect of Sample Size

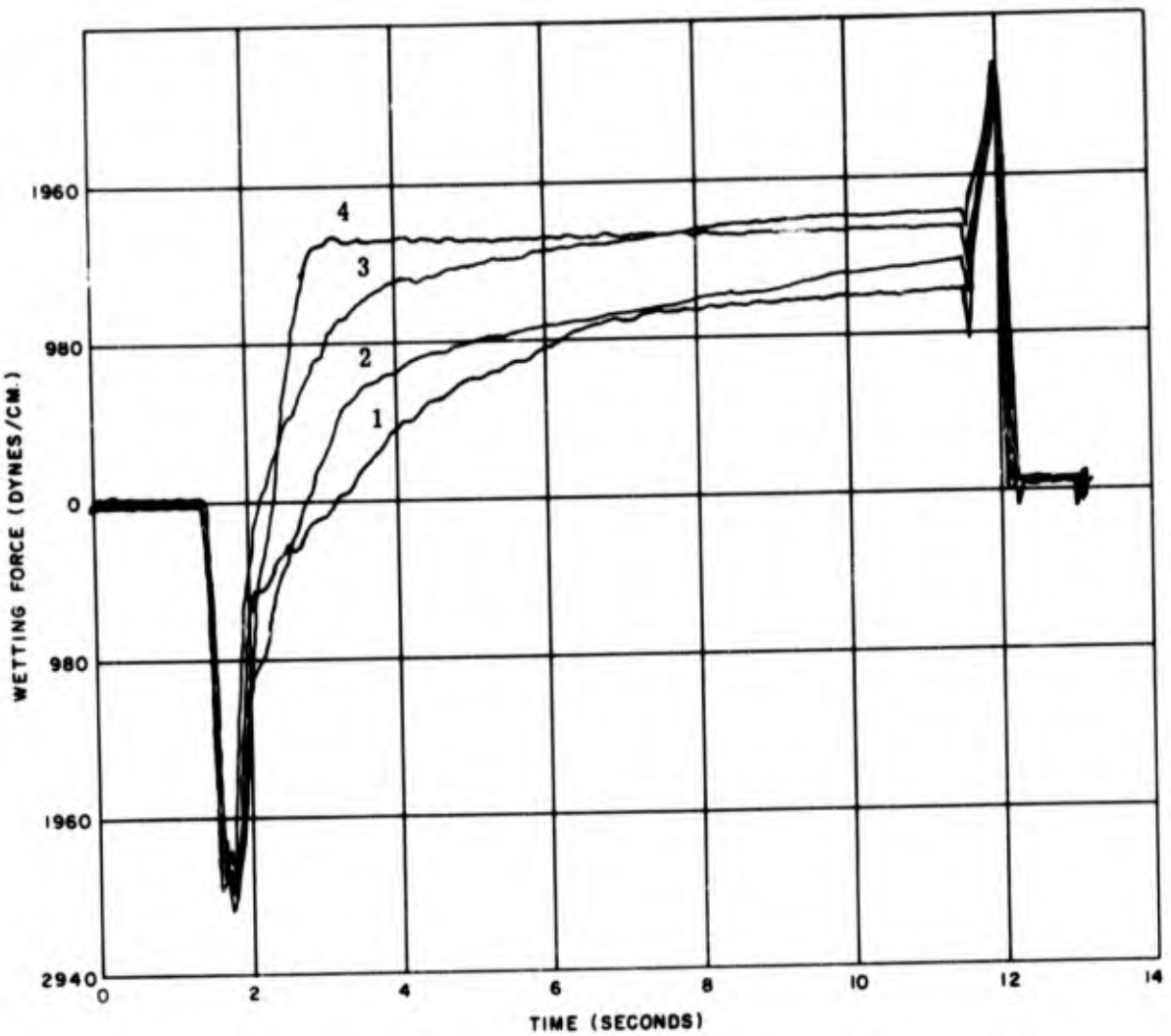

Base Material: Copper
Flux: Water White Rosin
Solder Bath Temperature: 260° C
Curve 1: Au1, 50 · 10^{-6} in.
Curve 2: Au2, 50 · 10^{-6} in.
Curve 3: BAT, 100 · 10^{-6} in.
Curve 4: BAS, 100 · 10^{-6} in.

Figure 43. Effect of Type of Material Plated (Copper Base Material)

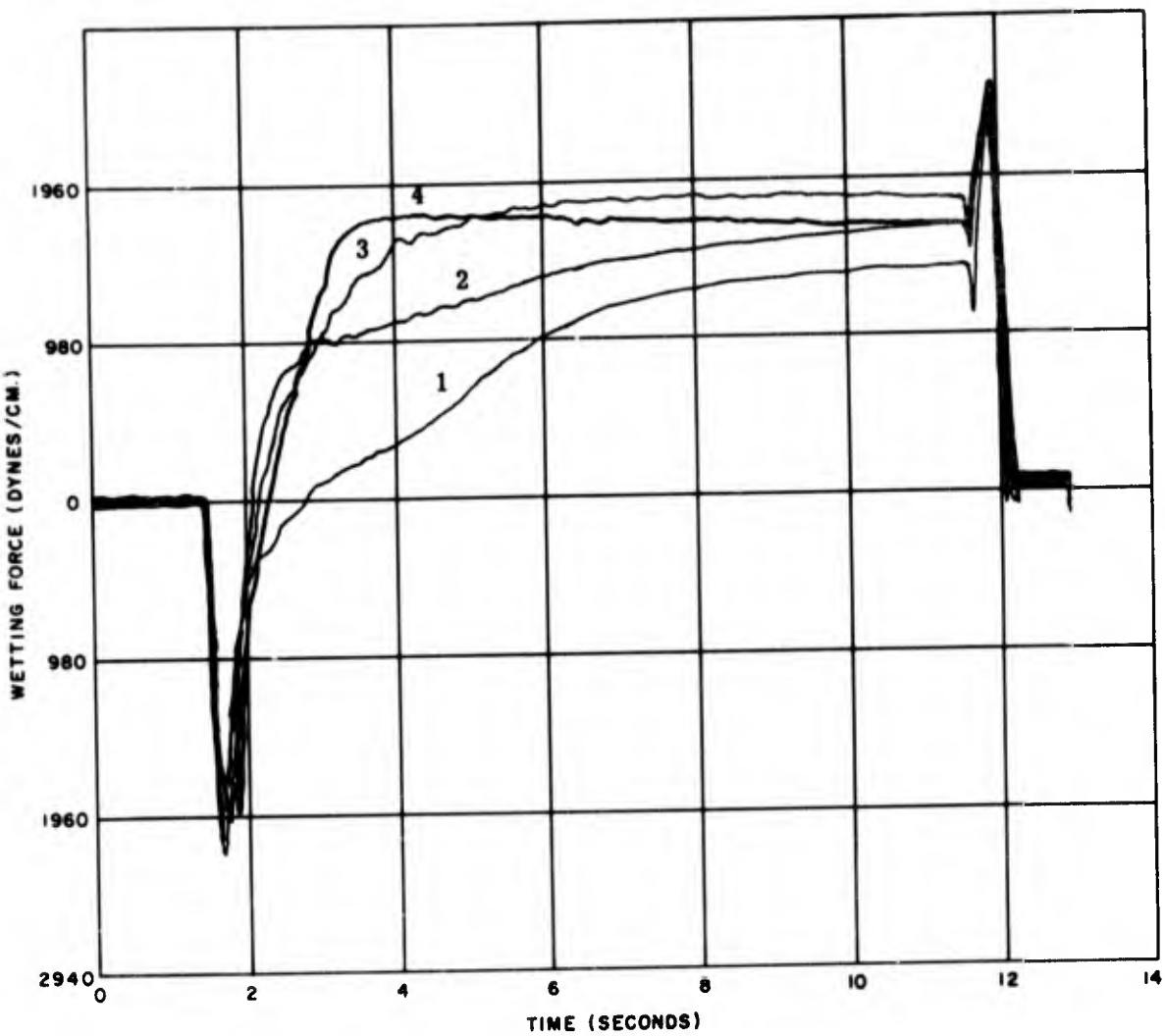

Base Material: ASTM-F15 Fe-Ni-Co
Flux: Water White Rosin
Solder Bath Temperature: 260° C
Curve 1: Au2, $50 \cdot 10^{-6}$ in.
Curve 2: Au1, $50 \cdot 10^{-6}$ in.
Curve 3: BAT, $100 \cdot 10^{-6}$ in.
Curve 4: BAS, $100 \cdot 10^{-6}$ in.

Figure 44. Effect of Type of Material Plated (ASTM-F15 Fe-Ni-Co Base Material)

base material. These curves are typical of those found for the as-plated condition. In the as-plated condition, the typical Meniscograph curve is basically independent of the vendor of the ASTM-F15 alloy base material whether the base material was in the as-received condition or had been previously oxidized with the oxidation removed.

For copper base material (Figures 43 and 44), the typical (for this experiment) Meniscograph curves of BAS reach equilibrium faster than the other types of plating. This is followed closely by BAT and then by Au2 and Au1.

For ASTM-F15 alloy base material the same order exists, except that the BAT curve is followed closely by Au1 and then Au2. It was noted (as shown on Figure 44) that with the fuseable BAS coating, a drop was sometimes obtained in the wetting force, presumably after equilibrium was reached.

Comparison of Thickness of Coating, As-Plated Samples

Figures 45, 46 and 47 show the effect of different thicknesses of BAT, gold type Au1 and gold type Au2. As shown in Figure 45, there is little difference in the Meniscograph curve for the samples with 100 microinches and 250 microinches of BAT.

The effect of the thickness of gold type Au1 on the shape of the Meniscograph curve is displayed in the earlier stages of the curve in Figure 46. The final curve height is generally slightly lower for the greater thickness of plate.

Curves for different thicknesses of gold type Au2 are shown in Figure 47. The initial stages of wetting are about the same, with the wetting force dropping off in the later stages for the greater thickness of the coating. The effect of thickness appears to be significantly greater for gold coatings than for BAT. No comparison was made for BAS because it was used in only one thickness.

Comparison of Duplex (Under and Over) Platings, As-Plated Samples

Figure 48 shows a Meniscograph curve for Au1, 10 microinches thick, as an underplating and an overplating on Au2, 40 microinches thick. Typical curves for the 50 microinches of Au1 and Au2 are shown for comparison. Also shown is the curve of Au1 as an overplate; this curve follows closely the curve of Au1 (50 microinches). It should be noted that in the later stages of wetting, the wetting force drops down to the final height of the underplating curve. This characteristic of falling off to the underplating curve height was

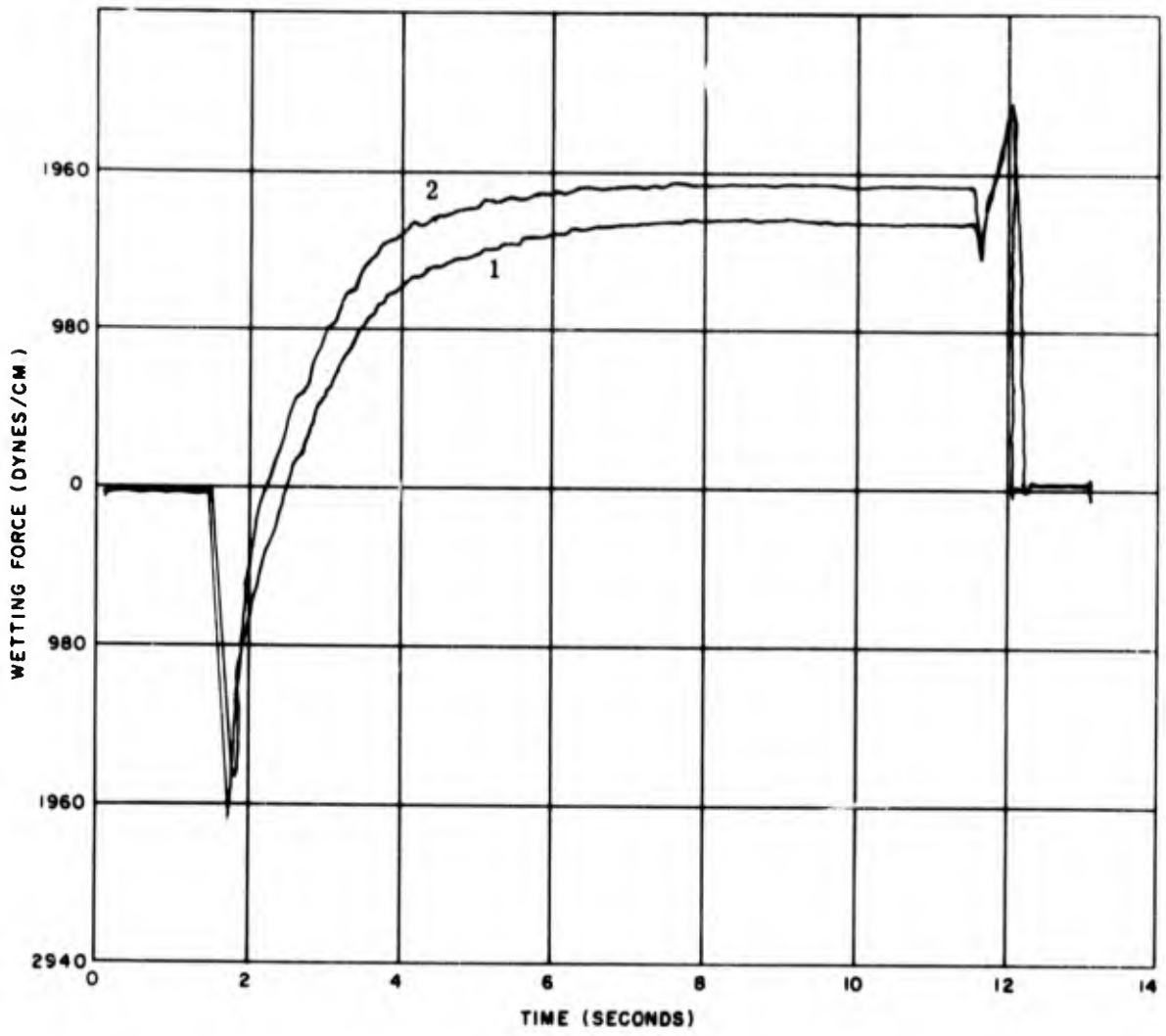

Base Material: ASTM-F15 Fe-Ni-Co
Flux: Water White Rosin
Solder Bath Temperature: 260°C
Curve 1: BAT, 250 · 10^{-6} in.
Curve 2: BAT, 100 · 10^{-6} in.

Figure 45. Effect of Thickness of Plate (ASTM-F15 Base, BAT Plate)

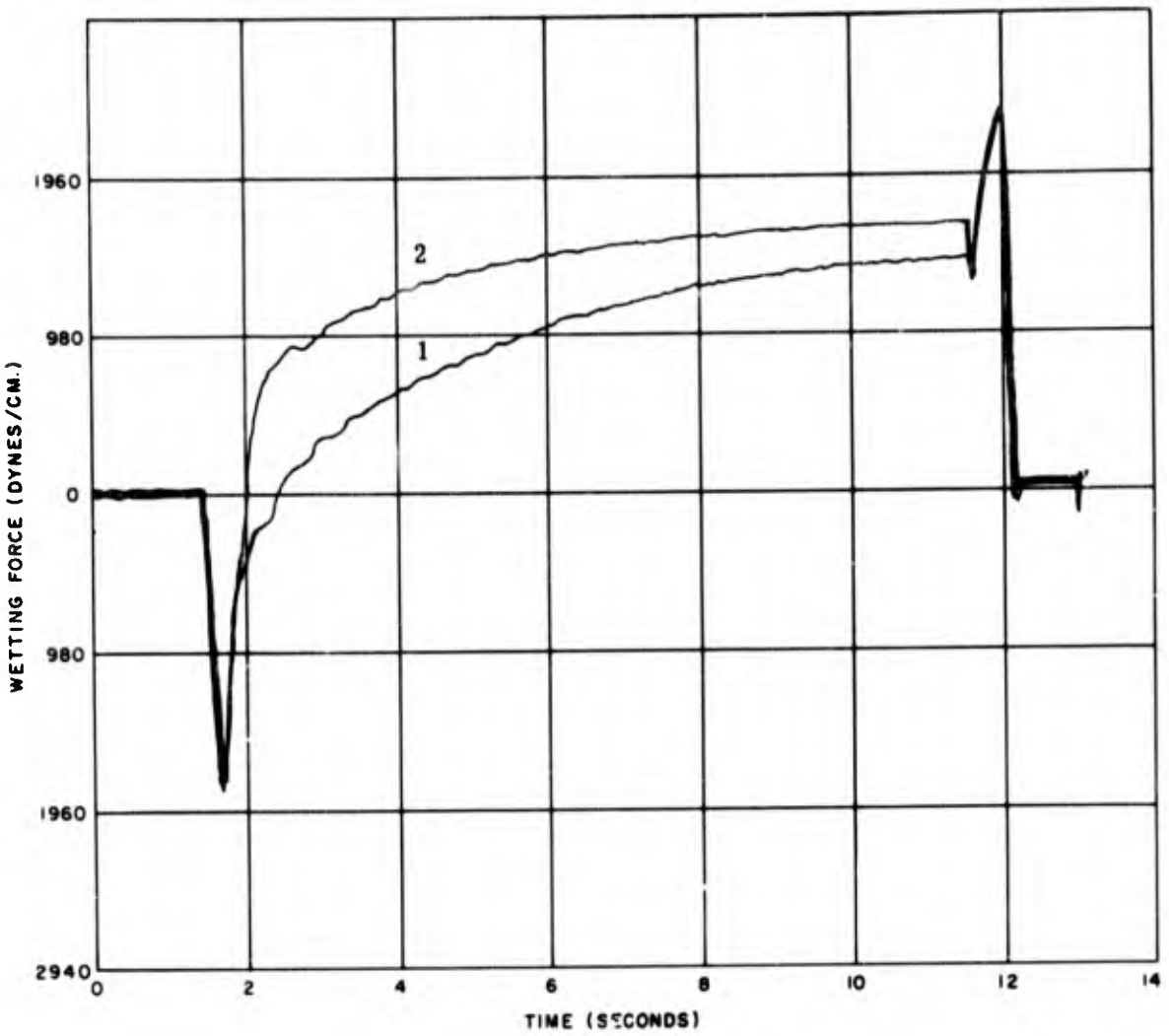

Base Material: ASTM-F15 Fe-Ni-Co
Flux: Water White Rosin
Solder Bath Temperature: 260° C
Curve 1: Au1, $200 \cdot 10^{-6}$ in.
Curve 2: Au1, $50 \cdot 10^{-6}$ in.

Figure 46. Effect of Thickness of Plate (ASTM-F15 Base, Au1 Plate)

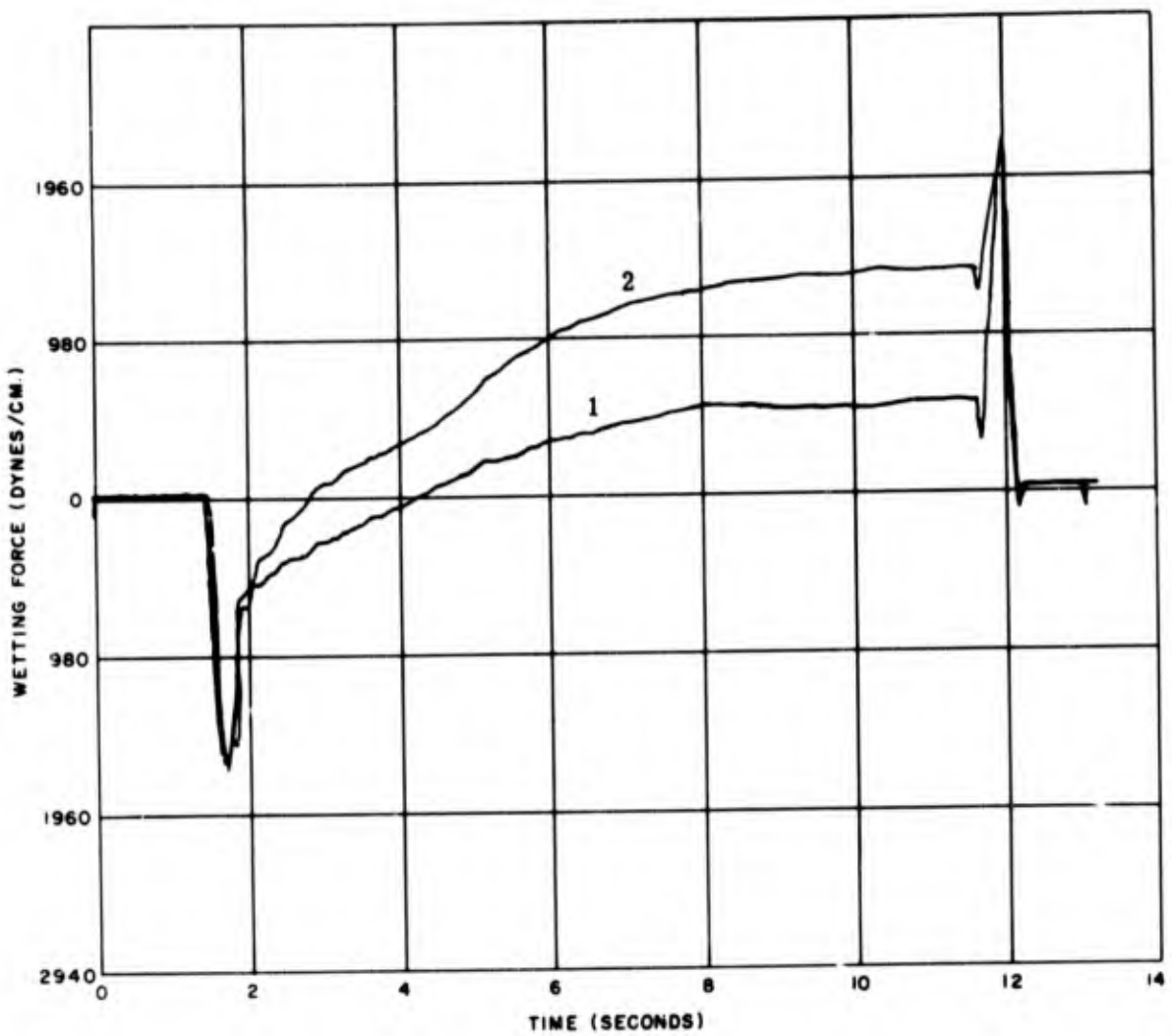

Base Material: ASTM-F15 Fe-Ni-Co
Flux: Water White Rosin
Solder Bath Temperature: 260° C
Curve 1: Au2, $150 \cdot 10^{-6}$ in.
Curve 2: Au2, $50 \cdot 10^{-6}$ in.

Figure 47. Effect of Thickness of Plate (ASTM-F15 Base, Au2 Plate)

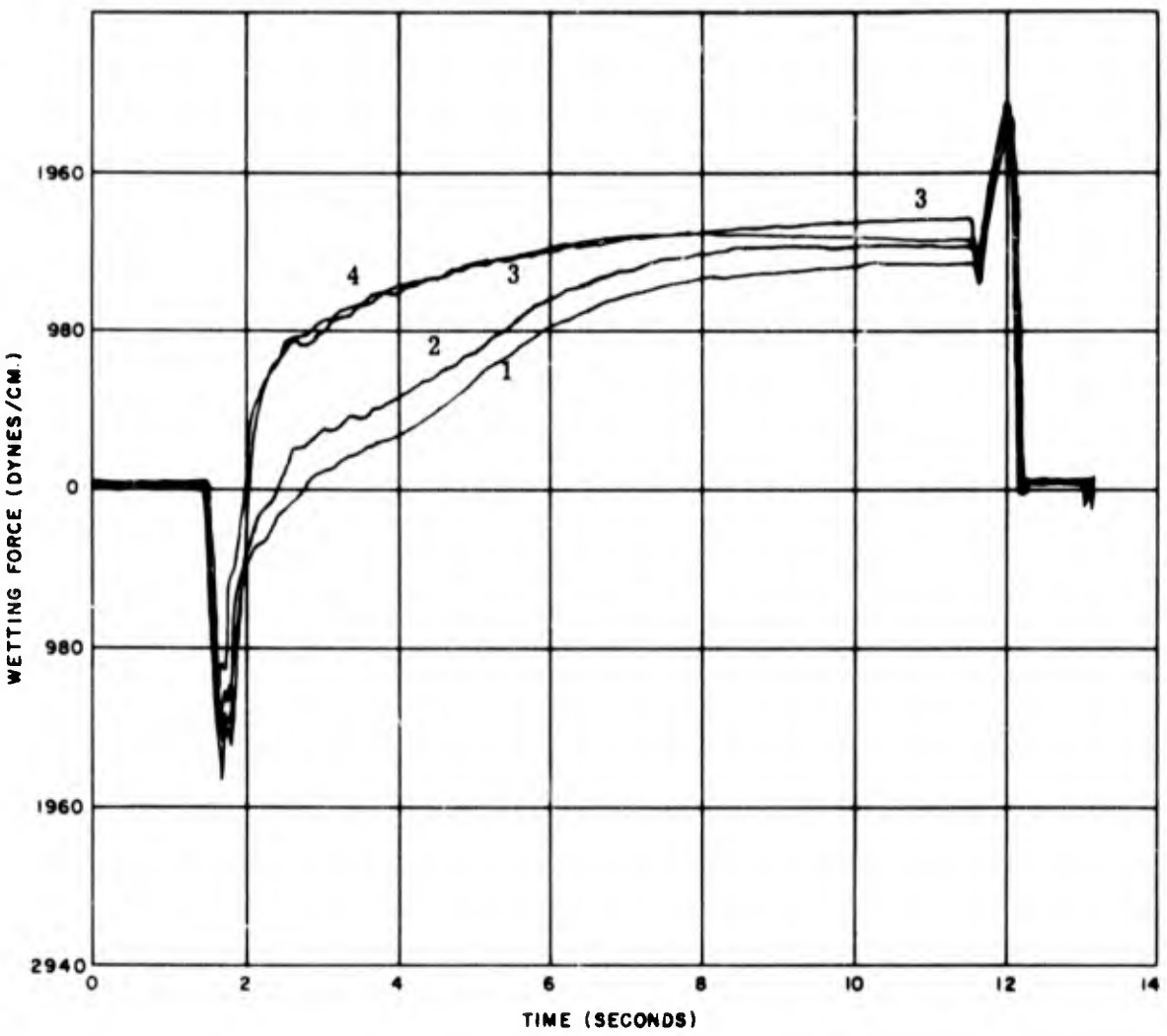

Base Material: ASTM-F15 Fe-Ni-Co
Flux: Water White Rosin
Solder Bath Temperature: 260° C
Curve 1: Au2, $50 \cdot 10^{-6}$ in.
Curve 2: Au2, 40 over Au1, 10 ($\cdot 10^{-6}$ in.)
Curve 3: Au1, $50 \cdot 10^{-6}$ in.
Curve 4: Au1, 10 over Au2, 40 ($\cdot 10^{-6}$ in.)

Figure 48. Effect of Duplex Plates (10 Microinches of Au1 Over or Under Au2)

noticed on other samples overplated with Au1; however, not all samples overplated with Au1 exhibited this trend. The curve of the underplating of Au1 on Au2 shown in Figure 48 follows closely that of the basic curve of Au2 (50 microinches) with only a slight change in curve height.

Figure 49 is similar to Figure 48 and presents the same type of information except for thicker duplex coatings. Also shown in Figure 49 are curves of gold type Au1, 100 microinches thick, with a nickel undercoat 30 microinches. The curves for the thicker gold coating are reproduced here for comparison with the thicker duplex coatings. Curves of each of the thicker duplex coatings are given in order to show some of the variability obtained with these types of gold coatings.

STEAM AGING

Meniscograph curves illustrating a gradual decrease in the wetting of 20×10^{-6} inches of gold, Au1, plated samples aged for 0, 2, and 4 hours in a steam bath are shown in Figure 50. The thickness of plate shown above was selected on the basis of obtaining some porosity of plate for possible reaction of the base metal to the steam atmosphere. The curves do show a gradual decrease in wetting rate with an increase in time in the steam atmosphere; however, samples with a thicker plate, 50×10^{-6} inches, aged for the same length of time yielded curves (not shown) with much greater crowding. Not all curves for other plating thicknesses when steam aged produced the consistency shown above, but these differences in reaction to both solderability and steam have been attributed to differences in porosity or differences in plate purity or thickness, despite attempts to make all samples uniform. There was no evidence of dewetting on any of the samples used in these steam aging tests. Table 12 gives, in tabular form, the decrease in wetting time and wetting force with an increase in steam atmosphere exposure.

EFFECT OF AMBIENT ATMOSPHERES ON SOLDERABILITY

The purpose of this phase of the experiment was to identify those coatings commonly found on lead materials, which would show the best solderability after exposure to room temperature storage. It also was desirable to evaluate several solderability tests using these or similar samples.

Two series of plated 1 inch x 1 inch samples sufficient for 0, 4, 8, 12 and 16 week exposures were placed in two different environments, namely a normal factory atmosphere and a slightly more corrosive laboratory atmosphere for room temperature exposure. Longer exposure times were considered and were desirable; however, time limitations negated these studies.

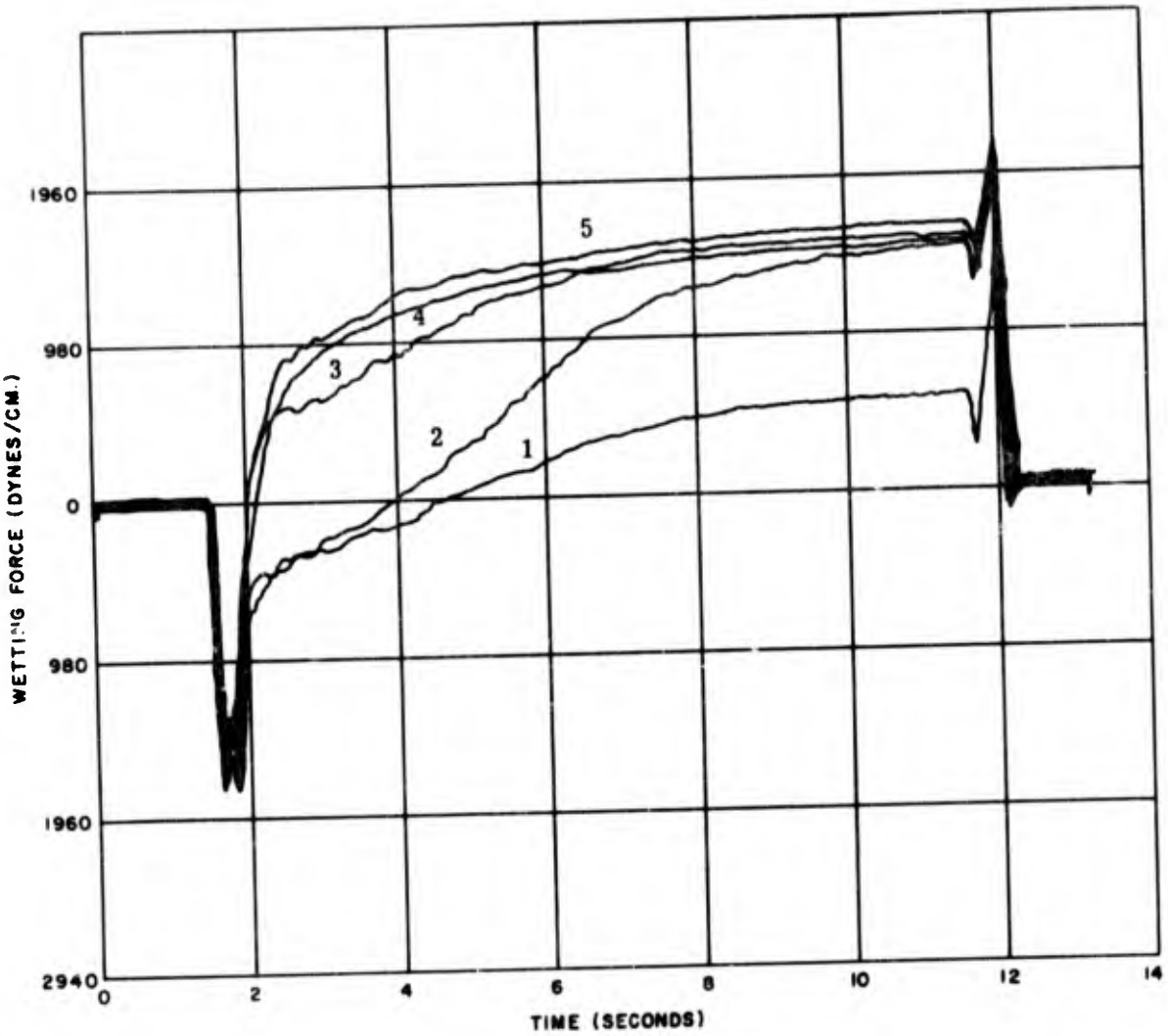

Base Material: ASTM-15 Fe-Ni-Co
Flux: Water White Rosin
Solder Bath Temperature: 260° C
Curve 1: Au2, 150 · 10^{-6} in.
Curve 2: Au2, 80 over Au1, 20 (· 10^{-6} in.)
Curve 3: Au1, 20 over Au2, 80 (· 10^{-6} in.)
Curve 4: Au1, 100 over NiS, 30 (· 10^{-6} in.)
Curve 5: Au1, 200 · 10^{-6} in.

Figure 49. Effect of Duplex Plates (20 Microinches of Au1 Over or Under Au2; 100 Microinches of Au1 Over NiS)

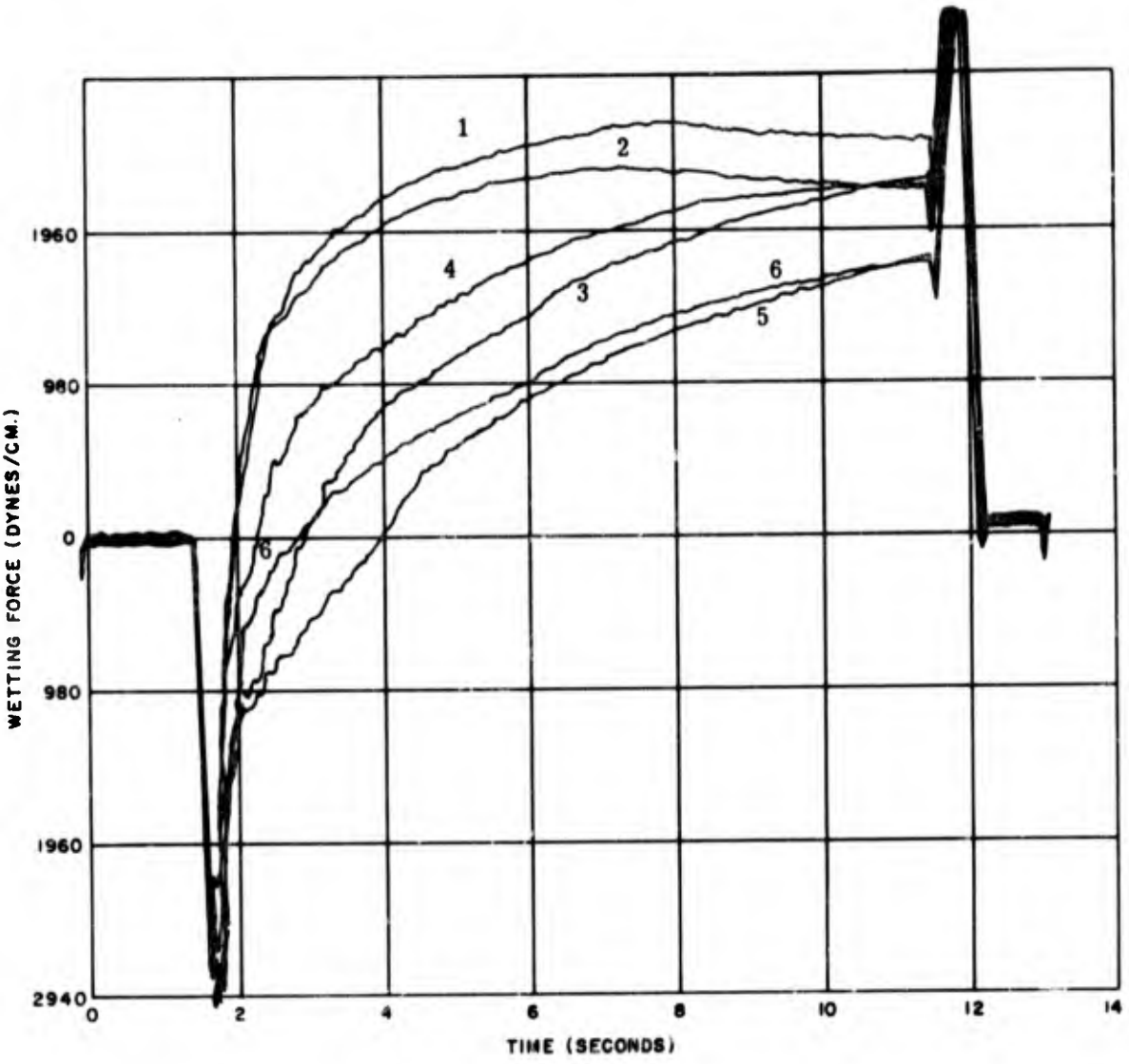

Base Material: ASTM-F15 Fe-Ni-Co
Flux: Water White Rosin
Solder Bath Temperature: 260°C
Curve 1: 0 Hours Steam Time
Curve 2: 0 Hours Steam Time
Curve 3: 2 Hours Steam Time
Curve 4: 2 Hours Steam Time
Curve 5: 4 Hours Steam Time
Curve 6: 4 Hours Steam Time

Figure 50. Effect of Steam Aging

TABLE 12. WETTING TIME AND FORCE VERSUS STEAM EXPOSURE

Steam Exposure (Hours)	Curve Nos.	Wetting Time (θ = 90°)	Wetting Force at 10 Seconds (dyne-cm)
0	1, 2	0.3	2400
2	3, 4	0.6 - 1.1	2300
4	5, 6	1.2 - 2.2	1700

Meniscograph data along with the results of the bend-peel, MIL-STD-883 and Hot Iron tests for all samples after 0, 8, and 16 week exposure for each environment are given in Appendix A.

Meniscograph curves of zero time for each given type and thickness of coating established a base for comparing differences that might occur over the full aging spectrum of 16 weeks exposure.

Although there were some 500 plus curves produced in this study in the hope that aging trends of the different platings could be correlated, the time spans were too short to detect significant differences attributable to aging; therefore, only a few curves typical of the results of a few coatings are shown. (See Figures 51, 52 and 53.) The three figures show curves characteristic of the individual coatings. The spread between curves, in most cases, was attributed to slight variations in sample to sample plating.

A comparison of samples displaying dewetting revealed that a majority of the dewetted samples were samples coated with the less pure gold (99.7% Au2). These dewetting occurrences cannot be observed on the Meniscograph curve since dewetting generally occurs after the sample is withdrawn from the molten solder. A significantly slower wetting time and lower equilibrium force were observed on those curves taken on samples with the heavier gold deposits (Figure 54). These results were attributed to the large quantities of gold dissolving in the advancing solder at the meniscus tip.

MENISCOGRAPH VERSUS MIL-STD-883 METHOD 2003 VERSUS HOT IRON SOLDERABILITY TEST

After Meniscograph curves were obtained, different but similarly exposed samples from the same plating lots were tested by means of the Hot Iron solderability test and the MIL-STD-883 test. Evaluation of the data

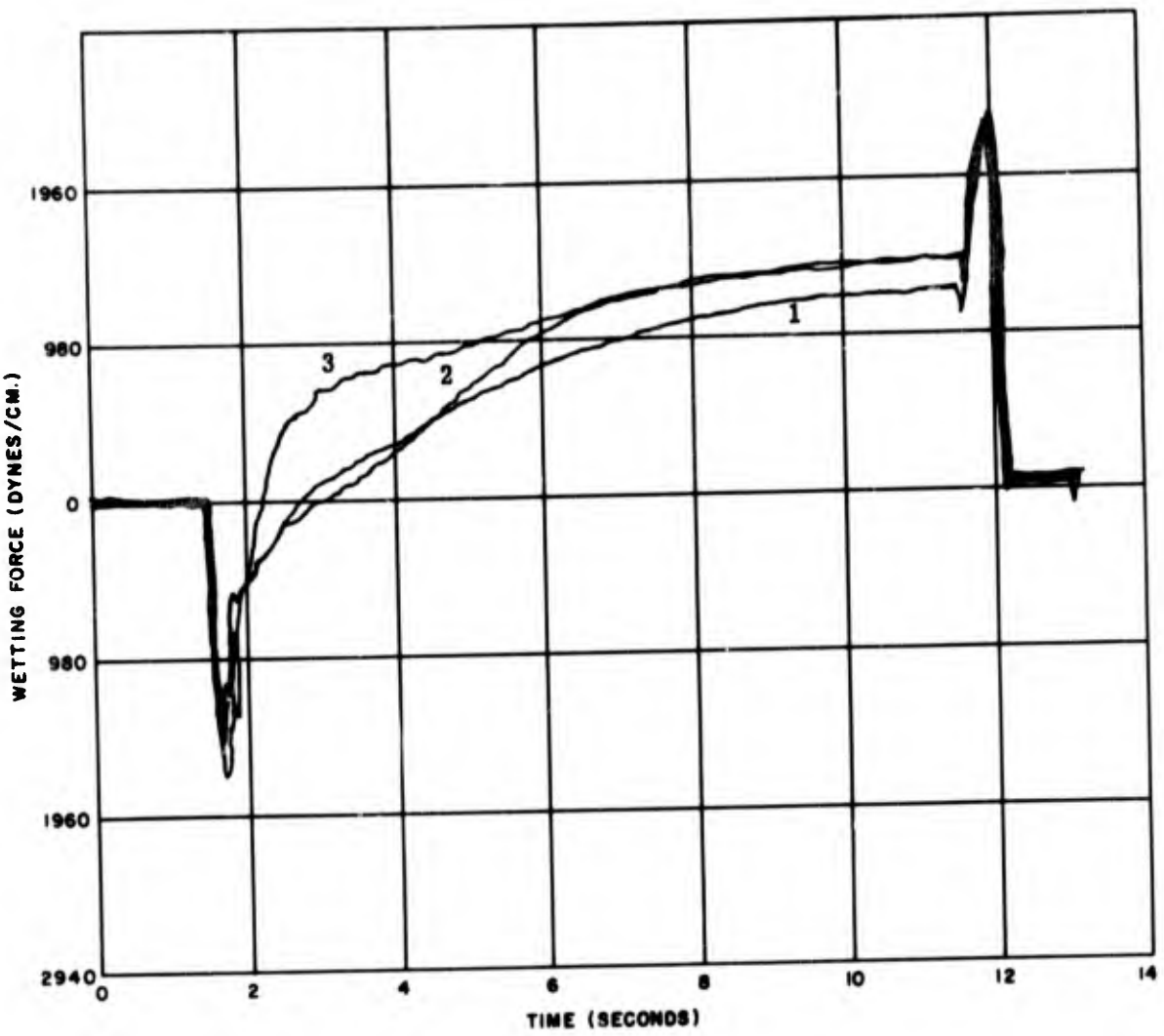

Base Material: ASTM-F15 Fe-Ni-Co
Flux: Water White Rosin
Solder Bath Temperature: 260° C
Plating: Au2, $50 \cdot 10^{-6}$ in.
Curve 1: Aged for 8 weeks
Curve 2: Aged for 0 weeks
Curve 3: Aged for 16 weeks

Figure 51. Effect of Environmental Exposure on Wetting Force (Au2 Plating)

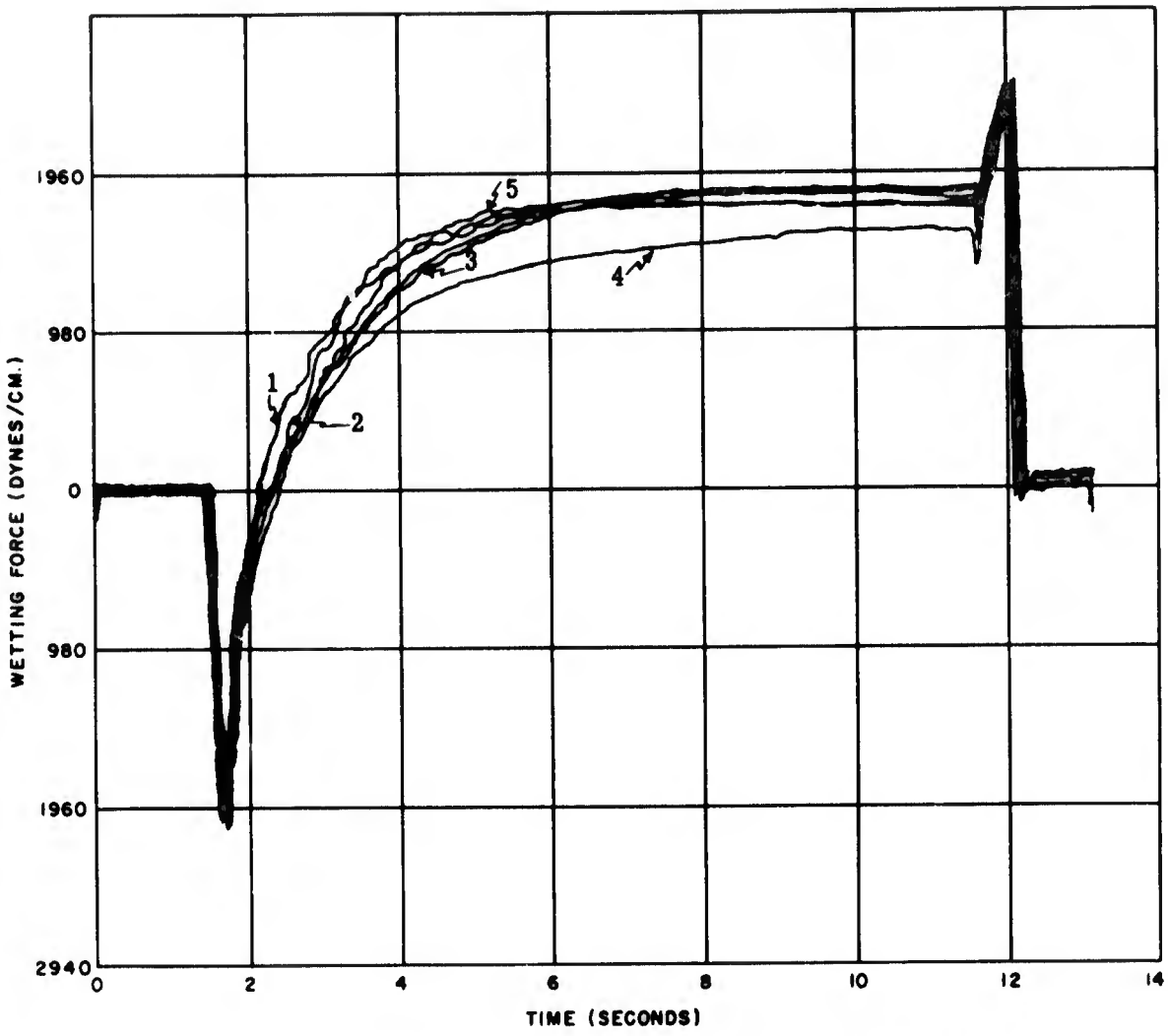

Base Material: ASTM-F15 Fe-Ni-Co Vendor A
Flux: Water White Rosin
Solder Bath Temperature: 260°C
Plating: BAT; $100 \cdot 10^{-6}$ in.
Curve 1: Aged for 0 weeks
Curve 2: Aged for 4 weeks
Curve 3: Aged for 8 weeks
Curve 4: Aged for 12 weeks
Curve 5: Aged for 16 weeks

Figure 52. Effect of Environmental Exposure on Wetting Force (BAT Plating)

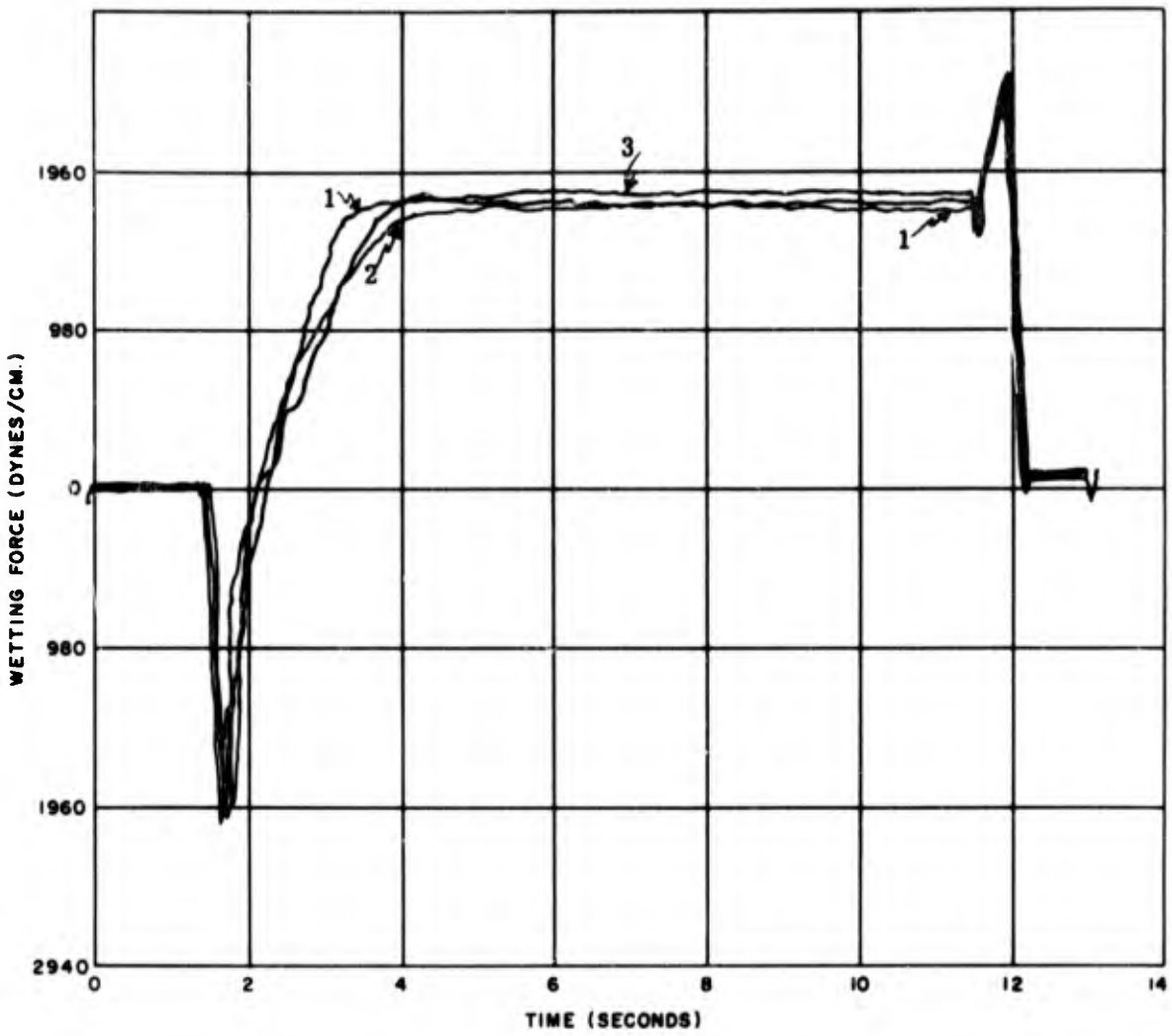

Base Material: ASTM-F15 Fe-Ni-Co Vendor A
Flux: Water White Rosin
Solder Bath Temperature: 260-C
Plating: BAS, $100 \cdot 10^{-6}$ in.
Curve 1: Aged for 0 weeks
Curve 2: Aged for 8 weeks
Curve 3: Aged for 16 weeks

Figure 53. Effect of Environmental Exposure on Wetting Force (BAS Plating)

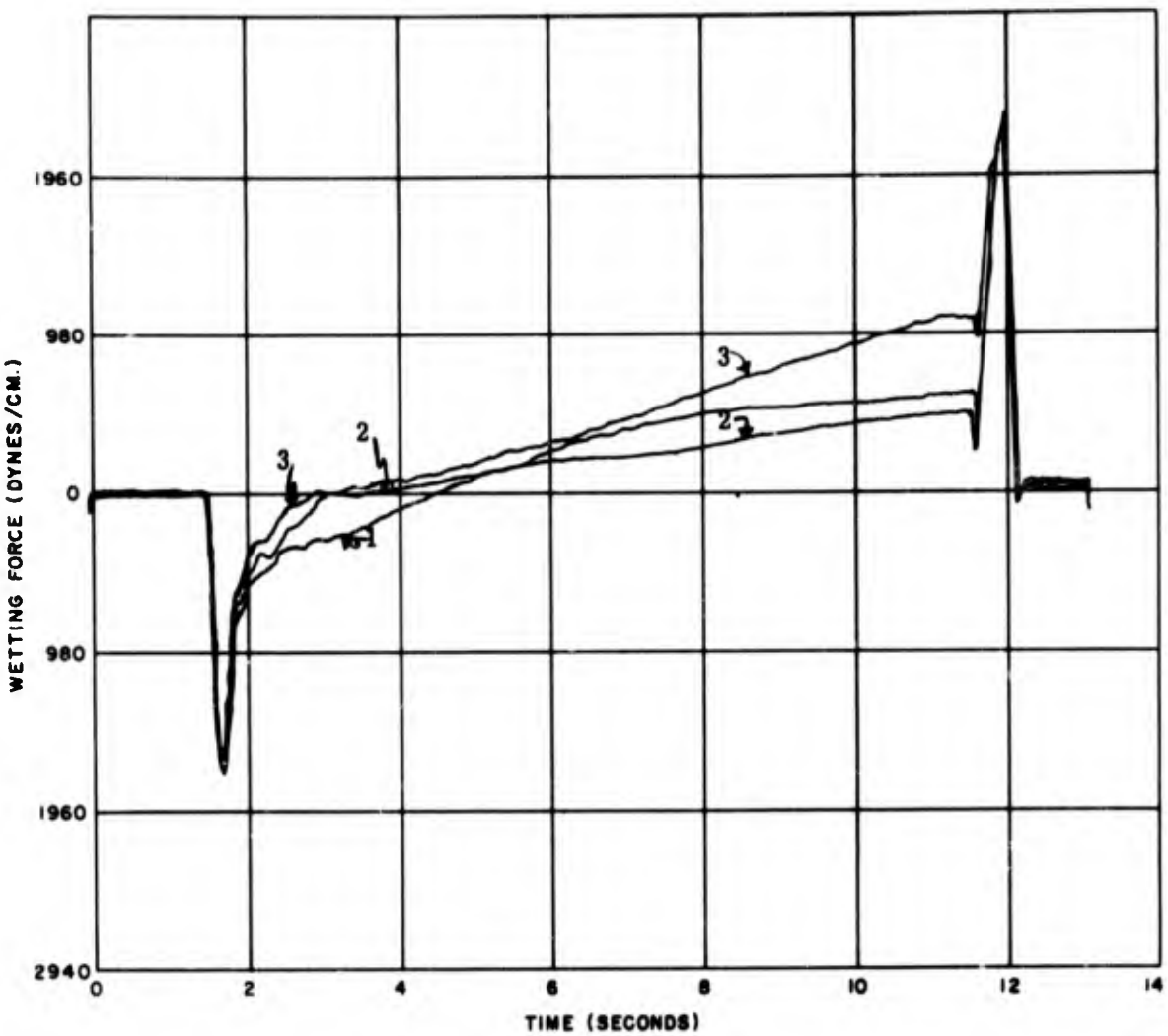

Base Material: ASTM-F15 Fe-Ni-Co Vendor A
Flux: Water White Rosin
Solder Bath Temperature: 260° C
Plating: Au2, $150 \cdot 10^{-6}$ in.
Curve 1: Aged for 0 weeks
Curve 2: Aged for 8 weeks
Curve 3: Aged for 16 weeks

Figure 54. Effect of Environmental Exposure on Wetting Force (Heavier Au2 Plating)

generated by these three test methods revealed no correlation among any of these tests nor with these tests and aging time. These three tests measure solderability somewhat differently and therefore are not necessarily comparable. MIL-STD-883 Method 2003 is based upon the amount of dewetting as determined visually; the Hot Iron test upon flow characteristics plus dewetting; and the Meniscograph test upon measurements of wetting rate as well as meniscus weight or height.

Additional investigations are required to understand the relationships of these solderability test methods from the standpoint of sensitivity, applicability, resolution and repeatability.

PHASE V - ULTRASONIC SOLDERING

Normally, when a purchaser secures flat packs from a vendor, one specification put on the devices is that the leads of the flat packs will have solderable surfaces. Occasionally, however (and often, too frequently), these flat pack leads will demonstrate dewetting when tested to MIL-STD-883 Method 2003, in the purchaser's plant. Because of a number of factors, such as delayed delivery of replacements, disagreement on solderability results etc., these dewetted leads are repaired by ultrasonic soldering.

To evaluate the effectiveness of ultrasonic soldering, it was decided that it was necessary to produce, consistently, a dewetted condition on the samples to be studied. Two methods most likely to produce consistent dewetting were investigated -- contamination of the base metal prior to plate, and the oxidation of samples plated with a slightly porous plate. Both conditions also were sought to determine if differences in sample preparation might show differences in ultrasonic soldering results. The samples were prepared as follows:

(a) Base Metal Contamination

Samples prepared by this method were degreased only and electroplated with a previously used and contaminated gold bath. All preliminary surface cleaning and activation steps were eliminated from the standard plating process. The omission of the cleaning and activation permitted residual oxides to remain on the base metal surface to aid in dewetting during soldering.

(b) Post-Plate Oxidation

These samples were processed through a complete cleaning and activation treatment followed by a 50 x 10^{-6} inch gold plate (Au2). After plating, the samples were placed in an oven for three days at 250°C.

Although other conditions could produce dewetting, these were the only ones investigated in this experiment.

To determine the suitability of these samples for the experiment, the samples were solderability tested on the Meniscograph. This not only yields a curve of the wetting action but also can duplicate the conditions specified in MIL-STD-883 Method 2003. These samples were so evaluated. All samples tested exhibited extreme dewetting after this soldering operation.

A group of samples was prepared by each method discussed above and solderability tested. This was done, not only to insure dewetting but to prepare the samples as they normally would be seen by ultrasonics. The samples prepared by each method were divided to have approximately ten samples from each method soldered in each of two ultrasonic soldering equipments, one with a vertical transducer and the other with two horizontal transducers. Pertinent ultrasonic soldering equipment details and soldering operating details were:

	Horizontal	Vertical
Manufacturer	Redford Corp.	Blackstone Corp.
Model	SG300A	TP-3
Solder Capacity	25 lbs	2.5 lbs
Power Input	300 watts	200 watts
Solder Temperature	260°C (500°F)	260°C (500°F)
Soldering Time	5 seconds	5 seconds
Soldering Composition	63/37	63/37

Examination of the samples upon removal from ultrasonic soldering showed all traces of dewetting to have disappeared from all samples. Retesting these samples both with the Hot Iron and the MIL-STD-883 Method 2003 tests on the Meniscograph produced no dewetting on any of the samples visible at a magnification of 12X.

PHASE VI - WIRE BONDING

Gold wire bonding was done to the gold plated surfaces used for preservation in the solderability section. This bonding and testing was accomplished using procedures reported in the Technical Report RADC-TR-73-123.[12] The only difference was that these bonds were totally gold-to-gold; no chip bonding was involved. Test Method 2011 of MIL-STD-883, Test Condition D was used.

Aluminum bonding was done on the same surfaces using the same type of procedural setup.

Gold and aluminum wires were 0.001 inch in diameter and were pulled to destruction. Table 13 contains the test results showing the average number of grams to failure of ten bonds on each surface. These are shown graphically in Figures 55 and 56.

It was found that gold wire bonds could be attached successfully to nearly all of the gold plated surfaces. As one approaches the complete or nearly complete Au2 exterior, the bond strength decreases and also tends to decrease when there is a nickel underplate. A minimum pull strength of 4 grams is considered acceptable for 0.001 inch diameter gold wires.

Aluminum wire bond test results were more dramatic in determining that the exterior surface and underplate which is less successful for gold wire is almost impossible for aluminum bonding. A minimum pull strength of 8 grams is considered acceptable for 0.001 inch diameter aluminum wires.

In both cases, standard setup procedures were held constant for all bonds of that type. No attempt was made to determine conditions which would more successfully cause better bonding to occur.

---

[12] Bertin, A., Development of Microcircuit Bond-Pull Screening Techniques, Technical Report RADC-TR-73-123. Rome, N. Y.: Griffiss Air Force Base, Rome Air Development Center, April 1973.

TABLE 13. WIRE BONDING RESULTS

Surface	Average No. of Grams to Failure for Ten Bonds							
	Vendor A Material		Vendor A Oxidized Material		Vendor B Material		Vendor B Oxidized Material	
	0.001 Inch Gold Bonds							
	Avg	Std Dev	Avg	Std Dev	Avg	Std Dev	Avg	Std Dev
Au1-10 Au2-40	7.45	0.76	7.55	0.64	7.00	1.20	8.05	0.64
Au1-20 Au2-80	7.65	1.29	6.75	1.14	7.50	0.91	7.70	1.01
Au1-100 NiS-30	6.80	1.36	7.10	0.46	7.95	0.83	6.05	1.55
Au1-50	7.00	0.85	7.45	1.04	7.45	0.83	7.50	0.94
Au1-200	7.20	1.30	7.30	0.71	7.65	0.63	7.60	1.43
Au2-40 Au1-10	7.00	0.85	7.50	0.78	7.50	0.97	7.90	0.77
Au2-80 Au1-20	6.95	0.64	7.15	1.23	7.05	0.60	7.10	0.74
Au2-50	7.50	0.71	7.15	0.91	6.70	1.09	6.80	1.34
Au2-150	6.90	1.05	6.40	1.33	6.10*	2.13	4.20	1.51
	0.001 Inch Aluminum Bonds							
Au1-10 Au2-40	11.75	2.81	10.40	3.06	9.90	3.28	11.00	3.25
Au1-20 Au2-80	12.40	0.97	14.00	2.67	10.20	1.67	12.75	1.60
Au1-100 NiS-30	---**	----	12.85	2.15	7.80*	2.58	---**	----
Au1-50	12.65	1.47	14.85	2.14	13.20	1.46	15.80	1.53
Au1-200	13.00	1.22	14.05	2.27	12.75	2.25	14.44	1.61
Au2-40 Au1-10	14.55	0.96	11.10	1.81	10.50	2.99	12.25	2.15
Au2-80 Au1-20	9.78	2.17	10.55	1.79	9.65	9.65	10.10	1.91
Au2-50	9.40	2.60	6.65*	1.93	6.55*	1.69	---**	----
Au2-150	---**	----	---**	----	---**	----	---**	----

*Excessive percent of stitch bonds lifted from plated surface. (>40%)

**Plated surface would not accept aluminum bonds.

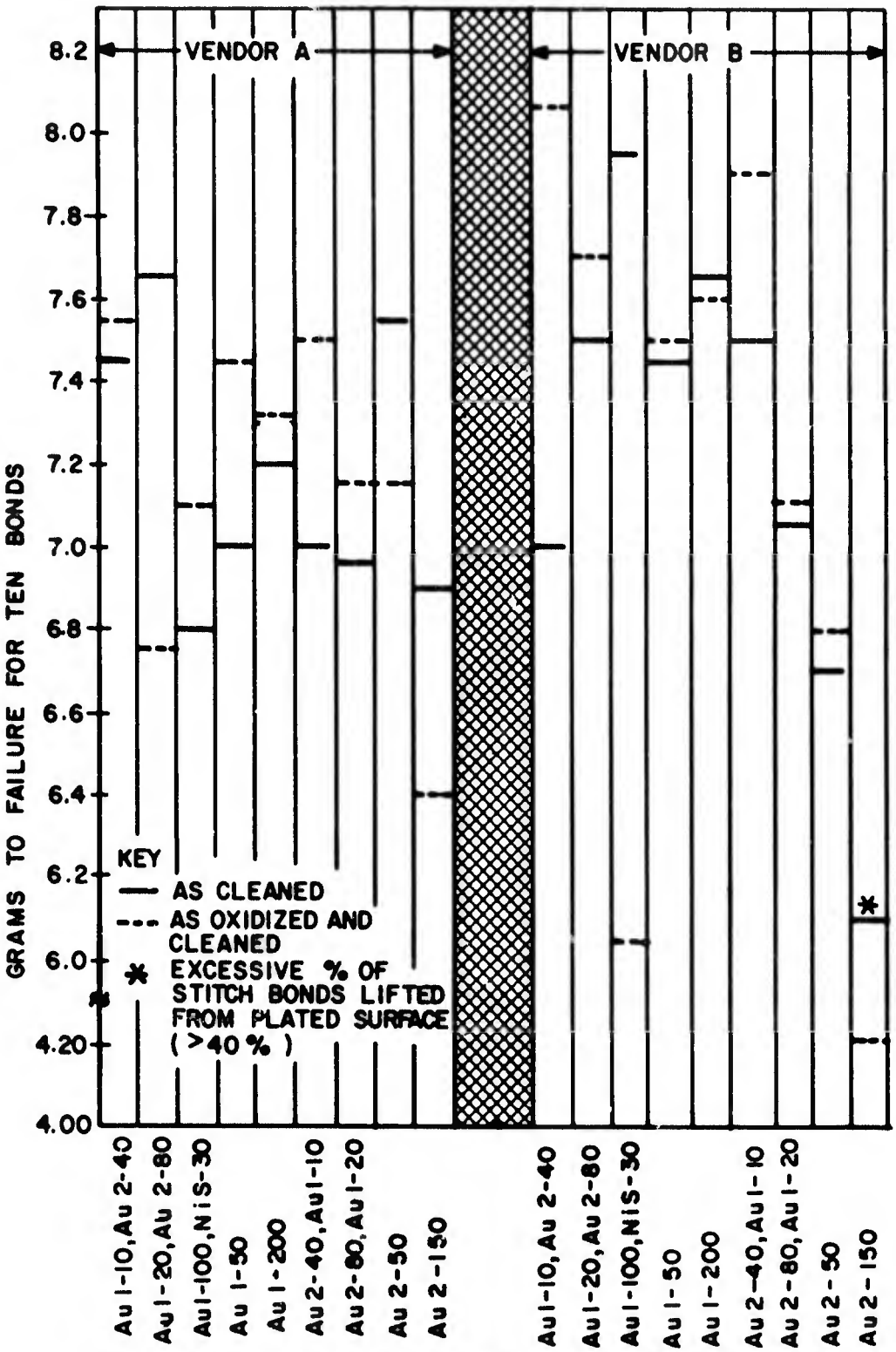

Figure 55. Average 0.001 Inch Gold Bond Pull Strength versus Surface Preparation

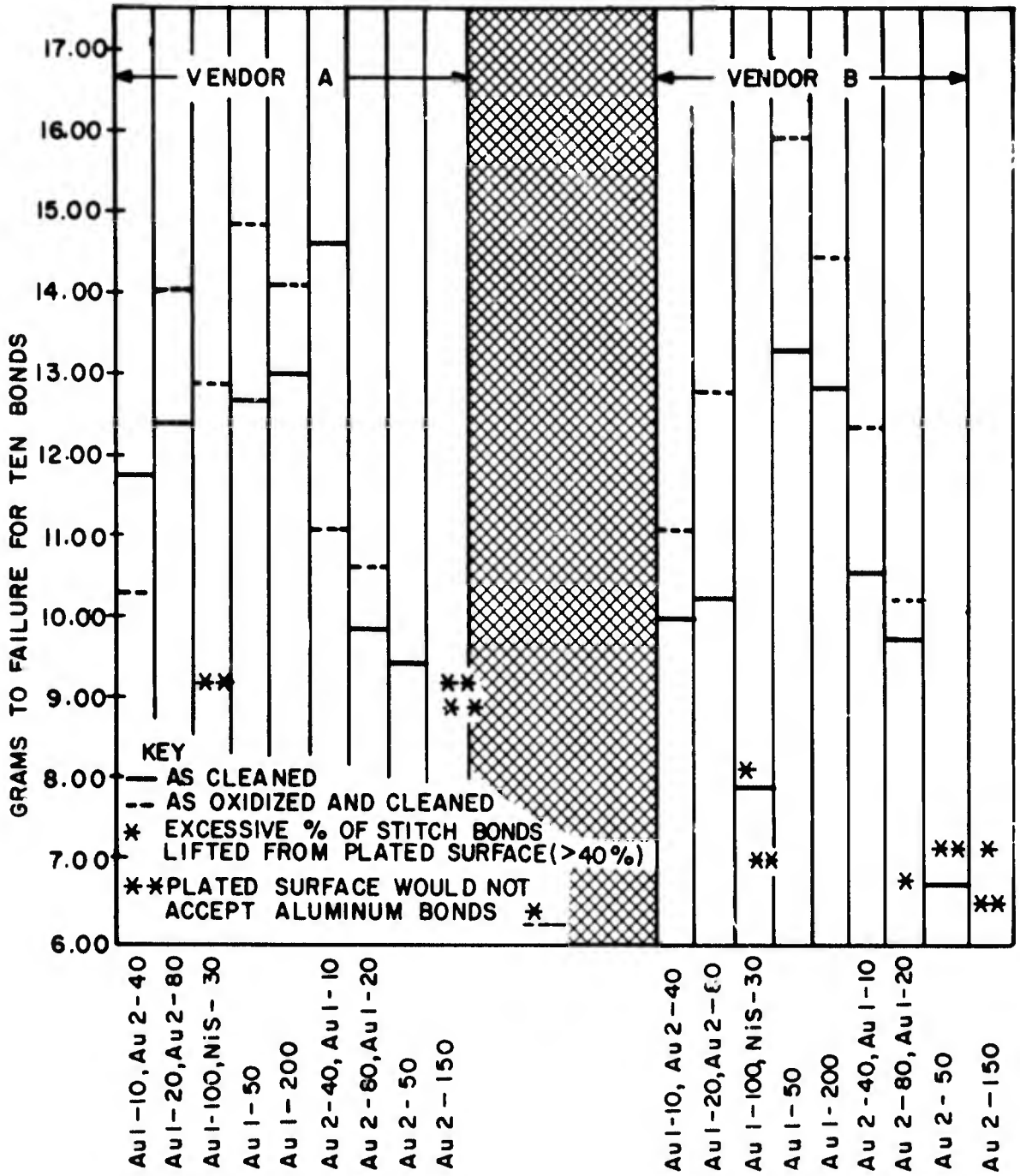

Figure 56. Average 0.001 Inch Aluminum Bond Pull Strength versus Surface Preparation

SECTION 4

CONCLUSIONS

1. Iron-nickel-cobalt glass sealing (ASTM-F15) alloys secured from different vendors show significantly different rates of oxidation and, in the single investigation made, significantly different rates were obtained between two different lots from one vendor.

2. Oxidation is more rapid at the grain boundaries, and the type of scale formed at these sites differs in composition from that scale formed on the body of the grain.

3. Grain growth characteristics of these different vendor alloys show significant differences when heated to temperatures customarily used for decarburization. Growth of the grains at these temperatures appears to be by nucleation and growth. Grain growth also appears to be related to the degree and the type of preferred grain orientation, hence, probably is dependent upon fabrication history.

4. Contrary to reports in the literature and within the range of carbon contents in the materials used, decarburization of the alloys was not required for adherence of the oxide to the metal. The degree of adherence of the scale is shown to be dependent upon the atmosphere (moisture content), temperature, time and surface roughness. Exposure to a wet hydrogen atmosphere at elevated temperatures (decarburization) prior to oxidation may relax the controls necessary on other variables to obtain adherence. A comparison of the adherence of oxides on as-received and decarburized samples of the same material was not investigated.

5. Experiments have shown that the rate of oxidation is greater at grain boundaries and the composition of the grain boundary oxide in the scale is higher in iron oxide than that of the body of the grain. It seems reasonable to assume that grain growth may be desirable both to increase oxide adherence and to decrease the total amount of oxygen penetration into the metal. These factors may outweigh the decrease in mechanical properties associated with large grains.

6. Experimental evidence seems to indicate that the ratio of scale thickness to depth of oxygen penetration at the grain boundaries changes with temperature; this result does not seem entirely reasonable. Because boundaries used for measurement (scale-to-air, scale-to-metal, and metal surface to the deepest oxide particles in grain boundaries) are irregular and inaccuracies in measurement make such correlations difficult, additional measurements should be made over larger temperatures and time spans to more realistically evaluate these relative rates.

7. Simple test samples, easy to handle in oxidation studies and in studies of glass sealing, were found to yield low stresses in the glass and appear to give a representative picture of package sealing. Limited studies on the shape of the meniscus of these samples show it to be relatively insensitive to temperature, time and oxide dissolution.

8. Glass-oxide-metal adhesion plotted both on a temperature versus oxide weight gain matrix and on an energy input versus weight gain matrix indicates that the oxide thickness necessary for good adhesion shifts to larger values at the higher sealing temperatures and energy inputs. At these higher temperatures and energy inputs, good adhesion is obtained over a range of oxide thicknesses. With reasonable control of the oxidation process, it would appear that no difficulties should be experienced with adherence in glass sealing.

9. Although no formal program was established to study the occurrence of bubbles in the glass, observations by microscopic examination at low power indicate that bubbles occurred infrequently and at random with respect to sealing temperature and oxide thickness.

10. No differences were found in either plating or solderability characteristics between as-received and cleaned materials or oxidized and cleaned materials.

11. After oxide removal, the care taken in the cleaning and activation for plating is dependent upon the type of plating bath used. For bright acid tin and bright acid solder plating, the plating baths proved efficient and effective in removing oxides and producing adherent plate.

12. In applications where corrosive environments exist and mechanical integrity of the leads is critical, bright acid tin and bright acid

solder coatings should prove advantageous because the coatings are sacrificial to the lead material. Some samples, either bright acid tin or bright acid solder coated, showed dewetting in both the aged and unaged condition. The cause for this dewetting was not investigated.

13. When gold coatings are to be used, high purity gold coatings are superior in bend, corrosion resistance, solderability and bondability to those of lower purity.

14. Either insufficient cleaning of the lead surface or contamination of the gold bath will be revealed by a dewetting action during solderability testing per MIL-STD-883 Method 2003.

15. No relationship was established between the curves obtained by the Meniscograph and the results of solderability testing by MIL-STD-883 Method 2003 and the Hot Iron test in either as-plated or 4 month aging tests. It appears that in spite of the plating controls imposed, slight variations in the plates obtained caused greater differences in the meniscus curves and the dewetting observed than was obtained by atmospheric exposures. The Meniscograph measures the speed of wetting and size of meniscus for given periods of time; the latter two tests are measures of dewetting.

16. The Meniscograph does not reflect dewetting; however, nonwetting can be observed. Some differences in the type of metal and the thickness of the metal plated are reflected by the Meniscograph curve.

17. In general, with duplex coatings of gold, the characteristics of the plate are reflected in the characteristics of the top plate. With the nickel undercoatings used, one half of the samples showed cracks but little dewetting was observed; the sample size is too small for firm conclusions.

18. Ultrasonics is beneficial to removing a dewet condition and improving solderability by the Hot Iron and MIL-STD-883 tests, when this dewet condition is caused by either contamination in or under the plate.

19. Except for surface appearance after ultrasonic soldering, no differences in results can be observed between the two different ultrasonics equipments used.

20. Both gold and aluminum bonding to a high purity plate are superior to plates of lower purity in pull strength values.

SECTION 5

RECOMMENDATIONS

1. Vendor alloys should be investigated to determine differences in oxidation rates and adherence of oxides as well as grain orientation and grain growth. These studies should be aimed at determining the causes for vendor alloy differences with an ultimate goal of establishing the best process and controls. With those alloys having a small tonnage output, fabricators may not be induced to change; however, simple tests may be determined to evaluate those alloys for suitability to flat pack processing.

2. In view of the extra costs to flat pack vendors, the decarburization process should be studied with an aim at establishing not only the maximum allowable carbon content of these alloys but also the advantages or disadvantages of the decarburizing gas on adhesion of the oxides and glass sealing.

3. The small test samples used in these experiments for evaluating adherence of the glass-oxide-metal interface should be further evaluated to determine the relation of their results to package hermeticity. Further evaluations are required both of oxide weight gains in other alloys and of glass sealing using other glasses.

4. For applications having severe corrosion exposure, bright acid tin and bright acid solder platings appear to have definite advantages. In applications where gold is either specified or desired, high purity gold is superior for solderability, bending, corrosion and bondability.

5. Studies are required to determine the feasibility of the use of the Meniscograph and Hot Iron tests as alternate tests to MIL-STD-883 Method 2003. Since dewetting is the basis for both the MIL-STD-883 and Hot Iron tests, and is the cause for many rejections and increased costs in many users' plants, basic studies should be made to determine its causes and prevention.

APPENDIX A

TEST RESULTS SUMMARY

TABLE A-1. TEST RESULTS SUMMARY -- ENVIRONMENT 1

Coating and Base Material	Sample Number	Zero Time: Meniscograph Visual	Zero Time: Meniscograph Final Curve Height	Zero Time: Meniscograph Final Curve Trend	Zero Time: MIL-883 Visual	Zero Time: Bend Pool	Zero Time: Hot Iron	8 Weeks: Meniscograph Visual	8 Weeks: Meniscograph Final Curve Height	8 Weeks: Meniscograph Final Curve Trend	8 Weeks: MIL-883 Visual	8 Weeks: Hot Iron	16 Weeks: Meniscograph Visual	16 Weeks: Meniscograph Final Curve Height	16 Weeks: Meniscograph Final Curve Trend	16 Weeks: MIL-883 Visual	16 Weeks: Hot Iron
BAT-100-A	1	DW20	1.83	0	P	C	P	DW15	1.70	0		P	P	1.80	0	P	P
BAT-250 - A	2	P	1.68	0	P	P	P						P	1.80	-	P	P
BAS-100 - A	3	P	1.68	-	DW85	P	P	P	1.70	0		P	P	1.78	-	P	P
Au1-50 - A	4	P	1.67	+	P	P	P	P	1.48	+		P	P	1.50	+	P	P
Au1-200 - A	5	P	1.70	+	P	P	P	P	1.45	+		DW	P	1.50	+	P	DW
Au2-50 - A	6	P	1.70	0	DW80	P	DW	P	1.20	+		DW	DW	1.00	+	P	P
Au2-150 - A	7	P	0.60	+	DW50	C	P	P	0.47	+		DW	DW	-		P	DW
BAT-100 - A0	8	P	1.54	-	DW20	C	P	P	1.62	-		P	DW	1.85	0	DW	DW
BAT-250 - A0	9	P	1.69	0	DW25	C	P						P	1.73	0	P	P
BAS-100 - A0	10	P	1.54	-	DW60	C	P	P	1 40	-		P	P	1.85	0	P	DW
Au1-50 - A0	11	P	1.56	0	P	P	P	P	1.44	0		P	P	1.55	+	P	P
Au1-200 - A0	12	P	1.50	0	P	P	P	P	1.50	+		P	P	1.50	+	P	P
Au2-50 - A0	13	DW20	1.43	+	DW80	P	P	DW50	1.83	+		P	DW	1.40	+	DW	DW
Au2-150-A0	14	DW10	0.65	+	P	C	P	P	0.35	+		P	P	0.55	0	P	P
BAT-100-B	30	DW20	1.75	0	P	P	DW	DW15	1.60	-		P	P	1.51	-	P	P
BAT-250-B	31	DW20	1.70	0	P	C	P						P	1.70	-	P	P
BAS-100-B	32	P	1.74	0	P	P	P	P	1.86	-		P	P	1.85	-	P	P
Au1-50-B	18	P	1.50	0	P	P	P	P	1.46	+		P	P	1.60	+	P	P
Au1-200-B	19	P	1.50	0	P	P	P	P	1.47	0		P	P	1.50	+	P	P
Au2-50-B	20	DW45	1.30	+	DW30	C	DW	DW	1.07	+		P	DW	1.10	+	P	DW
Au2-150-B	21	P	0.48	+	P	C	DW	P	0.57	+		DW	DW	0.60	+	P	DW
BAT-100-B0	22	P	1.72	-	DW15	P	P	P	1.70	-		P	P	1.82	-	P	DW
BAT-250-B0	23	P	1.51	0	DW15	P	P						P	1.72	-	P	P
BAS-100-B0	24	P	1.53	-	DW15	P	P	P	1.39	-		DW	P	1.55	-	P	P
Au1-50-B0	25	P	1.53	0	P	P	P	P	1.48	0		P	P	1.69	+	P	P
Au1-200-B0	26	P	1.60	0	P	P	P	P	1.47	+		P	P	1.55	+	P	P
Au2-50-B0	27	P	1.24	+	DW20	P	DW	DW30	1.13	+		DW	DW	1.20	+	DW	DW
Au2-150 B0	28	DW25	0.48	+	P	C	P	DW10	0.57	+		DW	DW	0.75	+	DW	DW
BAT-100-Cu	49	P	1.66	+	P	C	P	P	1.78	+		P	P	1.79	0	P	P
BAT-250-Cu	50	P	1.38	0	P	P	P						P	1.75	0	P	P
BAS-100-Cu	51	P	1.62	0	DW10	C	P	P	1.43	-		P	P	1.59	-	P	P
Au1-50-Cu	52	P	1.48	+	P	P	P	P	1.13	+		P	P	1.30	+	P	P
Au1-200-Cu	53	P	1.50	+	P	P	P	P	1.16	+		P	P	1.45	+	P	P
Au2-50-Cu	54	P	1.52	+	P	P	P	P	1.27	-		P	P	1.45	+	P	P
Au2-150-Cu	55	P	1.38	+	P	P	P	P	1.12	+		P	P	0.80	+	P	P
Au1-100 + NiS-30-A	29	P	1.48	0	P	C	P	P	1.53	0		P	P			P	P
Au1-10 + Au2-40-A	15	P	1.14	-	DW25	C	DW	P	1.20	-		P	DW	1.51	+	DW	P
Au2-40 + Au1-10-A	16	P	1.56	0	P	P	P	P	1.44	+		P	P	1.50	+	P	DW
Au1-20 + Au2-80-A	17	P	1.66	+	DW45	P	P	P	0.78	0		P	P	1.45	+	P	P
Au2-80 + Au1-20-A	33	P	1.60	+	DW10	P	P	P	1.50	0		DW	P	1.45	+	P	P
Au1-100 + NiS-30-A0	34	P	1.53	0	P	P	P	P	1.48	0		P	P	----		P	P
Au1-10 + Au2-40-A0	35	P	1.52	0	P	P	P	P	1.43	0		DW	P	1.65	0	P	P
Au2-40 + Au1-10-A0	36	P	1.57	+	P	P	P	P	1.56	0		DW	P	1.65	+	P	P
Au1-20 + Au2-80-A0	37	P	1.52	0	P	P	P						P	1.50	+	P	P
Au2-80 + Au1-20-A0	38	P	1.50	+	DW15	C	P						P	----		P	P
Au1-100 + NiS-30-B	39	P	1.62	0	P	P	P	P	1.51	0		P	P	----		P	P
Au1-10 + Au2-40-B	40	DW15	1.51	0	DW10	P	P	DW	1.30	0		P	DW	1.59	+	DW	P
Au2-40 + Au1-10-B	41	P	1.72	+	P	C	P	P	1.51	0		DW	P	1.70	0	P	P
Au1-20 + Au2-80-B	42	DW10	0.97	0	P	P	DW						DW	1.45	+	DW	P
Au2-80 + Au1-20-B	43	P	1.55	0	P	P	DW						P	----		P	P
Au1-100 + NiS-30-B0	44	P	1.56	0	P	C	P	P	1.46	0		P	P	----		P	P
Au1-10 + Au2-40-B0	45	P	1 50	+	DW10	P	DW	P	1.52	0		P	P	1.55	+	P	P
Au2-40 + Au1-10-B0	46	P	1.53	0	P	C	DW	P	1.52	0		P	P	1.65	+	P	P
Au1-20 + Au2-80-B0	47	P	1.56	0	P	C	DW						P	1.60		P	P
Au2-30 + Au1-20-B0	48	P	1.50	+	DW40	P	DW						P	----		P	P

For meniscus force - multiply given curve height by 980 dyne centimeters

A Vendor A Alloy

A0 Vendor A Alloy Oxidized

B Vendor B Alloy

B0 Vendor B Alloy Oxidized

C Cracked

DW25 = Dewet 25% (All DW = 5% or Greater Dewet)

P = Pass

+ = Increasing Slope

- = Decreasing Slope

0 = Equilibrium

TABLE A-3. TEST RESULTS SUMMARY -- ENVIRONMENT 2

Coating and Base Material	Sample Number	Zero Time						8 Weeks					16 Weeks				
		Meniscograph Visual	Meniscograph Final Curve Height	Meniscograph Final Curve Trend	MIL-883 Visual	Bend Test	Hot Iron	Meniscograph Visual	Meniscograph Final Curve Height	Meniscograph Final Curve Trend	MIL-883 Visual	Hot Iron	Meniscograph Visual	Meniscograph Final Curve Height	Meniscograph Final Curve Trend	MIL-883 Visual	Hot Iron
BAT-100-A	1	DW20	1.03	0	P	C P	P	P	1.08	0		P	P	1.05	0	P	P
BAT-250-A	2	P	1.08	0	P	P P											
BAS-100-A	3	P	1.08	-	DW85	P P	P	P	1.01	-		P	P	1.05	0	P	P
Au1-50-A	4	P	1.07	+	P	P P	P	P	1.56	+		P	P	1.05	+	P	P
Au1-200-A	5	P	1.70	+	P	P P											
Au2-50-A	6	P	1.70	0	DW80	P DW	DW45	1.12	0		DW	DW	1.13	+	P	DW	
Au2-150-A	7	P	0.60	+	DW50	C P											
BAT-100-A0	8	P	1.54	-	DW30	C P	P	P	1.77	-		P	P	1.90	0	P	P
BAT-250-A0	9	P	1.60	0	DW25	C P											
BAS-100-A0	10	P	1.54	-	DW80	C P											
Au1-50-A0	11	P	1.56	0	P	P P	P	P	1.60	+		P	P	1.70	+	P	P
Au1-200-A0	12	P	1.50	+	P	P P											
Au2-50-A0	13	DW20	1.43	+	DW80	P P	DW20	1.33	0		P	P	1.60	+	P	P	
Au2-150-A0	14	DW10	0.65	+	P	C P											
BAT-100-B	30	DW20	1.75	0	P	P DW	DW20	1.86	0		P	P	1.85	0	P	P	
BAT-250-B	31	DW20	1.70	0	P	C P											
BAS-100-B	32	P	1.74	-	P	P P											
Au1-50-B	18	P	1.50	0	P	P P	P	P	1.60	+		P	DW	1.65	+	P	DW
Au1-200-B	19	P	1.50	0	P	P P											
Au2-50-B	20	DW45	1.30	+	DW30	C DW	DW80	1.10	0		DW	P	1.55	+	P	P	
Au2-150-B	21	P	0.46	+	P	C DW											
BAT-100-B0	22	P	1.72	-	DW15	P P	P	P	1.84	-		P	P	1.95	0	P	P
BAT-250-B0	23	P	1.58	0	DW15	P P											
BAS-100-B0	24	P	1.53	-	DW15	P P											
Au1-50-B0	25	P	1.53	0	P	P P	P	P	1.54	+		P	P	1.75	+	P	P
Au1-200-B0	26	P	1.60	0	P	P P											
Au2-50-B0	27	P	1.24	+	DW20	P DW	DW20	1.23	0		DW	DW	1.80	0	DW	DW	
Au2-150-B0	28	DW25	0.48	+	P	C P											
BAT-100-Cu	49	P	1.66	+	P	C P	P	P	1.66	+		P	P	1.65	+	P	P
BAT-250-Cu	50	P	1.38	+	P	P P											
BAS-100-Cu	51	P	1.62	0	DW10	C P	P	P	1.73	0		P	P	1.70	0	P	P
Au1-50-Cu	52	P	1.48	+	P	P P	DW	0.15	+		P	P	1.50	+	P	P	
Au1-200-Cu	53	P	1.50	+	P	P P											
Au2-50-Cu	54	P	1.52	+	P	P P	P	P	1.44	0+		P	P	1.60		P	P
Au2-150-Cu	55	P	1.38	+	P	P P											
Au1-100 + NiS-30-A	29	P	1.48	-	P	C P	P	P	1.50	0		P	P			P	P
Au1-10 + Au2-40-A	15	P	1.14	-	DW25	C DW	DW30	1.29	0		DW	DW	1.70	+	DW	DW	
Au2-40 + Au1-10-A	16	P	1.56	0	P	P P	P	P	1.66	+		DW	P	1.65	0	P	P
Au1-20 + Au2-80-A	17	P	1.66	+	DW45	P P	DW15	1.13	0		DW	P			P	P	
Au2-80 + Au1-20-A	33	P	1.60	0	DW10	P P	P	P	1.20	-		DW	P			P	P
Au1-100 + NiS-30-A0	34	P	1.53	0	P	P P	P	P	1.56	0		P	P	1.60	0	P	P
Au1-10 + Au2-40-A0	35	P	1.52	0	P	P P	P	P	1.58	0		DW	P	1.70	0	P	P
Au2-40 + Au1-10-A0	36	P	1.57	0	P	P P	P	P	1.52	0		DW	P	1.55	0	P	P
Au1-20 + Au2-80-A0	37	P	1.52	0	P	P P	P	P									
Au2-80 + Au1-20-A0	38	P	1.50	+	DW15	C P											
Au1-100 + NiS-30-B	39	P	1.62	-	P	P P	P	P	1.50	0		DW	P	1.70	+	P	P
Au1-10 + Au2-40-B	40	DW15	1.51	0	DW10	P P	DW20	1.17	-		DW	DW	1.45	+	DW	P	
Au2-40 + Au1-10-B	41	P	1.72	+	P	C P	P	P	1.53	0		DW	P	1.65	+	P	P
Au1-20 + Au2-80-B	42	DW10	0.97	0	P	P DW											
Au2-80 + Au1-20-B	43	P	1.55	0	P	P DW											
Au1-100 + NiS-30-B0	44	P	1.56	0	P	C P	P	P	1.58	0		P	P	1.75	+	P	P
Au1-10 + Au2-40-B0	45	P	1.50	0	DW10	P DW	P	P	1.58	+		DW	P	1.70	+	P	P
Au2-40 + Au1-10-B0	46	P	1.53	0	P	C DW	P	P	1.58	0		DW	P	1.75	+	P	P
Au1-20 + Au2-80-B0	47	P	1.56	0	P	C DW											
Au2-80 + Au1-20-B0	48	P	1.50	+	DW40	P DW											

For meniscus force multiply given curve height by 980 dyne centimeters

A Vendor A Alloy

A0 Vendor A Alloy Oxidized

B Vendor B Alloy

B0 Vendor B Alloy Oxidized

C Cracked

DW25 = Dewet 25% (All DW = 5% or Greater Dewet)

P = Pass

+ = Increasing Slope

- = Decreasing Slope

0 = Equilibrium

MISSION
of
Rome Air Development Center

RADC is the principal AFSC organization charged with planning and executing the USAF exploratory and advanced development programs for information sciences, intelligence, command, control and communications technology, products and services oriented to the needs of the USAF. Primary RADC mission areas are communications, electromagnetic guidance and control, surveillance of ground and aerospace objects, intelligence data collection and handling, information system technology, and electronic reliability, maintainability and compatibility. RADC has mission responsibility as assigned by AFSC for demonstration and acquisition of selected subsystems and systems in the intelligence, mapping, charting, command, control and communications areas.

Printed by
United States Air Force
Hanscom AFB, Mass. 01731